



Delft University of Technology

## Shoreline response to detached breakwaters in prototype

Khuong, Chien

**DOI**

[10.4233/uuid:cdae6a2f-78dc-45fe-af01-43ed39c02ccc](https://doi.org/10.4233/uuid:cdae6a2f-78dc-45fe-af01-43ed39c02ccc)

**Publication date**

2016

**Document Version**

Final published version

**Citation (APA)**

Khuong, C. (2016). Shoreline response to detached breakwaters in prototype. <https://doi.org/10.4233/uuid:cdae6a2f-78dc-45fe-af01-43ed39c02ccc>

**Important note**

To cite this publication, please use the final published version (if applicable). Please check the document version above.

**Copyright**

Other than for strictly personal use, it is not permitted to download, forward or distribute the text or part of it, without the consent of the author(s) and/or copyright holder(s), unless the work is under an open content license such as Creative Commons.

**Takedown policy**

Please contact us and provide details if you believe this document breaches copyrights. We will remove access to the work immediately and investigate your claim.

# **Shoreline Response to Detached Breakwaters in Prototype**

Proefschrift

ter verkrijging van de graad van doctor  
aan de Technische Universiteit Delft,  
op gezag van de Rector Magnificus prof. ir. K. C. A. M. Luyben,  
voorzitter van het College voor Promoties,  
in het openbaar te verdedigen op maandag 30 mei 2016 om 12:30 uur

door

**Tat Chien KHUONG**

Master in Hydraulic Engineering  
National University of Civil Engineering, Vietnam  
geboren te Namdinh, Vietnam

This dissertation has been approved by the  
promotors: Prof.dr.s.ir. J.K. Vrijling and ir. H. J. Verhagen

Composition of the doctoral committee:

Rector Magnificus	chairman
Prof.dr.s.ir. J.K. Vrijling	Delft University of Technology
ir. H. J. Verhagen	Delft University of Technology

Independent members:

Prof.dr.ir. M.J.F. Stive	Delft University of Technology
Prof.dr.ir. P.H.A.J.M. van Gelder	Delft University of Technology
Prof.Dr.-Ing. H. Schüttrumpf	RWTH Aachen University
Dr.ir. B. Hofland	Delft University of Technology
Dr.ir. N.T. Hoan	Hanoi University of Civil Engineering
Prof.dr.ir. S.N. Jonkman	Delft University of Technology, reserve member

This research has been financially supported by the Ministry of Education and Training of Vietnam and Delft University of Technology.

*Keywords:* Detached breakwater, offshore breakwater, shoreline response, shoreline changes, estimate shoreline changes, aerial photography.

This dissertation should be referred to as: Khuong Tat Chien (2016). *Shoreline response to detached breakwaters in prototype*. Ph.D dissertation, Delft University of Technology.

An electronic version of this dissertation is available at: <http://repository.tudelft.nl/>.

Cover image by Dawn at Tel Aviv Beach.

Printed by Gildeprint, Enschede

ISBN 978-94-6233-301-7

Copyright © 2016 by Khuong Tat Chien

All rights reserved. No part of the material protected by this copyright notice may be reproduced or utilized in any form or by any means, electronic or mechanical, including photocopying, recording or by any information storage and retrieval system, without the prior permission of the author.

Author email: [chienbmcang@yahoo.com](mailto:chienbmcang@yahoo.com)

# CONTENTS

<b>CONTENTS</b> .....	<b>I</b>
<b>SUMMARY</b> .....	<b>V</b>
<b>SAMENVATTING</b> .....	<b>VII</b>
<b>CHAPTER 1: INTRODUCTION</b> .....	<b>1</b>
1.1 BACKGROUND AND PROBLEM STATEMENT .....	1
1.2 OBJECTIVES .....	2
1.3 RESEARCH QUESTIONS .....	2
1.4 RESEARCH METHODOLOGY .....	3
1.5 SCOPE OF RESEARCH .....	4
1.6 OUTLINE OF THIS RESEARCH .....	4
<b>CHAPTER 2: LITERATURE REVIEW OF EMERGED DETACHED BREAKWATERS OF SHORE PROTECTION</b> .....	<b>7</b>
2.1 INTRODUCTION .....	7
2.2 COASTAL PROCESSES WITHOUT DETACHED BREAKWATERS .....	8
2.2.1 <i>Waves in the nearshore</i> .....	9
2.2.2 <i>Currents in the nearshore</i> .....	10
2.2.3 <i>Sediment transport in the surf zone</i> .....	11
2.3 COASTAL IMPACTS OF DETACHED BREAKWATERS .....	15
2.3.1 <i>Waves change</i> .....	15
2.3.2 <i>Currents change</i> .....	16
2.3.3 <i>Change of sediment transport in the surf zone</i> .....	17
2.3.4 <i>Shoreline erosion impact</i> .....	18
2.3.5 <i>Erosion around structure</i> .....	19
2.3.6 <i>Other impacts</i> .....	19
2.4 SHORELINE RESPONSE PREDICTION METHODS .....	19
2.4.1 <i>Physical model</i> .....	20
2.4.2 <i>Numerical model</i> .....	23
2.4.3 <i>Empirical relationships</i> .....	24
2.5 CONCLUDING AND REMARKS .....	29
<b>CHAPTER 3: DATABASE OF OBSERVATIONS OF THE PROTOTYPES</b> .....	<b>31</b>
3.1 INTRODUCTION .....	31

3.2 DATA SOURCES .....	31
3.2.1 Sources of structure parameters .....	31
3.2.2 Sources of physical conditions: waves, currents, water level .....	33
3.2.3 Sources of observation results .....	33
3.3 PROJECTS INVENTORY .....	34
3.3.1 Inventory for the US.....	34
3.3.2 Inventory for Israel .....	34
3.3.3 Inventory for Spain .....	36
3.3.4 Inventory for Denmark, Italy, and the UK.....	37
3.3.5 Inventory for Japan.....	37
3.4 DATA COLLECTION OF STRUCTURE PARAMETERS.....	38
3.5 DATA COLLECTION OF SEDIMENT PROPERTIES .....	42
3.6 DATA ACHIEVEMENT OF WAVES, TIDES, AND OCEANIC CURRENTS .....	43
3.6.1 Waves.....	43
3.6.2 Tides .....	49
3.6.3 Oceanic currents.....	50
3.7 DATA MEASUREMENT OF SHORELINE RESPONSE .....	50
3.7.1 General .....	50
3.7.2 Measurement of the accretion .....	51
3.7.3 Measurement of the shoreline opposite the gap .....	53
3.7.4 Measurement of the shoreline at up and down-drift .....	54
3.8 CONCLUDING REMARKS .....	55
<b>CHAPTER 4: ANALYSIS OF PROTOTYPES DATA.....</b>	<b>57</b>
4.1 INTRODUCTION .....	57
4.2 ANALYSIS OF SHORELINE SILTATION .....	58
4.2.1 Classification based on the ratio of the breakwater length and the breakwater offshore distance ( $L_B/X_B$ ).....	58
4.2.2 The effect of dimensionless parameter of the breakwater length to the offshore distance .....	60
4.2.3 The effect of dimensionless parameter of the gap width to the representative wavelength.....	62
4.2.4 The effect of dimensionless parameter of the oblique incident wave ( $\sin\alpha_0$ ).....	63
4.2.5 The effect of dimensionless parameter of the tidal range to the representative wave height .....	65
4.2.6 Effect of dimensionless representative wave height to median sand diameter .....	65
4.2.7 Combination of the effects .....	66
4.2.8 Validation of the proposed formulation .....	70

4.3 ANALYSIS OF SHORELINE AT OPPOSITE THE GAP .....	75
4.3.1 States of the shoreline opposite the gaps .....	75
4.3.2 Develop the relationships.....	76
4.4 ANALYSIS OF SHORELINE AT UP AND DOWN-DRIFT AREA .....	82
4.4.1 Comparison of locations between the up-drift and the down-drift .....	82
4.4.2 Development of basic relationships .....	84
4.4.3 General relationships .....	87
4.5 DISCUSSION .....	90
4.6 CONCLUSIONS .....	91
<b>CHAPTER 5: INFLUENCE OF THE PARAMETERS ON THE SHORELINE CHANGES .....</b>	<b>93</b>
5.1 INTRODUCTION.....	93
5.2 INFLUENCE OF THE PARAMETERS ON THE CROSS SHORE AXIS .....	94
5.2.1 Effect of the breakwater length ( $L_B$ ).....	95
5.2.2 Effect of the breakwater offshore distance ( $X_B$ ).....	96
5.2.3 Effect of the gap width ( $G_B$ ) .....	98
5.2.4 Effect of the representative wave height ( $H_{repr}$ ).....	99
5.2.5 Effect of the representative wave length ( $L_{repr}$ ).....	100
5.2.6 Effect of the representative wave direction ( $\alpha_0$ ).....	102
5.2.7 Effect of the tidal range ( $h_{tide}$ ).....	103
5.2.8 Effect of the median sediment size ( $D_{50}$ ).....	104
5.3 INFLUENCE OF THE PARAMETERS ON THE ALONGSHORE AXIS .....	106
5.3.1 Effect of the offshore distance ( $X_B$ ) .....	106
5.3.2 Effect of the wave height ( $H_{repr}$ ).....	106
5.3.3 Effect of the oblique wave angle ( $\alpha_0$ ).....	107
5.3.4 Effect of the tidal range ( $h_{tide}$ ).....	108
5.3.5 Effect of the sediment size ( $D_{50}$ ).....	108
5.4 DISCUSSION .....	109
5.5 CONCLUSIONS .....	110
<b>CHAPTER 6: CONCLUSIONS AND RECOMMENDATIONS .....</b>	<b>113</b>
6.1 CONCLUSIONS .....	113
6.2 RECOMMENDATIONS.....	117
<b>REFERENCES .....</b>	<b>119</b>
<b>WEBSITES .....</b>	<b>123</b>
<b>LIST OF SYMBOLS.....</b>	<b>125</b>
<b>LIST OF FIGURES .....</b>	<b>129</b>

<b>LIST OF TABLES.....</b>	<b>133</b>
<b>ACKNOWLEDGEMENT .....</b>	<b>135</b>
<b>CURRICULUM VITAE.....</b>	<b>137</b>

## SUMMARY

An accurate prediction of shoreline changes behind detached breakwaters is, in regard to the adjustment to the environmental impact, still a challenge for designers and coastal managers. This research is expected to fill the gaps in the estimation of shoreline changes by developing new and generalized relationships of the shoreline changes to the detached breakwaters at several sensitive points, based on varying structure parameters, physical conditions and sediment properties of the prototypes. The generalization of relationships is intended to create new predictive possibilities.

Firstly, the background of detached breakwaters is presented in chapter 2, with the purpose of focusing on and narrowing down the specific problems. The background of the hydrodynamics and sediment transport with and without structures is reviewed to examine the changes of hydrodynamics and sediment transport in the field of detached breakwaters, and then, to approach the methods for the prediction of the shoreline response that have recently been applied. Chapter 2 presents the changes of waves and currents, leading to morphological changes in the sheltered areas of the breakwaters. As a consequence, the various positions of breakwaters' field change the morphology on the shoreline, such as the center of a structure, the shoreline opposite a gap, the up-drift and the down-drift position. To solve these problems, several methods are used to investigate the shoreline response, such as numerical, physical, and empirical models. However, the existing models still have a limited applicability for detached breakwaters. For example, numerical models are dependent on the accuracy of the mathematics of important morphological processes; physical models are problematic for laboratory scale effects as these use sediment scale or lightweight sediment material; empirical models are subject to the simplicity/limitation of relationships. Thus, new requirements are necessary for the estimation of the equilibrium shoreline responses.

Secondly, in chapter 3, the prototype approach is used as justifiable data for the development of the relationship models. In total 93 projects with 1144 structures were collected, including structure parameters, physical conditions, sediment properties and shoreline result measurements. The structural parameters are collected from a variety of sources, such as inquiry questionnaires, project reports, a selection of specific articles, journals and papers. The structural aspects, such as length of breakwater, offshore distance, gap width, freeboard, crest width, water depth at structure and structure orientation, are collected. The physical condition data, including wave, current and tidal range, were retrieved from online scientific resources and organizations. Waves were attained from two sources, the re-analysis of the global atmosphere and surface conditions for over 45 years by the European Centre for Medium-Range Weather Forecasts (ECMWF) and the model of estimating waves from past wind events (WIS). Currents were the subject of observation in the Ocean Surface Current Analyses – Real time (OSCAR); and tidal range values were extracted from reports of the projects. For the shoreline result measurements of aerial images were used to identify and



measure the magnitude of the affected shore; the time-series images of post-construction beach responses to detached breakwaters were obtained in the period from 1972 to 2013, of which the most appropriate images were chosen to be measured. In chapter 3, several types of data are validated with the other sources. To aid the research, the key parameters are established and their distribution is analysed.

Thirdly, in chapter 4 the predictive relationships of the shoreline changes are developed with the different accretion formations and the shore positions. The models start with the findings of the basic relationships of the shoreline changes and continue with the development of the relationships of the shoreline changes including the other parameters. The collective relationships of the shoreline changes are a combination of the total effects. The new relationships are developed to estimate the siltation of tombolo, salient and limited response; for the shoreline opposite the gap, for the up-drift and the down-drift. All these relationships are analysed for the goodness of fit (R-squared), the error of estimate and the correlation coefficients of the regression. Further on in this chapter, several existing models of the relationships are compared with the new basic relationships. However, there are no previous relationships to be compared with the complete relationships.

Fourthly, in chapter 5 the quantitative individual parameter effects on the shoreline changes are interpreted. The shoreline change functions relate to multiple parameters, therefore, the effect of each parameter needs to be analysed, while keeping the other parameters unchanged on the shoreline results. Comparison between the degree of the shoreline changes caused by the different parameters, thus, will show which parameters have more influence on the shoreline changes.

The findings of this research will contribute to a new understanding of the estimation of the detached breakwaters' behaviour on the shoreline. The new insight will also produce practical instructions when and where the shore will have accretion and erosion, including the main parameters with the most influence on the shore.

## SAMENVATTING

Een nauwkeurige voorspelling van veranderingen van de kustlijn achter kustparallelle golfbrekers is, met betrekking tot aanpassing aan de invloed op het milieu, nog steeds een uitdaging voor ontwerpers en beheerders van de kust. Dit onderzoek hoopt de ontbrekende kennis met betrekking tot de inschatting van de veranderingen van de kustlijn aan te vullen. Nieuwe en gegeneraliseerde verhoudingen van de veranderingen van de kustlijn in relatie tot kustparallelle golfbrekers zijn ontwikkeld, gebaseerd op verschillende parameters van constructie, fysieke omstandigheden en sediment eigenschappen van de prototypes. Deze gegeneraliseerde verhoudingen zijn bedoeld om nieuwe voorspellende mogelijkheden te creëren.

Allereerst wordt in hoofdstuk 2 de achtergrond van vrijstaande golfbrekers gepresenteerd, met als doel de specifieke problematiek te definiëren. Een overzicht wordt gegeven van de achtergrond van de hydrodynamica en sedimenttransport, met en zonder constructies, van de veranderingen in hydrodynamica en sediment transport in de zone van kustparallelle golfbrekers, om vervolgens de diverse voorspellingen van de kustlijnveranderingen te beoordelen. In hoofdstuk 2 worden eveneens de veranderingen van golven en stromingen gepresenteerd die tot morfologische veranderingen leiden rondom de golfbrekers. De verschillende posities in de zone van de golfbreker veranderen de morfologie van de kustlijn; zoals bijv. het middelpunt van de constructie, de kustlijn tegenover een gat, of een stroom-opwaartse en stroom-afwaartse positie. Verschillende methoden worden gebruikt om de respons van de kustlijn met behulp van numerieke, fysische en empirische modellen te onderzoeken, en om tot een oplossing van deze problematiek te komen. De bestaande modellen hebben echter een beperkte toepasbaarheid voor kustparallelle golfbrekers. Numerieke modellen zijn bijvoorbeeld afhankelijk van de nauwkeurigheid van de wiskundige beschrijving van belangrijke morfologische processen; fysische modellen zijn problematisch vanwege schaal-effecten in het laboratorium bij het gebruik sedimentschalen of lichtgewicht sediment materiaal; empirische modellen zijn onderworpen aan een te sterke vereenvoudiging en een beperkt toepassingsgebied van de relaties. Nieuwe eisen zijn dus nodig voor de schatting van de respons op de evenwichtstoestand van de kustlijn.

Ten tweede, wordt in hoofdstuk 3 de prototype-aanpak gebruikt ter onderbouwing van de ontwikkeling van de “Relatie-Modellen”. In totaal 93 projecten met 1144 constructies werden verzameld, inclusief constructieparameters, fysische randvoorwaarden, sediment eigenschappen en het resultaat van kustlijnmetingen. De informatie over de constructieparameters komt uit diverse bronnen, zoals vragenlijsten, projectrapporten, en uit een selectie van artikelen, tijdschriften en presentaties. De gegevens over diverse aspecten van de constructie werden verzameld, zoals lengte van golfbreker, afstand tot de kustlijn, breedte van opening, kruinhoogte, kruinbreedte, waterdiepte en oriëntatie van de constructie. De gegevens van fysische randvoorwaarden, met inbegrip van golf, stroming en getijde, zijn

afkomstig uit wetenschappelijke bronnen en online gegevens van organisaties. De gegevens over golven zijn verkregen via twee bronnen, namelijk de her-analyse van de wereldwijde atmosfeer- en oppervlakte voorwaarden, welke meer dan 45 jaar door het ‘European Centre for Medium-Range Weather Forecasts’ (ECMWF) zijn verzameld, en het model voor de schatting van de golven van windgebeurtenissen in het verleden (WIS). Stromingen waren het onderwerp van de waarnemingen van de ‘Ocean Surface Current Analyses – Real time’ (OSCAR); waarden van de getijslag werden uit verslagen van de projecten gehaald. Voor resultaten van de kustlijnmetingen werden luchtfoto's gebruikt om de omvang van de betrokken kust te identificeren en te meten; de beelden van de tijdreeksen van de respons van het strand op kustparallelle golfbrekers na de bouw werden verkregen in de periode van 1972 tot en met 2013 en hiervan werden de meest geschikte beelden gekozen voor meting. In hoofdstuk 3, worden verschillende soorten gegevens gevalideerd met de andere bronnen. Ter bevordering van het onderzoek, zijn de belangrijkste parameters nader gedefinieerd en is hun verdeling geanalyseerd.

In de derde plaats, in hoofdstuk 4 zijn de relaties van de wijzigingen van de kustlijn ontwikkeld aan de hand van de verschillende aanzandingsformaties en de positie van de kust. De modellen beginnen met de bevindingen van de fundamentele relaties van de veranderingen in de kustlijn en vervolgens met de ontwikkeling van deze relaties van de veranderingen met inbegrip van de andere parameters. Het totaal van relaties van de kustlijnveranderingen zijn het gevolg van een combinatie van gevolgen. De nieuwe relaties zijn ontwikkeld om de aanzanding van een tombolo, ‘salient,’ of geen van beide, in te schatten voor de kustlijn tegenover een gat, voor een stroom-opwaartse en een stroom-afwaartse positie. Al deze relaties worden onderzocht op ”goodness-of-fit” (R-kwadraat), foute inschattingen en correlatiecoëfficiënten van regressie. In dit hoofdstuk worden de verschillende bestaande modellen van de relaties vergeleken met de nieuwe basisrelaties. Er zijn echter geen voorafgaande relaties die vergeleken kunnen worden met de nieuwe overall-relaties.

Ten vierde, in hoofdstuk 5 worden de kwantitatieve gevolgen geïnterpreteerd van iedere afzonderlijke parameter op de veranderingen in de kustlijn. De functies van kustlijnverandering hebben betrekking op meerdere parameters, en daardoor moet het effect van elke parameter worden geanalyseerd, terwijl de andere parameters ongewijzigd blijven ten opzichte van de resultaten van de kustlijn. Vergelijking tussen de mate van de wijzigingen veroorzaakt door de verschillende parameters, zal aantonen welke parameters meer invloed hebben op de kustlijn en de veranderingen daarin.

De bevindingen van dit onderzoek zullen een bijdrage leveren aan een nieuw inzicht met betrekking tot de beoordeling van de invloed van kustparallelle golfbrekers op de kustlijn. De nieuwe inzichten zullen ook praktische instructies produceren waar en wanneer aanzanding en/of erosie aan de kust zal plaatsvinden, met inbegrip van inzicht in de parameters met de meeste invloed op de kustlijn.

# CHAPTER 1: INTRODUCTION

## 1.1 Background and problem statement

Since the 1960s nearshore detached breakwaters have increasingly been used in Japan, the United States and the Mediterranean. Nowadays, the nearshore breakwater structures are often considered an option for shore protection as part of coastal defence schemes. The main function of a detached break water is to reduce the incident wave energy on an embayment and, thereby, reduce the net sediment transport rate in the sheltered area. In this way, detached breakwaters promote the sediment deposition in the lee. In detail, the water areas behind the breakwater scheme induce complex circulation flows caused by the wave set-up, the wave-driven longshore- and tidal flows, leading to complex sediment transport patterns, which produce morphological changes in the vicinity of the structure, including sediment deposition in the lee, erosion/accretion in the gap, erosion/accretion at the up- and down-drift. Therefore, more accurate predictions of shoreline changes behind detached breakwaters are necessary for designers as well as for coastal managers for the adjustment of the environmental impact.

In previous studies, empirical methods, and physical and numerical models have investigated the morphological changes caused by detached breakwaters. Chasten et al. (1993) presented a review of the existing empirical methods to predict when siltation will form as a tombolo or a salient, and when a limited beach response can be expected. They concluded that the existing research has mostly investigated a geometrical layout of breakwater schemes creating the salient or tombolo. A physical model can observe the qualitative effects on a three-dimensional level and can observe the retention efficiency of structures. Ilic et al. (2005) commented on physical models as problematic for laboratory scale effects, by using sediment scale or lightweight sediment material, and, thus, not able to provide any accurate information

about the sediment transport rates and the sediment deposition speed, respectively. Although recently numerical models have been used as a leading method for beach nourishment and combined control structures design, the accuracy of the mathematic models of the important morphological processes is still limited. Therefore, when applying the previously discussed methods to the prototype, the empirical methods lack understanding of the shoreline changes in the vicinity of the breakwater opposite the gap, the up-drift and the down-drift; the physical models' prediction may be inaccurate to represent the actual morphological response and the long-term changes; the numerical models do not provide a high level of confidence.

In an attempt to bridge this gap, we will further improve the empirical relationships of the shoreline changes as a consequence of the detached breakwater scheme at all four positions of concern. The new relations are based on the data of the prototypes, including the primary geometrical parameters gathering the physical conditions and the equilibrium shoreline result measurements.

## **1.2 Objectives**

The aim of this research is to develop generalizations about the evaluation of the shoreline changes behind detached breakwaters from the assessment of the prototypes. Scientifically, this research is expected to fill the gaps of estimation of the sensitive positions on the shore of the breakwaters field. Therefore, the main objectives of this research of shoreline changes behind detached breakwaters are summarised below:

- To understand the background of coastal processes in an open coast and the occurring phenomena along a coast with structures, focusing on the geometric layout rather than the structural design of the emerged nearshore detached breakwaters;
- To synthesise the applicable existing methods of the evaluation of shoreline changes;
- To conduct a detailed analysis of the equilibrium shoreline parameters from the prototypes, in order to develop the general relationships of the effect of parameters on the result that detached breakwaters have on the behaviour of the shoreline;
- To produce practical instructions when the shore will have accretion and erosion, including the main parameters with the most influence on the shore behaviour.

## **1.3 Research questions**

As mentioned in the objectives, the outset of this research is intended, firstly, to identify the positions at the shoreline that are most affected by the breakwater scheme; secondly, to examine how many parameters possibly influence the shore at a specific position; thirdly, to develop generalizations on the empirical relationships between the influence parameters and the equilibrium shore parameters; and, fourthly, to quantify the effect of individual parameters on the shoreline changes.

On this basis, the following key research questions are formulated:

1. Where are the most sensitive positions on the equilibrium shoreline behind breakwaters?
2. Which parameters are involved in the shoreline behaviour?
3. What are relationships between variables and the shoreline response?
4. How do the individual variables influence the shoreline changes?

#### **1.4 Research methodology**

My research adopted an empirical relationship approach to estimate the shoreline changes. The methodology was divided into four steps: data collection, data measurement, developments and analysis.

Data collection was reviewed through the existing projects of detached breakwaters for shore protection, containing a range of conditions, such as geometrical layout, physical conditions and sediment properties. The structural layout parameters and sediment properties were collected from a variety of sources, such as inquiry questionnaires, data from project reports, and a selection of subject specific articles, journals, and papers. The information on physical conditions, such as waves, currents and tides, were retrieved from online scientific resources and organizations. To aid the research, the key parameters were constructed and their distribution was analysed.

Aerial images of the time-series observations were used for data measurement of post-construction beach responses to detached breakwaters. The image data were obtained during the inequitable period from 1972 to 2013. In order to make measurements, distinctions were made between the shoreline position, the placement of the structure and the water, using colours and appearances. During the measurements, several assumptions have been made to determine the magnitude of the affected shore.

However, as the previous studies have yet to establish the empirical relationships, these models were related to the simplicity of the parameters and the limitation of applicability. Therefore, development of the new models for shoreline changes prediction by using multiple variables formulae, which use an analysis software for regression, enable the application of generalizations.

The shoreline changes were affected by multiple parameters; then, the trends of the shore changes were separately analysed with each parameter, while keeping the other parameters unchanged. The resulting values of the shoreline changes were plotted in a sequence of changes for each particular parameter. Comparison between the degrees of the shoreline changes, caused by the different parameters, thus, will show which parameters have more influence on the shoreline response.

## **1.5 Scope of research**

The assessment was adapted for the emerged detached breakwaters used for shore protection with a permeable structure. The research focused on the investigation of the static equilibrium shoreline behind the structure, rather than on the structural design. The investigation was based on aerial image observations to expose morphological results. However, it cannot investigate morphological processes, but they were accepted from existing numerical and physical methods.

This research demonstrated the prediction models of plan shape of the long-term shoreline changes. It did not investigate beach response during individual storms, and recovery after storms and did not focus on the prediction of the bed morphology changes on the cross shore.

Several physical models have been applied to determine the effects of structures on the shoreline. Experimental results on the interaction between detached breakwaters and hydrodynamic fields in dominant waves were used to determine the limited morphological impacts on the vicinity shore of prototypes.

## **1.6 Outline of this research**

This dissertation focus is, the research on the development of generalizations about the estimation of shoreline changes behind detached breakwaters, and the main scientific results to be used to have a better understanding of the workings of a breakwater scheme. The description of this research is organised in this thesis as follows:

Chapter 2 contains a summary of the literature review of the research on hydrodynamics and sediment transport in the open coast and in the coastal areas with detached breakwaters; followed by a review on the existing methods for shoreline response prediction.

Chapter 3 presents the collection of data, consisting of the primary parameters and the resulting parameters, including the geometrical layout of breakwater schemes, wave characteristics, tidal range and sediment properties.

Chapter 4 contains an analysis of structure parameters, physical conditions, sediment properties data and the measurement of shoreline changes data. The aim of this analysis is to develop the relationships related to the shoreline response.

Chapter 5 contains an analysis of the impact parameters on the shoreline changes. The goal of this analysis is to carry out the main trends and the important parameters to describe the shoreline changes in the specific positions under varying values of each effect parameter.

Chapter 6 presents the overall conclusions and recommendations.

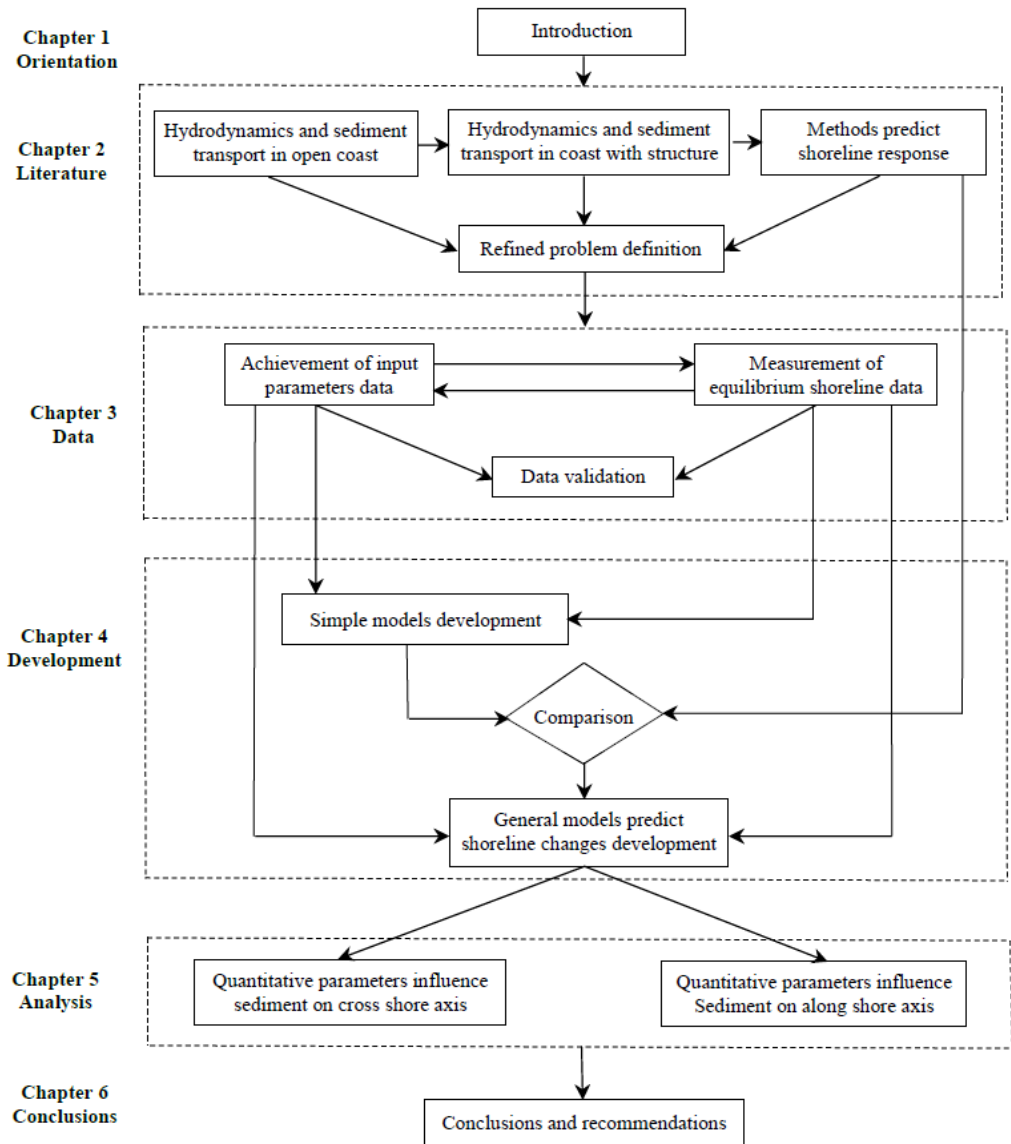


Figure 1.1: Schematic of this research





# CHAPTER 2: LITERATURE REVIEW OF EMERGED DETACHED BREAKWATERS OF SHORE PROTECTION

## 2.1 Introduction

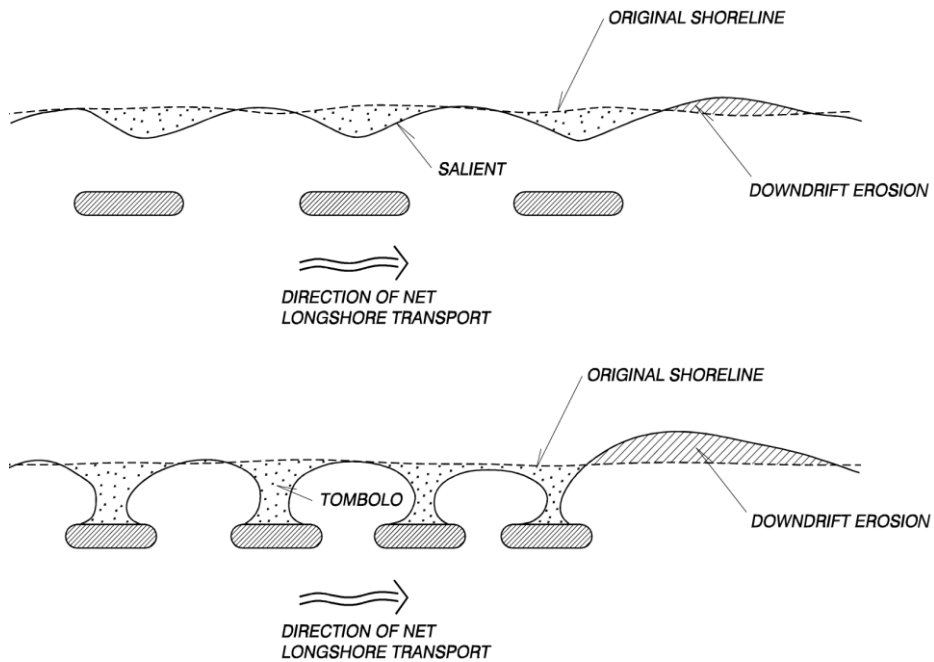
Detached breakwaters have been used more and more as coastline protection since the 1960s. Especially in Japan, the United States and the Mediterranean many of these breakwaters were built. In general, detached breakwater structures are constructed parallel to the shore and can be constructed as a single structure or in series. Construction a single structure is used to protect a narrow project area, whereas a multiple structure system is designed to protect a long shoreline. A multiple structure system consists of two or more structures isolated by gaps. See Figure 2.1 for a visual explanation.

The main purpose of detached breakwaters is the reduction of the amount of wave energy in an embayment by the reflection, the dissipation and the diffraction of incoming waves. The function is similar to that of a natural reef, an offshore bar or a nearshore island. Wave energy reduction leads to a decrease of transport capacity and sediment may be deposited in the basin area behind the structure. The siltation can form a salient or a tombolo, mainly based on the amount of wave energy transmitted into the sheltered water area of the breakwater and the sediment supply.

Although detached breakwaters can help to prevent beach erosion and can enable continued sediment movement through the project area by longshore transport, there are several disadvantages such as the limited design guidance, high construction cost, complicated hydrodynamic phenomena, a simplicity prediction of sediment accretion, a limited ability of

sediment state of the opposite gaps, and the up-and the downstream phenomena.

a, Plan view



b, Cross section

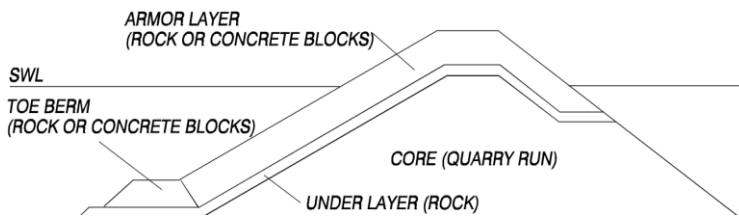


Figure 2.1: Detached breakwaters (Coastal Engineering Manual, 2002)

## 2.2 Coastal processes without detached breakwaters

Before understanding how a breakwater works, it is necessary to recognize coastal processes on the natural beach. Therein, tides and waves are two of the most important hydraulic aspects. In the sections below, tides and waves will be briefly discussed to understand their effects as well as sediment transport in the surf zone.

### 2.2.1 Waves in the nearshore

Wind waves are generated by the wind blowing over the water surface. In deep water where the ratio of water depth ( $h$ ) and wavelength ( $L_0$ ) is bigger than 0.5, it is generally assumed that there is no effect of the seabed on the waves. However, in shallow water waves may be subject to shoaling, refraction and the breaking of waves. In the following section the phenomena will be discussed.

#### a. Refraction and shoaling wave

When waves propagate toward the coastline, the water depth reduction leads to the wavelength decreasing and, refraction and shoaling waves will occur. Refraction can only occur if the waves approach underwater contours at an angle, while shoaling will occur when waves approach the contours perpendicular. A convenient formula of wave height that expresses both effects of wave shoaling and refraction is

$$H = H_0 K_s K_r \quad (2.1)$$

Where:  $H_0$  is the deep water wave height,  $K_s$  is the shoaling coefficient.

$$K_s = \sqrt{\frac{c_{g0}}{c_g}} \quad (2.2)$$

and  $K_r$  is the refraction coefficient, which for straight and parallel shoreline contours can be expressed in terms of the wave angles as follows:

$$K_r = \sqrt{\frac{\cos \alpha_0}{\cos \alpha}} \quad (2.3)$$

Given the deep water wave height  $H_0$ , the group velocity  $C_{g0}$ , and the wave angle  $\alpha_0$ .

#### b. Breaking wave

Wave breaking is one of the most important subjects to coastal engineers because it highly influences both the sediment behaviour on beaches and the magnitudes of the forces on coastal structures. Breaking is difficult to describe mathematically because it is the most complicated wave phenomenon. Unfortunately, at present, only limited properties of breaking waves can be predicted accurately.

Waves may break in several different ways: spilling, plunging, surging, and collapsing. Spilling breakers are usually found along flat beaches. Spilling is very small reflection of wave energy back towards the sea. Plunging breakers are forms that are often found on mid slope beaches. Some energy of plunging waves is reflected back to sea and some is transmitted to the coast. Surging breakers occur along steep coasts for relative long swell waves. Energy of the surging breaker zone is more than half reflected back into deeper water. A collapsing breaker is a breaker between a plunging and a surging breaker.

In general, the maximum wave height at any particular location, depends on the wavelength,  $L$ , the water depth,  $h$ , and the slope of seabed,  $\tan\beta$ . Based on Stokes wave theory, Miche (1944) gave the limiting wave steepness as:

$$\left[\frac{H}{L}\right]_{max} = 0.142 \tanh\left(\frac{2\pi h}{L}\right) \quad (2.4)$$

However, in the case of deep water ( $h/L \geq 0.5$ ) only the wavelength is important and breaking occurs when the wave steepness  $H/L$  is approximately 0.142. In shallow water depths, the breaking wave is relative to both water depth and wavelength; the conditions are  $h/L \leq 0.05$ , and the maximum wave height  $H_{max}/h \approx 0.88$ , but **the largest number of waves are breaking when  $H_s/h \approx 0.4-0.5$ .**

### 2.2.2 Currents in the nearshore

The current in the surf zone is a combination of currents driven by breaking waves, the tidal current, the wind-driven current, and the oscillatory flows due to wind waves and infra-gravity waves.

#### a. Longshore current

When oblique incoming waves are breaking, the radiation shear stress component shoreward decreases as a result of which a longshore current can develop. This longshore current can only occur there, where energy dissipation happens, this means in the surf zone. The wave height ( $H$ ) and the oblique wave angle ( $\alpha$ ) are the main effect on the strength of the longshore current. If they decrease, the longshore current decreases as well. (See Eq. 2.5)

$$S_{xy} = nE \sin \alpha \cos \alpha = \frac{n}{8} \rho g H^2 \sin \alpha \cos \alpha \quad (2.5)$$

Where:  $n$  is the ratio of wave group speed and phase speed.

#### b. Cross-shore current

A cross-shore current is not constant over depth. The mass transport carried shoreward due to waves is concentrated between the wave trough and the crest elevations, because the beach forms a barrier for mass flux landward movement and in a balanced situation the mean directed flow onshore should equal to zero. Therefore, to compensate the wave-induced mass movement in the upper layers, an opposite flow or undertow follows in the lower layers. The undertow current may be strong close to the bottom. The vertical profile of the undertow is determined as a balance between radiation stresses, the pressure gradient from the sloping mean water surface and vertical mixing.

#### c. Rip current

The nearshore circulation system happening at the beach often includes non-uniform longshore currents, rip currents, and cross-shore flows. Rip currents are narrow jets of water

issuing from the inner surf zone out through the breaker line that carries sand offshore. Rip currents on a long straight beach have been observed from one horizon to the other with roughly a uniform spacing, with approximately wavelength. Figure 2.2 shows rip currents and feeder currents.

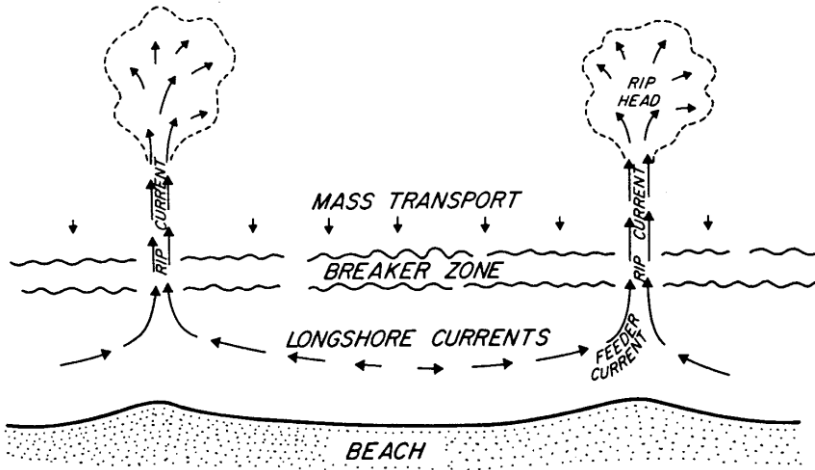


Figure 2.2: Nearshore circulation system showing the rip currents and the feeder currents (modified from Shepard and Inman (1951)).

### 2.2.3 Sediment transport in the surf zone

#### a. Longshore transport

Under the action of the waves and the longshore currents, the sediment moved along a shoreline. In general, three modes of sediment transport are recognized: bed load transport, suspended load and swash load. In the bed load mode, the particles are rolled, shifted or have a small jumps over in the seabed. In the suspended load mode, the particles are lifted up from the seabed within the fluid column and moved in suspension by currents. And in the swash load mode, the particles are moved on the surface of the beach by the swash. It is difficult to fully understand which of these predominant motions for various wave conditions, sediment types, and the profile of locations or even whether it is important to identify the different mechanisms. Several of sediment transport formulations of these modes are treated below:

*Energy flux model* : Inman and Bagnold (1963) showed that the total amount of material moved along the shoreline was related to the amount of energy available in the waves arriving at the shoreline:

$$Q = \frac{K P_I}{(\rho_s - \rho) g (1 - p)} \quad (2.6)$$

$$F \cos \theta \sin \theta \equiv P_l = E C_g \sin \theta \cos \theta = \frac{1}{16} \rho g H^2 C_g \sin 2\theta \quad (2.7)$$

Where,  $\theta$  : is the angle the wave ray makes with the onshore;

H : wave height;

E : the energy per unit surface area;

$C_g$  : the group velocity;

$F = E C_g$ : the energy flux per unit width;

K : the dimensionless parameter ( K = 0.77 by Komar and Inman (1970); K = 0.2 to 0.22 by Kraus et al. (1982); K = 1.23 by Dean et al. (1982)).

g : gravity;

$\rho$  : mass density of the water;

$\rho_s$  : mass density of the sediment grains;

p : in-place sediment porosity (p= 0.4).

*Energetics model:* Bagnold (1963) created a model for sediment transport based on the amount of the flow energy uses to transport of the sediment. Inman and Bagnold (1963) then adapted the theory for oscillatory flow within the surf zone. They demonstrated that the final expression for the dynamic transport rate for the wave-induced sediment transport is:

$$I_c = K E C_g \frac{U_c}{U} \quad (2.8)$$

Where, U : the near bed velocity of the fluid;

$U_c$  : mean direction current.

*Suspended transport model:* Dean (1973) developed the model of the suspended load for sediment transport within the surf zone. As in the suspended sediment model, Inman and Bagnold (1963) supposed that the falling sand grains dissipate a part of the available energy flux into the surf zone. They expressed that the dissipation  $D$  for a single sand grain is due to the loss of potential energy by the particle and is related to the submerged weight of the particle and the fall velocity  $\omega$ :

$$D = (\rho_s - \rho) g \frac{\pi d^3}{6} \omega \quad (2.9)$$

where the grain is roughly spherical with diameter  $d$ , as it is assumed.

Dean calculated the number of suspended grains per unit length in the surf zone and then

obtained the final longshore current formula is:

$$Q = CP_1 \quad (2.10)$$

$$C = 34.3 \times 10^3 \epsilon \frac{\sqrt{H_b/\kappa} \tan \beta \cos \theta_b}{C_f \sqrt{g} (\rho_s - \rho) (1-p) \omega} \quad (2.11)$$

*Traction models:* Another class of sediment transport models outside the surf zone has been created, which is based on the information about traction models created for open channel flow. An important variable is the Shields parameter. The sediment will move when its critical value is lower than the bottom shear stress.

Madsen and Grant (1976) calculated a mean transport rate over half a wave period for the time that the oscillatory flow in one direction starts to the time when it stops to change direction, which is

$$\bar{\phi} = \frac{2}{T} \int_{t_1}^{T/2 - t_2} 40\psi(t)^3 dt \quad (2.12)$$

Where:  $t_1$  is the time at which the beginning motion criterion is exceeded and  $(T/2 - t_2)$  is the time when the transport finishes.

*Other relationship transport:* Kamphuis (1991) showed that the results of the sediment transport rate is a function of wave, fluid, sediment, and beach profile based on three-dimensional hydraulic model experiments. The Kamphuis relationship is:

$$Q = 2.27H_b^2 T_p^{1.5} \tan \alpha_b^{0.75} d^{-0.25} \sin^{0.6}(2\theta_b) \quad (2.13)$$

In which  $Q$  is the total longshore sediment in kg/s,  $\alpha_b$  is the beach slope of the break point seaward, and all other variables expressed in metric units. In this equation, the longshore sediment is related to the breaking wave characteristics, the beach slope and the median sediment size  $d$ .

#### b. Cross-shore transport

The breaking of oblique in coming waves induce a longshore current, which is the main cause of the longshore transport. However, the action of waves and the return flow (or undertow) lead to the sediment transport in the cross-shore. Various models of the cross-shore will be shown below.

*Fall time model :* Dean (1973) developed a model for cross-shore transport in the surf zone, in which he supposed that breaking waves suspend the sand grains in the water column and the eventual settling of sand to the bottom. Dean showed that the time that it will take for the sand to fall back to the bottom is:  $t = \frac{S}{\omega}$ , in which  $S = \beta H_b$  is an average distance wave breaking in the surf zone lifting sand from the bottom up into the water column,  $\omega$  is the fall



velocity of the sand,  $H_b$  is the breaking wave height and  $\beta$  is a constant. If the fall time of a sand grain is smaller than  $T/2$ , where  $T$  is the wave period, the sand grain should move shoreward. Alternatively, if the fall time is bigger the  $T/2$ , the sand grain will be carried shoreward.

*Simple cross-shore transport model* : Moore (1982) proposed a simple cross-shore model first and later Kriebel (1983) and Kriebel and Dean (1985) improved this model. The initial definition is that, if sediment across the profile is a uniform size and in an equilibrium beach, the energy dissipation rate per unit volume is constant, then they supposed to obtain the  $Ay^{2/3}$  profile. If the beach profile is different from this equilibrium state, then the energy dissipation rate is different from the constant value too. It is assumed that the amount of sediment moved will depend on the difference of the dissipation energy of the two states. Therefore, the volumetric cross-shore sediment transport rate per unit width in the seaward direction is

$$q_s = K(D - D_*) \quad (2.14)$$

In which,  $K$  is a new dimensional constant;

The equilibrium energy dissipation per unit volume  $D^*$  determined by the profile scale factor  $A$ , for:

$$A = \left( \frac{24D_*}{5\rho g \kappa^2 \sqrt{g}} \right)^{\frac{2}{3}} \quad (2.15)$$

$D$  is the dissipation per unit volume of the changed profile:

$$D = \frac{5}{16} \rho g \kappa^2 \sqrt{gh} \frac{dh}{dy} \quad (2.16)$$

*Energetics model* : Stive (1986) and Roelvink and Stive (1989) investigated the Bailard's formula sediment transport by cross-shore flows.

$$\overline{i(y)} = \rho C_f \frac{\epsilon_b}{\cos\beta \tan\phi} \left( \overline{|u|^2 u} - \frac{\tan\beta}{\tan\phi} \overline{|u|^3 j} \right) + \rho C_f \frac{\epsilon_s}{\omega} \left( \overline{|u|^2 u} \right) - \frac{\epsilon_s}{\omega} \tan\beta \overline{|u|^5 j} \quad (2.17)$$

Stive successfully investigated the evolution of offshore shoals that were a result of wave activity. Roelvink and Stive investigated Bailard's formula coupled with a conservation of sand formula  $\frac{\partial h}{\partial t} = \frac{\partial q_s}{\partial y}$  to model the behaviour of beach profiles. They used a model of a random wave breaking (Battjes and Janssen, 1978) and combined nonlinear waves, groups of waves, undertow, and wave-induced turbulence. They came to the conclusion that their model predicted the wave hydrodynamics well, however, the Bailard formulation might have been insufficient for locations outside the surf zone, because of the strong vertical variation of the flow. They were able to create sandbars with their model, but not in the same regions as the experiment results.

*Ripple model:* The bed of an offshore breaker line is often rippled, and the ripples influence the sediment transport in this location. As the wave-induced motion increases over a ripple, the flow separates from the crest of the ripple and forms a vortex in the trough before the next ripple. This vortex captures and carries sediment.

Dingler and Inman (1976) and Jette (1997) found that the mobility number is significant to the dynamics of ripples. The mobility number  $\Psi_m$  is the Shields parameter with the near-bottom orbital velocity replacing the shear velocity as

$$\Psi_m = \frac{(A\sigma)^2}{gd(s-1)} \quad (2.18)$$

where  $A$  is one-half the near-bottom water particle excursion, and  $\sigma$  is the angular frequency of the wave.

If  $\Psi_m > 150$ , ripples tend to be obliterated;  $50 < \Psi_m < 100$ , ripples can form rapidly;  $\Psi_m < 50$ , ripples can form slowly.

### 2.3 Coastal impacts of detached breakwaters

As mentioned in the introduction above, the main function of detached breakwaters is to reduce the amount of wave energy in sheltered areas behind the breakwaters. Behind breakwaters, actually, complicated mechanism of waves, currents, sediment transport, and morphology do occur. In the following section a detailed description of this process will be given.

#### 2.3.1 Waves change

When deep water waves propagate toward a shoreline they undergo refraction and shoaling processes. Depending on the location of the breakwaters, wave breaking may have started. When the waves run toward and into the breakwaters, wave energy is dissipated by wave breaking on the breakwaters. At the breakwater, a part of the wave energy will be reflected, another part will be dissipated on the surface of the breakwater, and the remaining part will be transmitted by overtopping or by waves permeated through the structure. At the head of the breakwater, waves turn into diffraction waves around the tips. See Figure 2.3.

In the lee - the water area behind the breakwater seems to be sheltered, but waves are still existing. The diffraction waves and transmitted waves will continue to propagate forward towards the shoreline. On the other hand, the refraction waves that do not meet the breakwater can reach the coast too. Hence, in the lee, all waves will be mixed: transmitted waves, diffraction waves, and refraction waves. Consequently, new waves set up will reduce significantly in the sheltered water area.

The fundamental function of detached breakwaters is a reduction of the wave climate behind

them. The magnitude of the modified wave depends on a large number of parameters. The most important parameters are: wave height, wave period, water depth at breakwater, gap width between two breakwaters and the structure's porosity and crest level of the breakwaters.

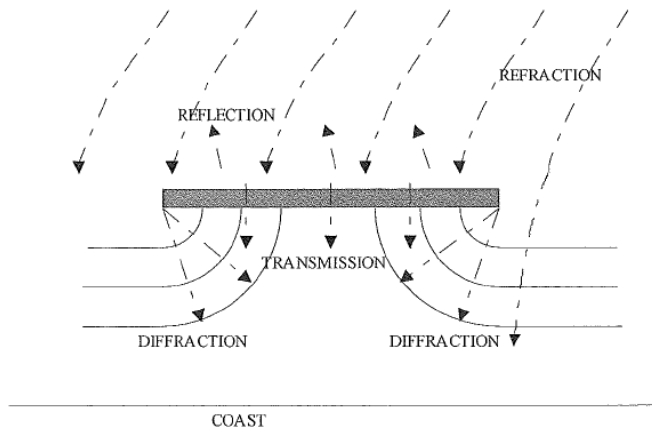


Figure 2.3: Waves near a single detached breakwater(CUR 97-2A, 1997)

### 2.3.2 Currents change

Detached breakwaters affect both the longshore current and the cross-shore current:

*a. Longshore currents:* The longshore currents are changed in both situations of a detached breakwater, just after a construction and after a state of equilibrium compared to the natural beach. On an open coast beach, the longshore currents are generated by oblique incoming waves when approaching the shoreline, and currents. The breakwater's placement interrupts the natural currents flow. The reduced wave height results in longshore currents by slowing or stopping when they move into the basin area. Additionally, waves setup in the lee is a combination of diffraction waves, transmitted waves and partly incident refraction waves, thus the dominant wave direction behind breakwaters is different from the wave direction without breakwaters. In the state of an equilibrium shoreline, sand bars are created and are connecting with the shore. Herein, longshore currents are also driven by sand bars like the working of groins. The currents must be further than the open coast, as well as the sand bars lengths. Moreover, rip currents appear at the downstream of structures. However, in both situations of the current, construction brings about advantages and disadvantages in terms of shore protection.

*b. Circulation currents :* The wave setup in the embayment area behind the segmented breakwaters will be reduced, but the wave setup just opposite the gap still maintains the same refraction wave. These two wave zones have a different wave gradient, therefore circulation currents can develop. Another flow of water behind the breakwaters is generated by transmitting and (or) overtopping. In the sheltered water area, a large volume of water can pull

up behind breakwaters. Without breakwaters a return current compensates this shoreward movement of water. But the breakwaters prevent the development of an undertow. Instead, the water will flow laterally towards the tips of the breakwater and forms a concentrated rip current (see Figure 2.4).

c. *Rip current* : When structures are placed in a segmented breakwaters there are gaps in between, and each gap causes a net seaward flow of water, called a rip current. This current can have a large velocity because the flow is concentrated. The magnitude of a rip current (return current) through the gap can be decreased by increasing the gap width, and (or) increasing the breakwater permeability. Other effects of rip current size are relative to wave height, length, and wave period; breakwater freeboard, length, and distance offshore; water depth, and shore attachment. If the velocity of a rip current is very strong, then there will be a problem of scour around the structures.

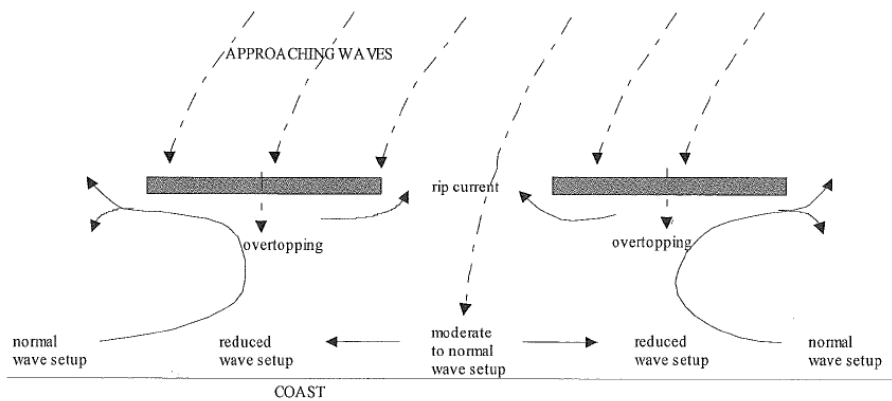


Figure 2.4: Wave induced currents around segmented detached breakwaters  
(CUR 97-2A, 1997)

### 2.3.3 Change of sediment transport in the surf zone

#### a. Longshore transport change

The area shoreward from the detached breakwater may be described as the shadow zone. Sediment transport along the coastline is a function of the activity of waves and currents, as well as sediment supply. Parallel structures have the ability to change all of these parameters and, therefore, sediment transport as well. Perhaps of more fundamental importance is that the construction of these structures prevents waves breaking on the beach; this may, as a result, hinder the generation of longshore currents, and may cause them to be reduced or even to stop. At the heads of a structure there is a generation of two diffractions and of which the waves move to the centre of breakwater. This, in turn, will impinge on the wave's ability to carry sediment and to mobilise beach sediment for longshore transport. The building of sediment

from the coast also represents a modification to longshore current patterns. A major sediment deposit, which develops behind such structures will, prevent currents from taking their original path and may produce several repercussions. First, the salient accretion may act in a similar way as a groin, actually forming a physical barrier to longshore sediment movement. While this will serve to accelerate the build-up of sediment on the up-drift side of the salient, it might trigger increased erosion at the opposite gaps and the down-drift end.

*b, Cross-shore transport change*

Placement of a detached breakwater can reduce offshore transport by presenting a physical barrier to offshore transport and promoting sediment accumulation close to the centre. In the lee, the diffraction waves approach the coastline at an angle, as a result of the wave run-up is oblique on the beach slope. While wave run-down is driven by gravity then wave run-down seems to be perpendicular to shoreline. The motions of wave run-up and wave run-down carry the sediment particles upward and backward to the shoreline as a zigzag route. If an incidental wave is orthogonal, the net sediment transports directly to centre of the breakwater (see Figure 2.5). In case of breakwaters that are constructed in a segmented way, they will have rip currents in the gaps between them. This current can carry a part of sediment from the lee seaward.

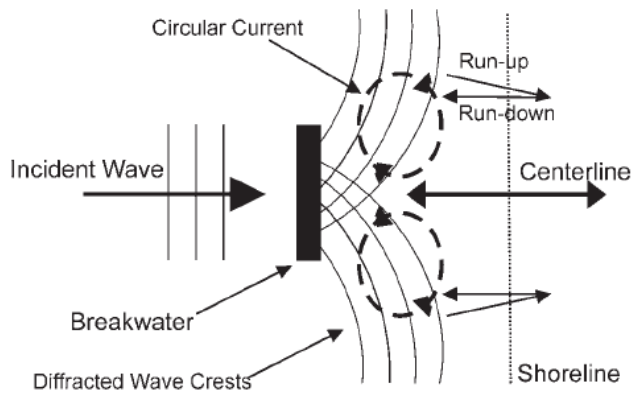


*Figure 2.5: Zigzag movement of sediment (Adapted from Ming and Chiew (2000))*

*2.3.4 Shoreline erosion impact*

When detached breakwaters are placed, in one part of the shoreline there will be a development of accumulation, some other parts may suffer erosion. Chasten et al. (1993) concluded from several observations on the shore opposite the gap that there might erosion, and that there can be erosion at the shore down-drift of the structures. However, the impact on the shore at the up-drift is unclear.

The shoreline opposite the gaps still attracted directly by wave refraction, followed by a stirring up of the sediment, while rip currents and circulation currents appearing in the lee, lead

to sediment stirring and moving offshore or to an adjacent place. The moving of sediment might lead to shore erosion.

Unprotected shorelines at the down-drift are continuously impacted by waves and currents. Another aspect, is that the longshore sediment supply is reduced when sand transport is trapped in the sheltered area. As a consequence, the net sediment at the down-drift location may be under zero, hence erosion may occur there too.

The unprotected shore at the up-drift of structures is still the under attack of normal refraction waves, however, the waves set up behind the breakwater is gradually reduced when it is closer the siltation. Two areas have different wave gradient, leads to turbulence develop. Hence, the shore at the up-drift has to changed.

Usually the shoreline erosion processes rapidly at the period just post-construction and then reduces gradually. This effect may cause harm to the adjacent sand beach by erosion or to the scour holes around structures nearby.

#### *2.3.5 Erosion around structure*

Breakwaters are constructed in a marine environment, where the presence of the structure will change the flow pattern in its immediate neighbourhood, resulting in one or more of the following phenomena: the contraction of flow; the formation of a horseshoe vortex in front of the structure; the formation of lee-wake vortices (with or without vortex shedding) behind the structure; the generation of turbulence; the occurrence of reflection and diffraction of waves; the occurrence of wave breaking; the creation of wave overtopping, and the pressure differentials in the soil that may produce “quick” condition/liquefaction, allowing material to be carried off by currents. These changes usually cause an increase in the local sediment transport capacity and thus lead to scour.

#### *2.3.6 Other impacts*

There are still several negative impacts when breakwaters are constructed, such as less safety, an interrupted view, and seaweed trapping. Swimmers may feel tempted to swim in the basin area in connection with detached breakwaters, but the circulation currents and rip currents can be dangerous. Detached breakwaters are normally built higher than mean sea level, which means that the visual impact can be undesirable. When segmented breakwaters are built with too small gaps, the water exchange in the basin between the breakwaters may be poor, leading to floating objects that are trapped.

### **2.4 Shoreline response prediction methods**

To understand the behaviour of detached breakwaters on the shoreline tools are needed. In the case of earlier structures, theory was used in the effort to explain. But theoretical approaches alone cannot guarantee that the hydrodynamic circumstances are fully understood.

Since the 1950s, small scale laboratory models have been exploited. Numerical models were booming in the 1990s, when computers were reasonably fast for that time. Another method is the empirical method, in which the current breakwaters practice is preferred to apply the data of experiments and prototypes to understand its results.

Hanson and Kraus (1990) indicated that in general there are at least fourteen parameters, including breakwater parameters, hydraulic conditions, and sediment properties which control the shoreline response of a sandy beach:

- *Breakwater parameters:* Length of structure ( $L_B$ ); distance from structure to the original shoreline ( $X_B$ ); gap width between structures ( $G_B$ ); structure transmissivity ( $K_T$ ); and orientation of structure to the original shore ( $\theta_B$ ).
- *Hydraulic conditions:* Wave characteristics and water level
  - Waves characteristics: Wave height ( $H_s$ ); wave period ( $T$ ); predominant wave angle ( $\alpha$ ); standard deviation of wave height ( $\sigma_H$ ); standard deviation of wave angle ( $\sigma_\alpha$ ); and standard deviation of period ( $\sigma_T$ ).
  - Water level: Water depth at structure ( $h_B$ ); and tidal range ( $h_{\text{tide}}$ ).
- *Sediment properties:* Sand median size ( $D_{50}$ ).

These parameters probably have an influence on an equilibrium coastline, however, some of them have been taken into account in the difference methods of shoreline prediction. In the following section a brief summary of the methods of evaluating shoreline response behind detached breakwater(s) will be given. The overview of the several methods before 1995 is partly used as presented by Birben et al. (2007).

#### *2.4.1 Physical model*

Since the 1950s, numerous scientists conducted research on physical models of detached breakwaters in the laboratory. This method endeavours to reproduce correctly the prototype conditions, such as the geometric, kinematic and dynamic. However, a physical model is seldom possible for complete similarity. Usually, several conditions, such as gravity waves, currents, surface tension, bottom friction, sediment motion, etc., are similar to attain. The problem of a physical model is distorted of the geometric scale and the sediment scale or by the lightweight sediment material. The previous experiments mostly focused on the interaction between structures and the shoreline under particular conditions. It seemed that the authors were concerned with tombolo or salient accretion, rather than erosion. Some of these authors are listed below.

- Shinohara and Tsubaki (1966) conducted a set-up experiment of a single detached breakwater in a rectangular water tank of 25 meter in length, 5 meter in width and 0.25 meter in depth. The non-cohesive sediment was used in the tests of 0.3 mm in the average

diameter of sand. They found the amount of sand deposits within the sheltered water area by breakwater and the sand movement at the sandy beach through the progress of beach deformation up to the accomplishment of an equilibrium profile with two kinds of wave steepness,  $S_0 = 0.0192$  for normal waves and  $S_0 = 0.0461$  for storm waves. They supposed that the amount of sand entrapment was a function of breakwater's geometrical layout parameters and wave properties, as

$$\frac{Q}{L_B X_B} = f\left(S_0, \frac{L_B}{L_0}, \frac{X_B}{L_B}, \frac{h_B}{L_0}\right) \quad (2.19)$$

Where,  $L_B$ : breakwater length;  $X_B$ : distance from original shoreline to breakwater;  $h_B$ : depth at structure;  $H_0, L_0$ : deep water wave height and wavelength.

- Rosen and Vajda (1982) made observations on small scale moveable bed models and measured the sand deposition parameters behind the breakwater. Then, they found that the relation among the equilibrium state factors based on the hypotheses are:

When salient formation :

$$\frac{S}{X_B} = \Phi_1\left(\frac{L_B}{X_B}, \frac{X_{br}}{X_B}, \frac{H_0}{V_f T}, \frac{H_0}{L_0}\right) \quad (2.20)$$

When tombolo formation:

$$\frac{L_B - Y_T}{2X_B} = \Phi_2\left(\frac{L_B}{X_B}, \frac{H_0}{V_f T}, \frac{H_0}{L_0}\right) \quad (2.21)$$

$$\frac{A_T}{X_B L_B} = \Phi_3\left(\frac{L_B}{X_B}, \frac{H_0}{V_f T}, \frac{H_0}{L_0}\right) \quad (2.22)$$

$$\frac{Q_b}{L_B X_B^2 \tan \beta} = \Phi_4\left(\frac{L_B}{X_B}, \frac{H_0}{V_f T}, \frac{H_0}{L_0}\right) \quad (2.23)$$

Where :

$L_B$  : the length of breakwater;

$X_B$  : the breakwater's distance from the initial shoreline;

$X_{br}$  : the breaker line's distance from the initial shoreline;

$H_0, L_0$  : deep water wave height;

$T$  : wave period;

$V_f$  : fall velocity;

$S$  : the distance from the land spit at its apex measured from the original shoreline;



$Y_T$  : the attachment width at the breakwater;

$A_T$  : the accreted sand area;

$Q_b$  : the total volume of sand trapped in the protected area;

$\beta$  : local bottom slope.

A series of eighteen moveable bed tests were conducted with varying deep-water wave steepness ( $H_0/L_0 = 0.015$ ;  $0.025$ ; and  $0.040$ ), different breakwater lengths ( $X_B = 1.0$ ;  $2.0$ ;  $3.0$  meters), three distances of the breakwater to the shoreline ( $L_B = 0.5$ ;  $1.0$ ; and  $2.0$  meters), with bed slope ( $\beta = 1/25$ ;  $1/30$ ; and  $1/40$ ) and beach slope ( $1/30$ ;  $1/20$ ; and  $1/10$ ), respectively. The artificial lightweight coarse sand of  $0.64\text{mm}$  in the average diameter size was used in these experiments. From the results of the experiments, they drew the conclusion that the sand deposit in the sheltered area could be well represented by the value of  $X_B$ ,  $L_B$ ,  $L_B/X_B$ , and  $H_0/L_0$ .

- Suh and Dalrymple (1987) tested on a model for both single and multiple breakwaters in a spiral wave basin to investigate the effects of breakwaters' geometric parameters on the changes of morphologic in the adjacent area. The test results were compared with previous experimental studies reported by others and with detached breakwaters in the field. All the horizontal lengths dimensionless ratios ( $X_b^* = \frac{X_b}{X_B}$ ;  $L_B^* = \frac{L_B}{X_B}$ ; and  $G_B^* = \frac{G_B}{X_B}$ ) were important with respect to the offshore distance of the breakwater from the original shoreline ( $X_B$ ). In which  $X_b$ ,  $L_B$ , and  $G_B$  were the surf zone width, the breakwater length, and the gap width between two breakwaters, respectively. They concluded that, for a single detached breakwater, the  $L_B^*$  parameter is the most important of sand accumulation, for multiple detached breakwaters, the ratio  $G_B^*/L_B^{*2}$  is the effectiveness of sand accumulation.
- Wen-Juinn and Ching-Ton (1995) showed based on laboratory results the following relationships between  $Q_b$  and  $X_B/L_B$ :

$$\frac{Q_b}{H_0^2 G_B} = 28.46 \left(\frac{X_B}{L_B}\right)^{3.67} \exp\left(-\left(\frac{X_B}{L_B}\right)^{2.1}\right) \quad (2.24)$$

$$\frac{Q_b}{X_B L_B h_B} = 1.13 \left(\frac{X_B}{L_B}\right)^{0.6} \exp\left(-\left(\frac{X_B}{L_B}\right)^{1.6}\right) \quad (2.25)$$

where  $Q_b$  is the amount of sand deposition in the lee,  $X_B$  is the distance of the breakwater from the shoreline,  $L_B$  is the breakwater length, and  $G_B$  is the gap between breakwaters,  $h_B$  is the water depth at breakwater.

- Ming and Chiew (2000) created experiments to study the shoreline changes as result of a single detached breakwater under the influence of pure wave action. They investigated

breakwater length ( $L_B$ ), and its distance from the initial shoreline ( $X_B$ ). The results of experiment showed the relation that:

$$\frac{Q_b}{X_B^2} = -0.384 + 0.043 \frac{X_B}{L_B} + 0.711 \frac{L_B}{X_B} \quad (2.26)$$

They drew the following conclusions :

- The size of salient (S) increases with  $L_B$ , but decreases with  $X_B$ ;
  - The sand deposited area of salient ( $Q_b$ ) increases with both  $L_B$  and  $X_B$  for  $X_B \leq L_B$ , but  $Q_b$  decreases when  $X_B > L_B$ ;
  - The width of the tombolo is directly related to  $L_B$  and inversely proportional to  $X_B$ .
- Several physical models for the projects were tested in the United States (Chasten et al., 1993), Japan, and Israel (Fried, 1976). The projects in the US, namely Presque Isle (Pennsylvania), Lakeview Park (Ohio), Oceanside Beach, and Imperial Beach (California), were conducted in the laboratory facilities at WES (Waterways Experiment Station, Vicksburg, Mississippi) from 1978 to 1983. The Tel Aviv, Israel breakwater project was tested in 1971 and 1972. The models were performed in a movable-bed facility. Physical model results have been used to validate results from the previously described numerical simulations. The model's scale for coastal applications typically ranged from 1:20 to 1:100, and in some cases near full-scale modeling or tracer studies were used to reproduce sediment movement observed at the actual site location. In these physical models the aspects of geometric, kinematic and dynamic similarity were reproduced with conditions of the prototype. However, **the models seldom succeeded to achieve of complete similarity**. Therefore, only several important physical conditions were the focus such as gravity waves, water currents, friction, surface tension, and sediment motion.

#### 2.4.2 Numerical model

Numerical models of beach change use sediment transport relationships and conservation of volume to simulate beach response to various driving forces (e.g., waves, currents, and water levels). There are two types of well-tested beach change models: short-term (hours to days) storm-induced profile predictions, and long-term (months to decades) shoreline response models.

Correct application of a storm-induced beach profile change model requires the assumption that longshore transport is constant for the project reach, and that the beach change occurs in the cross-shore direction. These models are primarily employed to design and evaluate beach fill projects, in conjunction with the shoreline change models. Another type of model - shoreline response models assumes that longshore sediment transport is the primary long-term

contributor to planform response. The underlying postulation is that cross-shore movement of sediment during storms equilibrates over the long term. Shoreline response models are best when applied to sites for which there is a clear trend in beach change. Thus, shoreline change models are well-suited to predict morphologic responses of the beach as a function of detached breakwater design. However, for those detached breakwater projects with beach fill that are intended to provide storm protection, storm-induced profile change models may also be applied in the design process to provide a worst-case evaluation of beach fill response to extreme events. Nowadays, there are a dozen existing multidimensional models, both two dimensional and three-dimensional, namely Delft3D, MIKE 21, GENESIS, UNIBEST, XBeach, ECOMSED, ROMS, STOMSED, SEDTRANS and so on.

### *2.4.3 Empirical relationships*

Empirical relationships, for the design and the prediction of shoreline response to a single detached breakwater or to segmented breakwaters, have been developed since the 1960s. In terms of the empirical relationship; this is a relationship or correlation based purely on observation and experiment rather than theory. Empirical relationships can be applied to detailed studies to rapidly assess prototype response to design and as a means of assessing model results. Most scientists focus on the conditions when tombolo or salient will form. Table 2.1 shows an overview of the authors and their studies on empirical relationships.

*Table 2.1: Empirical relationships for detached breakwater (from Chasten et al. (1993))*

<b>N<sub>0</sub></b>	<b>Author and year</b>	<b>Explanation</b>
1	Inman and Frautschy (1966)	Predicts accumulation condition; based on beach response at Venice in Santa Monica, CA.
2	Toyoshima (1972, 1974)	Recommendations for design guidance based on prototype observation of 86 breakwater systems along the Japanese coast.
3	Noble (1978)	Predicts shore impact of breakwaters in terms of offshore distance and length; based on California prototype breakwaters.
4	Walker, Clark, and Pope (1980)	Discusses method used to design the Lakeview Park, Lorain, OH, segmented system for salient formation; develops the Diffraction Energy Method based on diffraction coefficient isolines for representative waves from predominant directions.
5	Gourlay (1981)	Predicts beach response; based on physical model and field observations.
6	Nir (1982)	Predicts accumulation condition; based on performance of 12 Israeli breakwaters.
7	Rosen and Vadja (1982)	Graphically presents relationships to predict equilibrium salient and tombolo size; based on physical model/prototype data.
8	Hallermeier (1983)	Develops relationships for depth limit of sediment transport and prevention of tombolo formation; based on field/laboratory data.

No	Author and year	Explanation
9	Noda (1984)	Evaluates physical parameters controlling development of tombolos/salients; especially due to on-offshore transport; based on laboratory experiments
10	Shore Protection Manual (1984)	Presents limits of tombolo formation from structure length and distance offshore; based on the pattern of diffracting wave crests in the lee of a breakwater.
11	Dally and Pope (1986)	Recommends limits of structure-distance ratio based on type of shoreline advance desired and length of beach to be protected.
12	Harris and Herbich (1986)	Presents relationship for average quantity of sand deposited in lee and gap areas; based on laboratory tests.
13	Japanese Ministry of Construction (1986); Rosati and Truitt (1990)	Develops step-by-step iterative procedure, providing specific guidelines towards final design; tends to result in tombolo formation; based on Japanese breakwaters.
14	Pope and Dean (1986)	Presents bounds of beach response based on prototype performance; response given as a function of segment length-to-gap ratio and effective distance offshore-to-depth at structure ratio; provides beach response index classification.
15	Seiji, Uda, and Tanaka (1987)	Predicts gap erosion; based on performance of 1,500 Japanese breakwaters.
16	Sonu and Warwar (1987)	Presents relationship for tombolo growth at the Santa Monica, CA breakwater.
17	Suh and Dalrymple (1987)	Gives relationship for salient length given structure length and surf zone location; based on lab tests and prototype data.
18	Berenguer and Enriquez (1988)	Presents various relationships for pocket beaches including gap erosion and maximum stable surface area (i.e., beach fill); based on projects along the Spanish coast.
19	Ahrens and Cox (1990)	Uses Pope and Dean (1986) to develop a relationship for expected morphological response as function of segment-to-gap ratio.

The authors in the table above concluded that the shoreline response, mainly influenced by four parameters of structures, are  $X_B$ ,  $L_B$ ,  $G_B$ , and  $h_B$ , where:

$X_B$ : Distance of breakwater from original shoreline;

$L_B$ : breakwater length;

$G_B$ : Gap distance between two adjacent breakwaters in segment;

$h_B$ : Depth (average) at breakwater structure below mean water level.

Several authors developed an evaluation of empirical design methods based on the dimensionless breakwater length  $L_B/X_B$ , the separate conditions for salient formation, tombolo formation, and the limited response, respectively in the table 2.2.

In general, the simplicity of the empirical relationships is estimated and provides prototype data limitations. The results provide are a widely varying prediction for most design relations. However, several of the estimated relationships are careful on their reliability and their limitation during the process of design. For more details, the most remarkable studies and their results are summarized herein:

Table 2. 2: Conditions for shoreline response behind detached breakwater  
(Chasten et al., 1993)

<b>Condition for the tombolo formation</b>		
Condition	Comments	Reference
$L_B/X_B > 2.0$		Shore Protection Manual (1984)
$L_B/X_B > 2.0$	Double tombolo	Gourlay (1981)
$L_B/X_B > 0.67$ to 1.0	Tombolo (shallow water)	Gourlay (1981)
$L_B/X_B > 2.5$	Periodic tombolo	Ahrens and Cox (1990)
$L_B/X_B > 1.5$ to 2.0	Tombolo	Dally and Pope (1986)
$L_B/X_B > 1.5$	Tombolo (multiple breakwaters)	Dally and Pope (1986)
$L_B/X_B > 1.0$	Tombolo (single breakwaters)	Suh and Dalrymple (1987)
$L_B/X_B > 2 b/L_B$	Tombolo (multiple breakwaters)	Suh and Dalrymple (1987)
<b>Condition for the salient formation</b>		
$L_B/X_B < 1.0$	No tombolo	Shore Protection Manual (1984)
$L_B/X_B < 0.4$ to 0.5	Salient	Gourlay (1981)
$L_B/X_B = 0.5$ to 0.67	Salient	Dally and Pope (1986)
$L_B/X_B < 1.0$	No tombolo (single breakwater)	Suh and Dalrymple (1987)
$L_B/X_B < 2 b/L_B$	No tombolo (multiple breakwater)	Suh and Dalrymple (1987)
$L_B/X_B < 1.5$	Well-developed salient	Ahrens and Cox (1990)
$L_B/X_B < 0.8$ to 1.5	Subdued salient	Ahrens and Cox (1990)
<b>Condition for minimal shoreline response</b>		
$L_B/X_B \leq 0.17$ to 0.33	No response	Inman and Frautschy (1966)
$L_B/X_B \leq 0.27$	No sinuosity	Ahrens and Cox (1990)
$L_B/X_B \leq 0.5$	No deposition	Nir (1982)
$L_B/X_B \leq 0.125$	Uniform protection	Dally and Pope (1986)
$L_B/X_B \leq 0.17$	Minimal impact	Noble (1978)

- Dally and Pope (1986) showed several techniques for governing shoreline response to a single or segmented offshore breakwater project. They recommended for tombolo formation;

$$\frac{L_B}{X_B} = 1.5 \text{ to } 2 \quad \text{single breakwater} \quad (2.27)$$

$$\frac{L_B}{X_B} = 1.5 \quad L \leq G_B \leq L_B \text{ segmented breakwaters} \quad (2.28)$$

where L is the wavelength at the structure.

for salient formation is

$$\frac{L_B}{X_B} = 0.5 \text{ to } 0.67 \quad (2.29)$$

for both single and segmented breakwaters is

$$\frac{L_B}{X_B} = 0.125 \quad (\text{long systems}) \quad (2.30)$$

- Nir (1982), based on the prototype data in the Israel Mediterranean projects, finds the following relationship between the distance offshore to the breakwater length ratio ( $X_B/L_B$ ) and average tombolo sand layer thickness ( $d_t$ ):

$$d_t = 1.786 - 0.809 \frac{X_B}{L_B} \quad (2.31)$$

- Hallermeier (1983) suggested the following water depth at a structure as a guide for the position offshore breakwaters when tombolo formation is expected undesirable:

$$d_{sa} = \frac{2.9 H_e}{\sqrt{(s-1)}} - \frac{110 H_e^2}{(s-1)gT_e^2} \quad (\text{depth for salient formation}) \quad (2.32)$$

where  $d_{sa}$  is the annual seaward limit of the littoral zone,  $H_e$  is the deep-water wave height exceeding 12 hours per year,  $s$  is the ratio of sediment to fluid density,  $g$  is the acceleration of gravity, and  $T_e$  is the wave period corresponding to the wave height. For headland structures (tombolo formation), breakwaters should be placed at an approximate depth of  $h_B = \frac{d_{sa}}{3}$  (headland structures).

- Harris and Herbich (1986) showed equations, based on prototype and field data of the following relationship between the amount of sand deposition in the embayment area ( $Q_b$ ) and the distance of the breakwater from the shoreline ( $X_B$ ):

$$\frac{Q_b}{X_B L_B h_B} = \exp\left(0.315 - 1.922 \frac{X_B}{L_B}\right) \quad (2.33)$$

- (Seiji et al., 1987), gave conditions on the  $G_B/X_B$  ratio for no erosion, possible erosion, and certain erosion at the shoreline opposite the gap:

$$\frac{G_B}{X_B} < 0.8 \quad \text{no erosion opposite gap} \quad (2.34)$$

$$0.8 \leq \frac{G_B}{X_B} \leq 1.3 \quad \text{possible erosion opposite gap} \quad (2.35)$$

$$\frac{G_B}{X_B} \geq 1.3 \quad \text{certain erosion opposite gap} \quad (2.36)$$

- Suh and Dalrymple (1987) developed the following relationship for the prediction of salient length S by combining movable-bed laboratory results with prototype data:

$$\frac{S}{X_B} = 14.8 \frac{G_B X_B}{L_B^2} \exp \left[ -2.83 \sqrt{\frac{G_B X_B}{L_B^2}} \right] \quad (2.37)$$

And they concluded that tombolo usually formed for single and multiple breakwaters when

$$\frac{L_B}{X_B} \geq 1.0 \quad \text{single breakwater} \quad (2.38)$$

$$\frac{G_B X_B}{L_B^2} \approx 0.5 \quad \text{segmented breakwaters} \quad (2.39)$$

- Ahrens and Cox (1990) classified the beach response using the index scheme of Pope and Dean (1986) to develop an estimated relationship for beach response based on a ratio of the breakwater length to the distance from the initial shoreline. The relationship defining a beach response index ( $I_s$ ) is:

$$I_s = \exp \left[ 1.72 - 0.41 \frac{L_B}{X_B} \right] \quad (2.40)$$

where the five types of beach response (Pope and Dean (1986)) give  $I_s$  value as:

Permanent tombolo formation,  $I_s=1$

Periodic tombolos,  $I_s=2$

Well-developed salients,  $I_s=3$

Subdued salient,  $I_s=4$

No sinuosity,  $I_s=5$

- Hsu and Silvester (1990) created, based on the prototype data and laboratory results, the following relationship between the ratio of salient distance to breakwater length ( $X/L_B$ ) and the ratio of original shoreline distance to breakwater length ( $X_B/L_B$ ):

$$\frac{X}{L_B} = -0.1626 + 0.8439 \left( \frac{X_B}{L_B} \right) + 0.0274 \left( \frac{X_B}{L_B} \right)^2 \quad (2.41)$$

- McCormick (1993) assumed a notation for elliptical shoreline response to a single breakwater. The author developed empirical relationships based on experimental data, resulting in the following relationship for the prediction of salient and tombolo at Bay Ridge:

$$0.38 < \varepsilon_0 < 0.83 \text{ then } \varepsilon_0 = \frac{H_0/L_0}{m} \quad \text{tombolo} \quad (2.42)$$

$$\frac{X_B}{L_B} < 0.6 \quad \text{tombolo} \quad (2.43)$$

$$\frac{X_B}{L_B} > 0.6 \quad \text{salient} \quad (2.44)$$

To sum up, physical, numerical, and empirical methods are used to evaluate shoreline response, focused on the relationship between breakwater parameters, beach profile, wave properties, and magnitude or capacity of sediment accretion/erosion. **Despite the fact that at least fourteen parameters have an influence on shoreline change, almost all methods are unable to take all influence parameters into account. However, the most effective parameters are found to be breakwater length, distance from structure to the original shoreline, gap width between structures, depth at structure, grain median size, wave height, wave period, and wave angle.**

## 2.5 Concluding and remarks

1. In this chapter, we have seen that it is possible to protect a shore by the installation of detached breakwaters. The fundamental advantages are:

- Reduction in wave attacks directed at the shore;
- Increasing sediment deposition and promoting beach formation tombolo or salient;
- Reduction in shore erosion behind;
- Reduction in sediment loss through activity of circulation currents;
- Reduction of flood risk due to wave overtopping at the shore.

However, disadvantages still appear when detached breakwaters are placed, such as:

- Possible change of magnitude and direction of longshore currents;
- Sediment budgets with corresponding increased erosion elsewhere along shore;
- Scour problems around structure;
- Potential shoreline erosion through gaps in segmented breakwaters;
- Structure maybe damaged in storms;
- Expensive to construct and maintain;
- Less safety for swimmers and obstruction of sea view.



2. The complicated hydraulic mechanism of waves, currents and sediment motion changes in the sheltered water area due to breakwater works, leading the main causes of morphology changes in the breakwater field. The issue of most concern in the embayment of breakwaters, is sediment deposition promoted among the structure's length, such as tombolo and salient. However, morphological changes also appear at adjacent areas, such as the morphology opposite the gap, the up-drift and the down-drift. Most previous studies focused on the estimation of accretion; several studies investigated the gap erosion; limited studies examined the status of the up- and down-drift. Therefore, it is necessary to investigate the impact of breakwaters on the shore, to fill the gap of understanding.

3. Several important parameters with effects on shoreline response can be: length of structure, offshore distance, structure transmission, gap width, structure orientation, depth at structure, tidal range, wave height, wave period, wave oblique angle, and sediment size.

4. The methods applied for the prediction of shoreline response are the physical model, the numerical model, and the empirical relationship. Within the physical model, several results on the effects of a particular design can be shown, but these tools can be costly and time consuming; a scale model, similarity conditions and due to setup of a model may also be instable. Instead of laboratory tests, prototype tests are the visual method in detailing the workings of a breakwater, however, it can be very expensive and is not applicable in preliminary design. A major problem of the numerical model is the inaccuracy of the mathematics representing the morphological processes and the input data; the user can get the wrong results of the effects of detached breakwaters on shoreline response. Empirical relationships are a quick, inexpensive method, that can evaluate the beach response to a proposed design. But, this method is still subject to the simplicity / limitation of parameters relationships. Therefore, problems can happen when applying them to a wide variety of conditions.

In the next chapter, data of the prototypes for analysis of the shoreline changes behind detached breakwaters will be collected.

# CHAPTER 3: DATABASE OF OBSERVATIONS OF THE PROTOTYPES

## 3.1 Introduction

The previous chapter described the phenomenon related to detached breakwaters and the research performed. In this chapter, we describe how we achieved the process of data collection. The objects of concern, are the prototypes of the structures which are mostly constructed with the intention to protect the coast.

The layout and geometry of the detached breakwaters have been described in many publications with the purpose of describing the actual characteristics of these structures in a worldwide overview. The definition of the parameters for the structures was shown in Chasten et al. (1993) and K.J. MacIntosh (1988). However, in this chapter several new parameters will be added, as shown in the terminology used in this thesis, figure 3.1 below. A statistical study for detached breakwaters in Japan is shown in UDA (1988) and a similar study for such structures in Europe can be found in the DELOS (*Environmental Design of Low Crested Coastal Defence Structures*) project; the cases in the United States are reported by the Coastal Engineering Research Center (CERC).

The data related to breakwaters are the structure parameters, the physical conditions, and the equilibrium shoreline, which will be exposed in the next sections of this chapter.

## 3.2 Data Sources

### 3.2.1 Sources of structure parameters

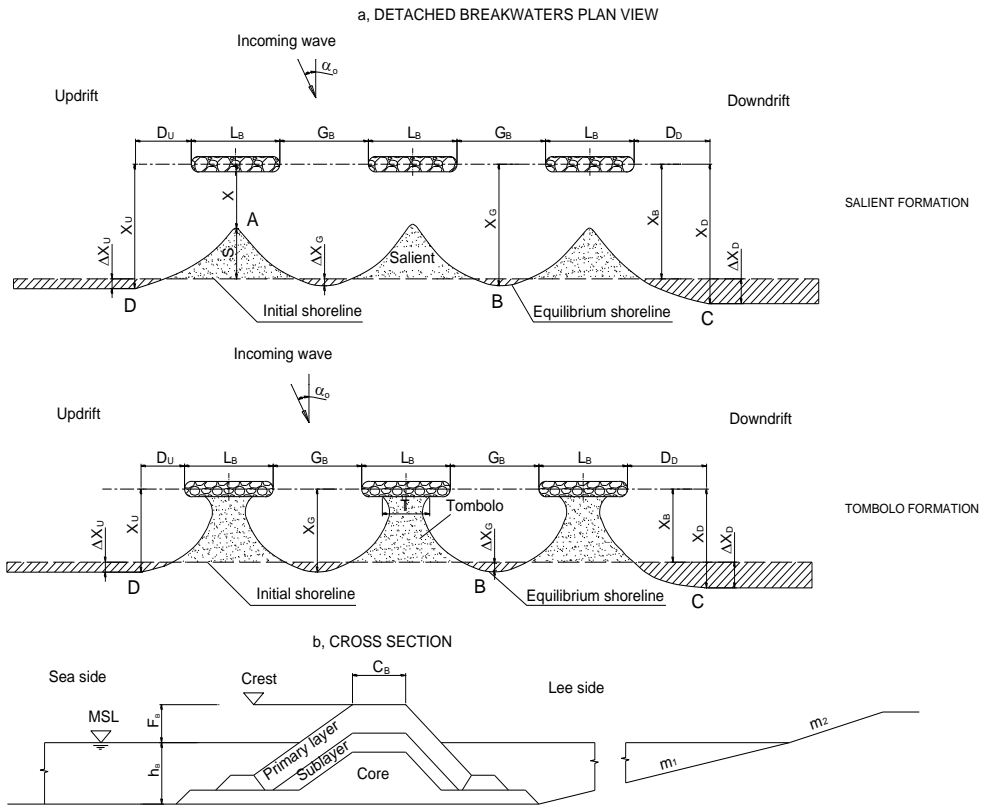


Figure 3.1: The definition of terms used in the thesis

The structure parameters data in this thesis was collected from a variety of cases in the different zones and countries. Three sources of information are used in the inquiry questionnaires, using data from project reports, and a selection of useful information from various articles, journals, and papers. First, we used the inquiry questionnaires as a source to collect data from the DELOS project. This project focussed on an inventory of detached breakwaters in Europe. The data bank was assembled from 150 completed survey series questions. Each full questionnaire contained information including location of the structure, main purpose of the scheme, type of breakwater, dimensional sketch, and other information. The collected data results are found in Lamberti et al. (2005). The second source consisted of data of exploitation from project reports. A database of detached breakwater projects in the United States and several other countries is maintained by the Coastal Engineering Research Center (CERC). The database includes detailed information such as detached breakwater types, construction dates, project dimensions, and other site data. A concise historical description of the project's performance is also included. The third source for our database was collected from papers. Each of these, public papers, journals and articles focused on different aspects of

detached breakwaters. However, these papers usually contained only part of the sketch of the structure parameters. The contribution of the collected data from the represented papers can be found in Mauricio González (2001), Bricio et al. (2008), José Ma Berenguer (1988), Rosen and Vajda (1982), Nir (1982) and Fried (1976). The three sources of data collection mentioned above were applied to review the detached breakwaters in Italy, Israel, Spain, the United Kingdom, and the United States.

### *3.2.2 Sources of physical conditions: waves, currents, water level*

In general, detached breakwaters designed for shore protection along the coastline, are placed in the littoral zone. Within this zone, waves, oceanic currents, and water level are a major physical influence on the effectiveness of the structures. Data of waves and currents has been retrieved from online sources. The first wave source is the ERA-40, which is a re-analysis of the global atmosphere and surface conditions for over 45 years (September 1957 to August 2002) by the European Centre for Medium-Range Weather Forecasts (ECMWF)([http://apps.ecmwf.int/datasets/data/era40\\_daily/](http://apps.ecmwf.int/datasets/data/era40_daily/)). The ECMWF used a database of meteorological collections from satellites, aircrafts, balloons, buoies, radiosondes, and scatterometers. This data was run through the ECMWF computer model and was stored in NetCDF format files. The second part of the wave source is the wave hindcast. Wave hindcast refers to the predictions of wind waves on the water surface in the past time. The Wave Information Studies (WIS) conducted by the US Army Corps of Engineering (USACE) has developed hindcast data for all ocean coasts of the United States and the coast of the Great Lakes in a period of 20 years (<http://wis.usace.army.mil/>). The next major physical aspect is the ocean current. The oceanic currents at all projects are the subject of observation in the Ocean Surface Current Analyses – Real time (OSCAR) project. Understanding ocean currents and their influence on structures is the basic information concerned with the existence of considerable currents or inconsiderable currents. The last physical aspect, discussed here, is the water level related to tidal range at the construction sites. The tidal range values were shown in the report of the projects or extracted from tidal charts. Thus, the physical conditions at structures in the littoral zone of waves and ocean currents were retrieved via reliable scientific organizations, while the physical conditions of the tides were gathered from project reports.

### *3.2.3 Sources of observation results*

Detached breakwaters interact with near-shore hydrodynamics in a very complicated way and are a consequence of coastal line changes. If the deposition forms a planform which connects a structure to the coastline, this is called a tombolo. If there is no connection a salient is formed. Post-construction beach responses to detached breakwater structures are analysed using the aerial photos of time-series observations. The image data were obtained at the inequitable period between 1972 and 2013. The selected photos are mostly of good quality, with few cloud effects. In this study a technique is used to estimate shoreline responses, using rule tool to measure distance between the objects. For instance, measuring the distance from

the centre of breakwater to the edge of the salient. Also, the place-mark tool can identify the global position of specific points. An example the place-mark of the Elmer, West Sussex project in figure 3.2 has a latitude of 50°47'28.00"N and a longitude of 0°36'11.00"W. In order to make measurements, distinctions must be made between the shoreline position, the structure placement and the water by colours and appearances. In aerial images, the shoreline of a sand beach usually appears bright in colour, the structures in grey, and the water in blue colour. In the aerial photo in figure 3.2 below the different colours of these objects are illustrated.

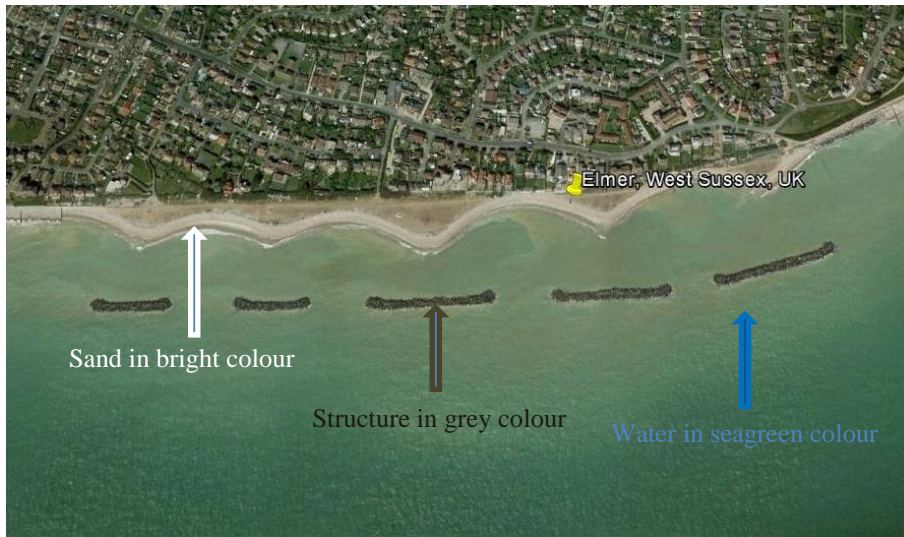


Figure 3.2: How to recognize the objects by colours that appear in the aerial image

### 3.3 Projects inventory

In the project inventory of the detached breakwater projects are listed by country. Several countries have combined reports, but most have not. Specific characteristics of the inventory of different the countries are:

#### 3.3.1 Inventory for the US

The document inventory for the US detached breakwater project information is mostly based on the report “Engineering Design Guidance for Detached Breakwaters as Shoreline Stabilization Structures” by Chasten, Rosati, McCormick, Coastal Engineering Research Center, U.S.Army Corps of Engineers, Waterways Experiment Station, CERC-93-19, December 1993. The breakwater projects in this report are included and summarized (see table 3.1)

#### 3.3.2 Inventory for Israel

Several papers and reports related to projects in Israel are found in the professional journals:

Table 3.1: Summary of the US breakwater projects (from technical report CERC-93-19)

Coast	Project	Location	Date of Construction	Number of Segments	Project Length	Segment Length	Gap Length	Distance Offshore Pre-project	Water Depth	Fill Placed	Beach* Response	Constructed by	Maintained by
Atlantic	Winthrop Beach (low tide)	Massachusetts	1935	5	625m	91m	30m	Unknown	3.0 (mlw)	No	1	State of Mass.	
Atlantic	Winthrop Beach (high tide)	Massachusetts	1935	1		100	30	305	3.0 (mhw)	No	3	State of Mass.	
Atlantic (Potomac River)	Colonial Beach (Central Beach)	Virginia	1982	4	427	61	46	64	1.2	Yes	2	USACE	
Atlantic (Potomac River)	Colonial Beach (Castlewood Park)	Virginia	1982	3	335	61,93	26,40	46	1.2	Yes	1	USACE	
Chesapeake Bay	Elm's Beach (wetland)	Maryland	1985	3	335	47	53	44	0.6-0.9	Yes	1	State of Maryland	
Chesapeake Bay	Elk Neck State Park (wetland)	Maryland	1989	4	107	15	15		0.6-0.9	No	2-4	USACE	USACE
Chesapeake Bay	Terrapin Beach (wetland)	Maryland	1989	4		23	15,31,23	38.1	0.6-0.9	Yes	5	USACE	USACE
Chesapeake Bay	Eastern Neck (wetland)	Maryland	1992-1993	26	1676	31	23		0.3-0.6	Yes		US fish and Wildlife Service, USACE	US fish and Wildlife Service
Chesapeake Bay	Bay Ridge	Maryland	1990-1991	11	686	31	31	42.7		Yes	4	Private	Private
Gulf of Mexico	Redington Shores	Florida	1985-1986	1	100	100	0	104		Yes	1	USACE	USACE
Gulf of Mexico	Holly Beach	Louisiana	1985	6	555	46,51,50	93,89	78,61	2.5	No	4	State of Louisiana	State of Louisiana
Gulf of Mexico	Holly Beach	Louisiana	1991-1993	76		46,53	91,84	122,183	1.4,1.6	Yes	3	State of Louisiana	State of Louisiana
Gulf of Mexico	Grand Isle	Louisiana		4	84	70	21	107	2	No	3	City of Grand Isle	City of Grand Isle
Lake Erie	Lakeview Park	Ohio	1977	3	403	76	49	152	3.7	Yes	4	USACE	City of Lorain
Lake Erie	Presque Isle	Pennsylvania	1978	3	440	38	61,91	60	0.9-1.2	Yes	2	USACE	USACE
Lake Erie	Presque Isle	Pennsylvania	1989-1992	55	8300	46	107	76-107	1.5-2.4	Yes	3-4	USACE	USACE
Lake Erie	Lakeshore Park	Ohio	1982	3	244	38	61	120	2.1	Yes	5	USACE	City of Ashtabula
Lake Erie	East harbour	Ohio	1983	4	550	46	90,105,120	170	2.3	No	5	State of Ohio	State of Ohio
Lake Erie	Maumee Bay (headland)	Ohio	1990	5	823	61	76		1.3	Yes	1	USACE	State of Ohio
Lake Erie	Sims Park (headland)	Ohio	1992	3	975	38	49		2.5	Yes	1	USACE	City of Euclid
Pacific	Venice	California	1905	1	180	180	0	370		No	5	Private	
Pacific	Haleiwa Beach	Hawaii	1965	1	49	49	0	90	2.1(msl)	Yes	3	USACE/state of HI	USACE
Pacific	Sand Island	Hawaii	1991	3	110	21	23					USACE	USACE

\*Beach response is coded as follows: 1- permanent tombolos, 2- periodic tombolos, 3- well developed salient, 4- subdued salient, 5- no sinuosity

In “Protection by means of offshore breakwaters” in which Fried (1976), Coastal Engineering 1976, mentions the project at the Sheraton Hilton, Tel Aviv in Israel and the central Tel Aviv coast.

In “Sedimentological influences of detached breakwaters” Rosen and Vajda (1982), Coastal Engineering 1982, make the inventory table of the projects in Haifa, Netanya, and Tel Aviv.

In the report “Investigations and Recommendations for Solutions to the Beach Erosion Problems in the City of Herzliya, Israel” Harris (2007) mentions the project in Herzliya, Israel.

### 3.3.3 Inventory for Spain

In “Geometric Detached Breakwater Indicators on the Spanish Northeast Coastline” Bricio et al. (2008), Coastal Research no. 245, they studied nourishment of the beach at several projects in Spain (table 3.2).

In “Beach nourishment in Altafulla, Spain: Verification of theoretical models” Galofré et al. (1997), Coastal Engineering 1996, the project in Altafulla beach, Spain is indicated.

In the DELOS inventory for Spanish projects, there are 28 brief questionnaires for 28 projects of offshore breakwaters. The questionnaires contained the information of construction motivation, system layout, water level variations, and breakwater impact on the environment. The list of the structures of emerged schemes and submerged schemes are included. However, herein the data collection is focused on emerged schemes.

Table 3. 2: Projects of detached breakwater in Spain

(modified from Bricio et al. (2008))

<b>N<sub>o</sub></b>	<b>Name of the detached breakwater</b>	<b>L<sub>B</sub> (m)</b>	<b>X<sub>B</sub> (m)</b>	<b>Coast’s response</b>
1	Gerona Calonge I	145	100	Tombolo
2	Gerona Calonge II	150	100	Tombolo
3	Gerona Calonge III	160	100	Tombolo
4	Barcelona Sitges	158	117	Tombolo
5	Barcelona Vilanova I la Geltrú	200	234	Tombolo
6	Barcelona Cubelles I	135	81	Tombolo
7	Barcelona Cubelles II	135	84	Tombolo
8	Mota de Sant Pere I	105	186	Limited response
9	Mota de Sant Pere II	100	206	Limited response
10	Mota de Sant Pere III	100	199	Limited response

No	Name of the detached breakwater	$L_B$ (m)	$X_B$ (m)	Coast's response
11	Tarragona Cunit I	236	198	Tombolo
12	Tarragona Cunit II	162	151	Tombolo
13	Tarragona Cunit III	115	108	Tombolo
14	Tarragona Cunit IV	131	100	Tombolo
15	Tarragona Cunit V	147	133	Tombolo
16	Tarragona Cunit VI	162	122	Tombolo
17	Tarragona Cunit VII	168	113	Tombolo
18	Tarragona Altafulla	93	204	Salient
19	Tarragona Cambrils I	60	115	Salient
20	Tarragona Cambrils II	138	97	Tombolo
21	Tarragona Cambrils III	82	78	Salient
22	Tarragona Cambrils IV	154	96	Tombolo
23	Tarragona Cambrils V	57	120	Limited response
24	Tarragona Cambrils VI	193	124	Tombolo
25	Tarragona Cambrils VII	72	97	Salient
26	Tarragona Cambrils VIII	194	120	Tombolo
27	Tarragona Cambrils IX	210	114	Tombolo

### 3.3.4 Inventory for Denmark, Italy, and the UK

The inventory for Denmark, Italy and the UK offshore breakwaters is mostly based on the 4, 57, and 34 number series questionnaires as used in the DELOS project, respectively. The information of the questionnaires consists of the same information as in the DELOS inventory in Spain. But, here the interest is focussed on statistics of emerged offshore structures.

### 3.3.5 Inventory for Japan

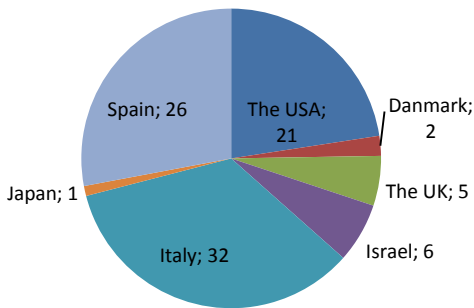
UDA (1988) investigated the effect and stability of the detached breakwaters along Japanese coasts on the statistics of 1552 breakwaters constructed until 1982. However, this investigation was shown in combined data only; therefore, individual parameters of each project cannot be extracted. Only data on the project in Kaike, Japan has been collected from the inventory by Toyoshima (1982).

To sum up, the inventory of the detached breakwater projects includes a total 93 of projects, resulting in 1144 structures, detailed in appendix 1 and submitted to the TUDelft Datacenterum



(<http://dx.doi.org/10.4121/uuid:9a2775c0-7c64-4fe1-bf02-221574825197>). The largest number of projects is located in Italy with 32 projects and 729 structures, marking a percentage of the total projects and structures of 34% and 64%, respectively. The projects in Spain are the second highest number of investigated projects with 26 (28%), but the number of breakwaters only count up to 67 (just 6%). In the USA, there are 21 projects and 266 structures, both adding up to 23%. Denmark, Israel, Japan, and the UK have considerably less selected projects and structures than other countries (figure 3.3). In the subsection below more details about the data collection will be explained.

a,



b,

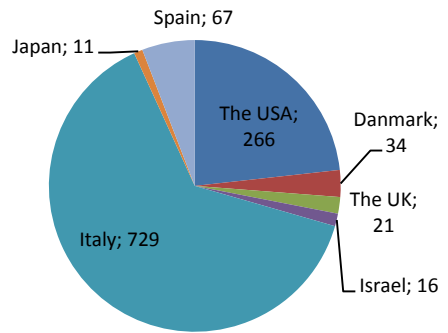


Figure 3.3: Number of the collected projects (a) and structures (b) in the different countries.

### 3.4 Data collection of structure parameters

Seven structure parameters were included and collected, in which, six of the seven parameters were indicated in the reports as the sketch parameters of the design, and another parameter was not shown, however, could be measured from aerial images.

The six selected parameters are chosen from the reports and papers, as follows:

$L_B$  : Length of detached breakwater at crest level (m);

$X_B$  : Distance between the original shore line and the centre of the breakwater (m);

$G_B$  : Gap width between two successive structures (m);

$F_B$  : Freeboard, the distance from mean water level (MWL) to breakwater's crest level (m);

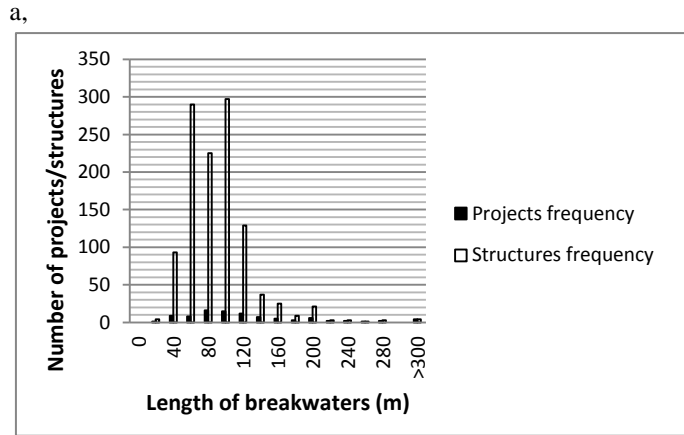
$C_B$  : Crest width of breakwater (m);

$h_B$  : Breakwater under water at MWL (m).

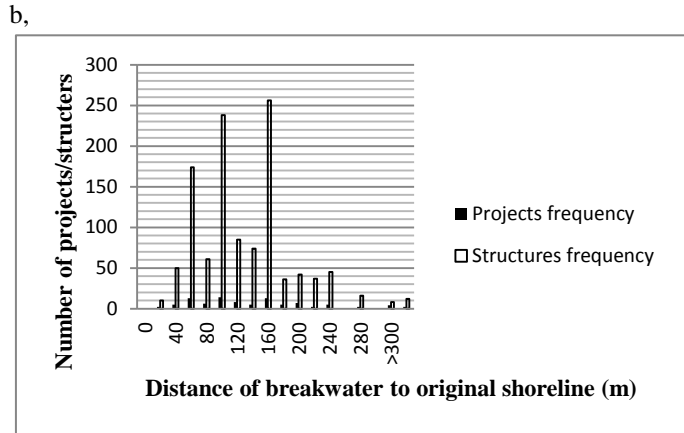
and the seventh parameter related to angle of the structure to the true North  $\theta_N$  (degree), is the orientation of the structure.

In the same projects, if the layout parameters (breakwater length, offshore distance and gap width) are not similar, they should be separated as different projects. The group of structures with a similar layout parameters determines the definition of study case. Each case has unique representative parameters, so that the total number of cases must be bigger than the number of projects. In turn, the analysis the of frequency distribution in both project and structure, with the first six of structure parameters, is shown:

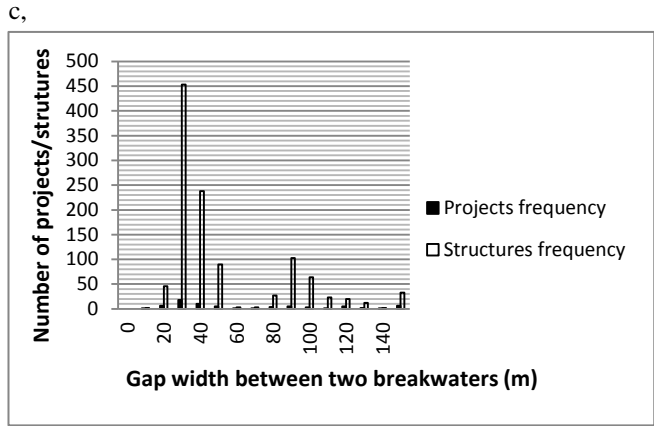
The six breakwater parameters in the inventory projects are of a variety of magnitudes. The length of breakwaters ( $L_B$ ) ranges from 15 to 1000m, and the largest frequency distribution of projects and structures varies the breakwater length from 40 to 120m (Fig. 3.4a).



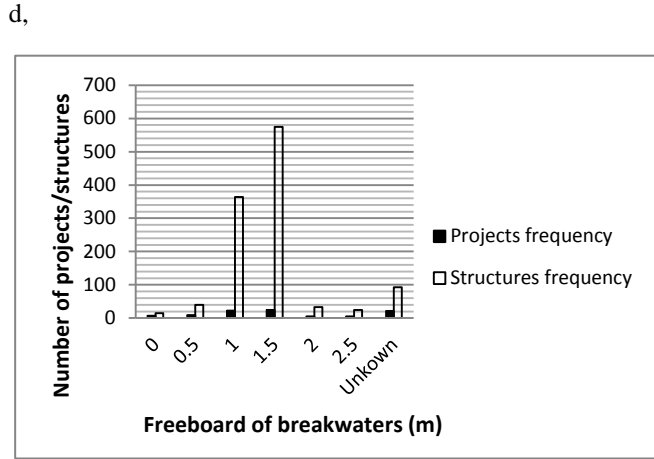
The offshore distance of the breakwater ( $X_B$ ) is spread between 20 and 610 m. The higher density of projects and structures are at around the offshore distance of 160, 100, and 60m (Fig. 3.4b).



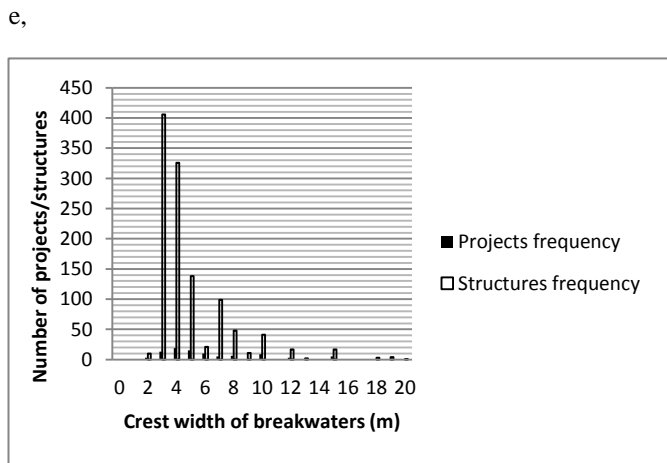
The gap between two successive breakwaters ( $G_B$ ) runs from 10 to 300m. The significant number of projects and structures are around 30 and 40 m of gap width (Fig. 3.4c).



The freeboards ( $F_B$ ) seem to be low, just lower than 2.5 meters above MWL. Most projects and structures contribute at the height of 1.0 and 1.5 m above MWL (Fig. 3.4d).



The crest width ( $C_B$ ) ranges from 1.8 to 20m, however, the crest width of the biggest frequency of projects and structures is mostly from 3.0 to 7.0 m of crest width (Fig. 3.4e).



f,

And the last parameter - the water depth at the breakwater at MWL ( $h_B$ ) is mostly from 0.5 to 8.5 m. The biggest number of cases and structures is around 2.5m depth (Fig. 3.4f).

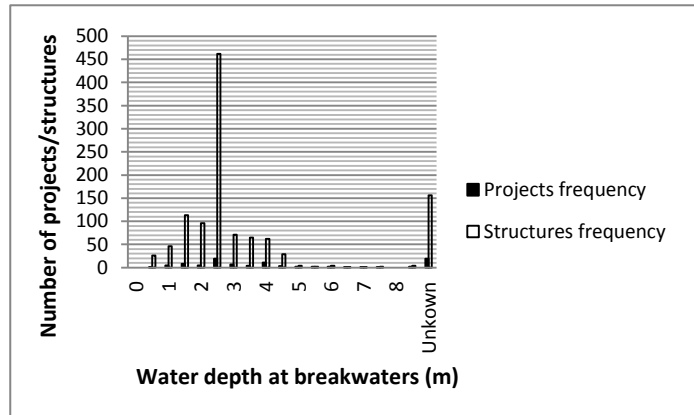


Figure 3.4: Histograms showing the distribution of cases and structures for each investigated parameters.

Although the six parameters above were investigated in each of the projects, however, some parameters has not been reported. The magnitude of freeboard ( $F_B$ ) is the biggest unknown parameter value in a total of 21 projects with 93 structures. The water depth at the breakwater ( $h_B$ ) has been missing in 19 projects with 156 structures. Also, the breakwater distance to the original shoreline ( $X_B$ ) was missing in 2 projects with 12 structures. The other parameters, the breakwater length ( $L_B$ ), the gap width ( $G_B$ ), and the crest level width ( $C_B$ ) were complete.

Another structure parameter is the orientation of structures to the North ( $\theta_N$ ) which was not shown in reports of the projects. However, the direction of segments can be measured after construction on the aerial photos, assuming that the direction of a structure does not change during its working life. Thus, the angle of the segment and the true North direction in the aerial photos is equal to the angle of the initial orientation of a structure.

The orientation angle of a structure is defined by taking the following steps: First to determine the centre line of the breakwater. The second step is to rotate the aerial photo into the true North direction. Next, set the centre point of the compass on the start point of the centre line of the structure. On the compass, the centre line indicates the angle of the structure to the true North. For instance, in figure 3.5 the measurement of the angle orientation of one of the breakwaters in San Antonio beach, in Calonge, Spain, is illustrated. The centre line indicates that the orientation angle is 60 degrees. Executing the measurement of the orientation angle in the other projects; then it adds information to the basic parameters of the projects.

In summary, seven sketch parameters of the projects were collected. In which the six parameters were sorted from the project reports and published articles, and one more parameter

was determined from the current situation through measurements.

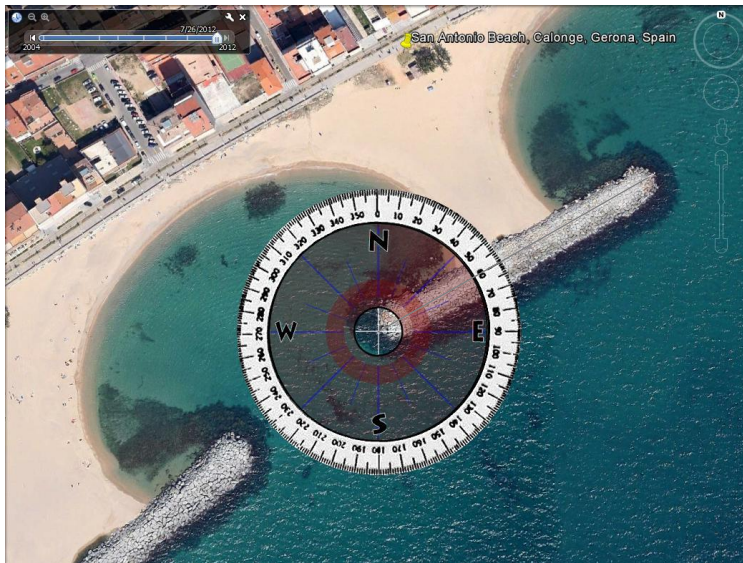


Figure 3.5: The direction measurement at San Antonio beach, Calonge, Spain project.

### 3.5 Data collection of sediment properties

In the projects of beach sand in detached breakwater projects, sediment transport depends on sediment properties, characteristics of sediment, and fluid flow properties. Therefore, the sediment properties are important in the beach profile changes. Sediment properties surveyed in the projects mentioned above are the non-cohesive grains in the sediment bed. The properties of individual sediment grains include sediment size, sediment density, sediment shape, and chemical composition. However, in the reports of the projects only the median grain size ( $D_{50}$ ) is indicated. The value of  $D_{50}$  is taken from the grain size distribution of a characteristic grain diameter. The middle of diameter size distribution (50%) can be described as the size class of the highest frequency ( $D_{50}$  means that half of the sediment is finer than this size).

Unfortunately, in the total of 93 projects, only 21 projects have shown values of median grain size, of which, one in the UK, 11 in the US, 7 in Spain, 2 in Italy. The value of  $D_{50}$  ranges from 0.115mm (fine sand) at Elmer, West Sussex, U.K. to 1.86mm (coarse sand) at Palo Beach, Málaga and at Pedregalejo, Málaga, Spain. For the details of the sediment diameter, see appendix 1 at TUDelft Datacentrum (<http://dx.doi.org/10.4121/uuid:9a2775c0-7c64-4fe1-bf02-221574825197>).

### 3.6 Data achievement of waves, tides, and oceanic currents

#### 3.6.1 Waves

To achieve deep water wave data in front of the projects, two database sources, one is the re-analysis of the global atmosphere and surface condition (the ERA-40), and another is the wave hind-cast models (WIS), are used. The database of the ERA-40 was applied to calculate deep-water waves for whole projects in Europe, Israel, Japan, and several projects in the US coast. The database of the WIS wave was applied to determine waves for the projects in the Great Lakes in the United States. Data of the two wave models will be explained in detail below.

##### *a. Waves in the database of re-analysis of meteorological observations (ERA-40)*

In the ERA-40, the significant wave height, mean wave period and mean wave direction can be retrieved from the domain of the ECMWF. The output of the wave characteristics data set takes place at particular hours 00, 06, 12, and 18 UTC in the full 3 years from the start in 1998 to the end of 2000. The grid resolution of the model is given on a  $1.5^\circ \times 1.5^\circ$  of the global latitude and longitude (approximately 125km x 125km). Because of projects identification, the wave model grid is split into smaller grids with  $0.25^\circ \times 0.25^\circ$  solution. However, waves in the sub grids between the model grid remain at the same values. The wave characteristics were obtained as the NetCDF file which contained numerical data and visual plots.

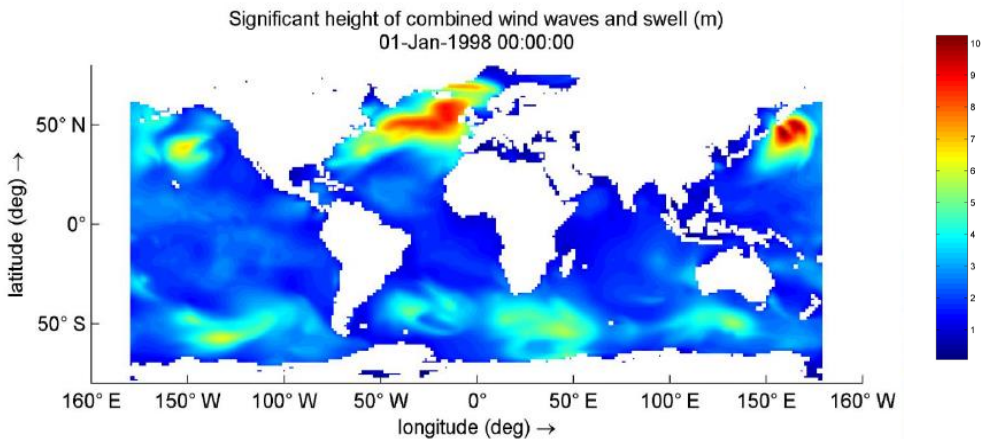


Figure 3.6: Significant waves height retrieved from the ERA-40

Using QUICKPLOT in the WAVE module of the Delft3D software will demonstrate the NetCDF file of deep water wave characteristics as a visual plot and numbers. The visual plot can be shown in an animation of significant wave height, wave period, and wave direction. In addition, it can show visual scatters when a specific point (M,N) in a defined grid is chosen. An explanation for the visual plot of wave achievement in Delft3D shows the spectra of

significant wave heights in the project locations in figure 3.6. In the computer grid we choose point (11,7) representing the global coordinate point of  $133^{\circ}30'00''$  longitude and  $35^{\circ}30'00''$  latitude; the quick view function then will display scatters of wave characteristics as in figure 3.7, which illustrates the scatters of recorded data at the project location. The wave data is used to calculate the deep-water wave in front of the Kaike, Japan project as an example. The project is located at  $133^{\circ}21'17''$  longitude and  $35^{\circ}47'34''$  latitude. To explain in more detail, at the site of the point in front of Kaike, three characteristics of deep water waves are significant: wave height, wave period, and wave direction.

This point (11,7) contained 4834 series of observations of wave characteristics. In figure 3.7a, a scatter of significant wave heights combined with wind waves and swell, is demonstrated in the chosen time interval. The highest significant wave height was around 4.5m, the lowest was about 0.15m. The higher frequency was around 0.5m of the wave height.

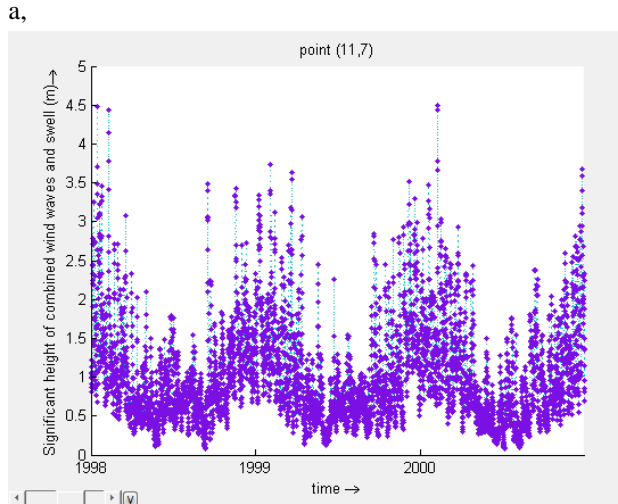


Figure 3.7b displays the correlative mean wave period. The maximum wave period was just under 14 seconds, while the minimum was 2.5 seconds. Overall, most wave periods fluctuated from 4.0 seconds to 8.0 seconds.

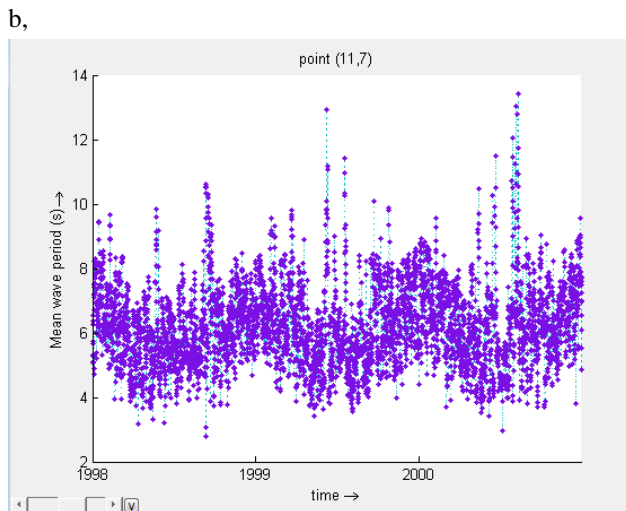


Figure 3.7c displays a distribution of mean wave direction. Wave directions more frequent from angle of -60 degree (or 300 degree) to 50 degrees. But the prominent direction was at the angle of 22.5 degrees.

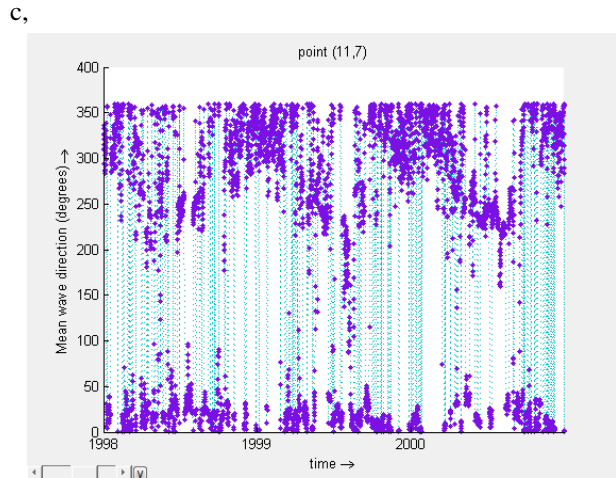


Figure 3. 7: Deep water wave at Kaike, Japan project

It can be noted that during the determination of a node of the grid, taking into account the wave data of the project, the node point must be in the water area in front of the project. Hence, when entering the computer grid (M,N) represented for the project location coordinates but for which the values of waves do not appear on the screen, we have to adjust the location to another computer grid in a water area nearby.

#### b. Waves achievement in model of hind-cast (WIS)

Hind-cast wave model was used for estimation wave characteristics at the nine projects in the Great Lakes in the US. Hind-cast is a numerical wave model, which has been developed by the US Army Corps of Engineers (USACE). The name of project is Wave Information Studies (WIS). The WIS hind-cast has been estimating waves from past wind events for thousands of stations near the US coast and the Great Lakes (<http://wis.usace.army.mil/>). Wave data at the detached breakwater projects in the United States has been selected through the WIS hind-cast. Data at each WIS station showed a contribution of wind and wave in figures in the wind rose for the period from January 1980 to December 2012.

The WIS wave stations have been established to contain wave data. From the coordination of the projects on the WIS web page we are able to find out the station closest to the project. The wave values at the WIS station are used for our wave project. An example in figure 3.8 indicates the characteristics of wind and wave at WIS station 92031 applied at the project at Presque Isle, Pennsylvania, the US. The WIS station 92031 is located at the point of 80°12'00"W longitude and 42°12'00"N latitude on the coast of Lake Erie. This wave station is also used for the detached breakwaters project of Holly Beach at the location of 80°06'58"W longitude and 42°09'57"N latitude. The occurrence frequency of wind and significant wave in difference directions can clearly be seen from the wind rose (a) and the wave rose (b). The



largest frequency of wind and wave came from the direction of 270 degrees from the true North with 10.5% and 23.5%, respectively. Other aspects were the strongest wind speed with 20 to 25m/s, and the highest significant wave height of 4 to 5m.

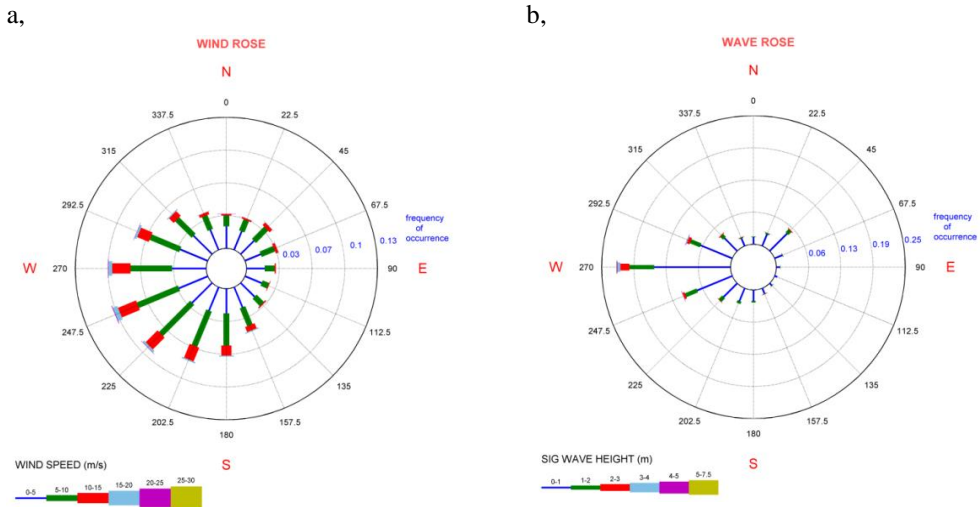


Figure 3.8: Wind rose (a) and wave rose (b) at the WIS station 92031 in Erie Lake. January 1980 – December 2012 (from USACE)

### c, Representative wave characteristics

From the wave data in the ERA-40 and in the WIS, to calculate the characteristics of a representative wave, which has an equivalent sediment transport for the whole wave climate, including the representative wave height, the representative wavelength and the representative period:

Terms of representative wave height are derived for the coast adjacent to the project. These wave heights are an equivalent morphology to a complete wave regime based on wave energy and on equivalent longshore sediment transport capacity over the beach profile. The most suitable wave regime is chosen by taking into account the predominant sediment transport processes at the project site. The representative waves should be used to significantly reduce computational time in morphological models. Following Komar and Inman (1970) and Ricardo del Vaile (1993) the longshore sediment transport is related to exponent two and half of a breaking wave height ( $H_b^{2.5}$ ). In this thesis we choose the representative deep water wave height, determined through exponent five over two of the deep water wave height ( $H_0^{2.5}$ ), is the equivalent wave energy for longshore sediment transport and the representative deep water wavelength and period, determined from the estimation of the deep water wave steepness of the predominant waves direction.

- The formula of the representative wave height on the predominant wave:

$$H_{repr} = \sqrt[2.5]{\frac{\sum_1^n H_0^{2.5}}{n_w}} \quad (3.1)$$

- The representative wavelength and wave period based on the estimation of the average wind **wave steepness** was obtained from Saville (1962) equation:

$$S_w = \frac{H_0}{L_0} = \frac{H_{repr}}{L_{repr}} = 0.04 \quad (3.2)$$

then  $T_{repr} = 4 H_{repr}^{0.5}$  (3.3)

Where :

$H_0, L_0$  - Deep water wave height and wavelength;

$H_{repr}, L_{repr}, T_{repr}$  - Representative wave height, wavelength, and wave period;

$n_w$  - number of waves in the dominant direction;

$S_w$  - Wave steepness.

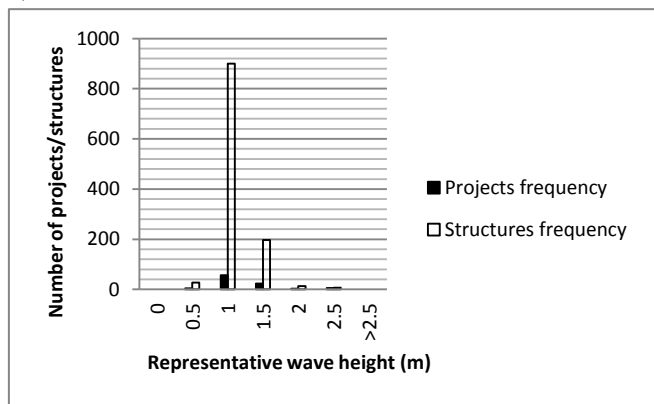
From the statistic wave data of the Kaike project in Fig 3.7 above is an example, to determine by the values of representative wave on the predominant wave direction of 22.5 degrees, which has:

$$H_{repr} = 1.076(m), \text{ then } L_{repr} = \frac{H_{repr}}{0.04} = 26.9(m) \quad \text{and } T_{repr} = 4 H_{repr}^{0.5} = 4.15(s).$$

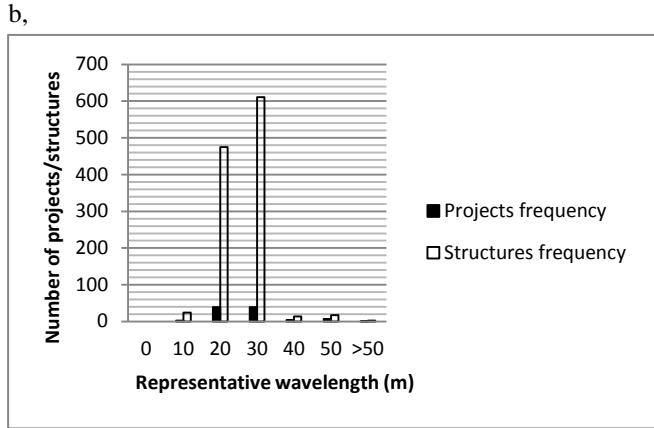
Similar to the Kaike project, continue to follow the same steps as mentioned above, to calculate deep-water wave at other projects. The results of the representative wave values for the projects is shown in detail in the electronic appendix 2 at TUDelft Datacenterum (<http://dx.doi.org/10.4121/uuid:9a2775c0-7c64-4fe1-bf02-221574825197>), and the distribution of projects and structures for representative wave characteristics show in figure 3.9.

a,

The representative wave height ( $H_{repr}$ ) ranges from under 0.5 to 2.5m, and the largest distribution of projects and structures varies the representative wave at 1.0 and 1.5m height (Fig. 3.9a).



Most projects and structures have the representative wavelength around 30m and 20m (Fig.3.9b)



The representative wave period vary from just under 3 seconds to slightly over 6 seconds. A majority wave period of projects and structures is around 4 seconds and the second biggest frequency wave period at 5 seconds (Fig.3.9c).

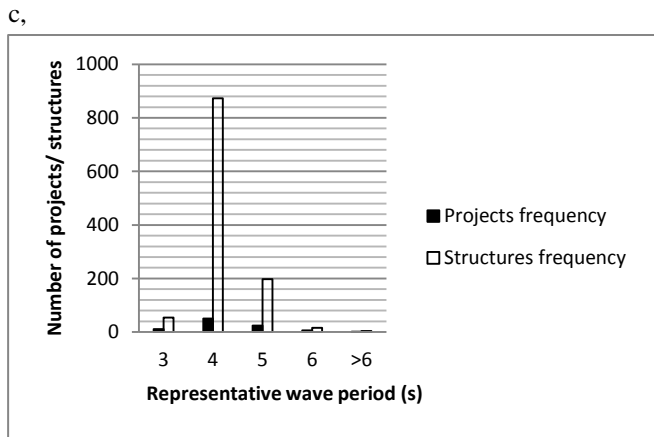


Figure 3.9: The distribution of projects and structures for representative wave parameters

To validate waves from the ERA-40 and WIS, waves in the report of projects are used for a comparison: There are limited reports of projects indicating the value of wave heights used for sediment transport. Only in nine projects a typical significant wave height is mentioned. The comparison of this wave height with the significant wave height in the ERA-40 and WIS, is shown in figure 3.10. From this figure it can be seen that six cases of wave heights in the reports are higher than the waves in the ERA-40 and WIS, with different gaps from 15.5% to 45.7%. There are three cases of waves in the reports that are lower than the waves in the ERA-40 and WIS, the different gaps seem to have a similar ratio, from 15.5% to 42.8%. Therefore, waves in the ERA-40 and WIS can be accepted for analysis.

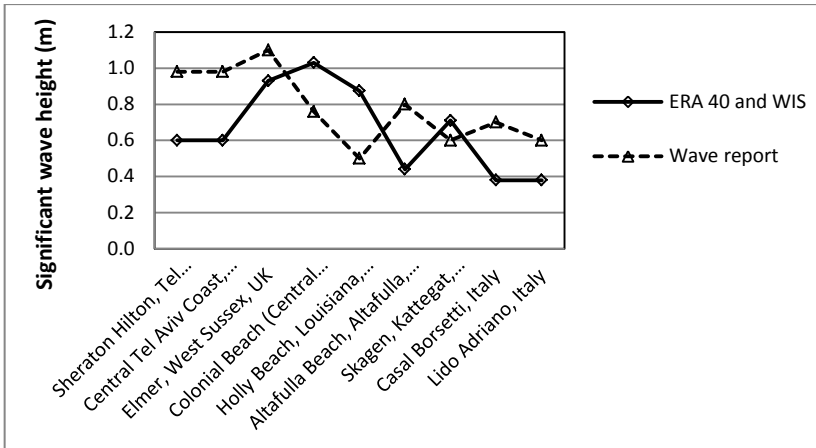


Figure 3.10: Comparison between waves collection and waves in the reports

To sum up, through re-analysis of the deep-water model – the ERA-40, we can estimate waves at most projects (84 over 93 projects) in Europe, Japan and some in the US and wave of the nine projects in the Great Lakes in US are from the WIS hind-cast. The achievement values are significant height of combined wind waves and swell, waves period, and dominant wave directions, therefore, the representative wave characteristics are identified.

### 3.6.2 Tides

Spring tidal ranges ( $h_{\text{tide}}$ ) at all the projects were collected from the reports. A majority of projects has a tidal range of less than 2.0m. The highest frequency of the projects occurred at the tidal range of 1.0m and 0.5m, occupied 38 and 34 projects, respectively. Seven projects had a tidal range between 2m and 4m. Only 3 projects have a tidal range higher than 4m (see figure 3.11). This seems to indicate that most of the collected projects are from micro-tidal coasts.

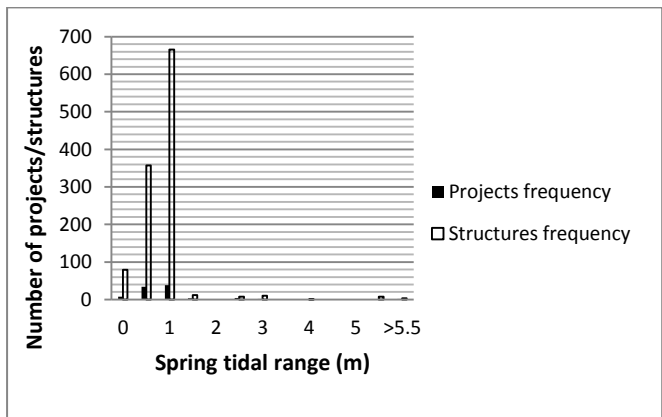


Figure 3.11: The spring tidal range distribution

### 3.6.3 Oceanic currents

Understanding oceanic currents comprises 3 parts: The rise and fall of the tides, the wind driven currents, and the temperature and salinity circulation process. However, the data of the oceanic currents at the projects' locations consist of basic survey data. The author only considers the projects that appear to have a significant or an insignificant influence on the oceanic currents. The results found that 22 projects are located at significant oceanic currents, while the other 71 projects are located at insignificant oceanic currents. For more details see appendix 2 in TUDelft Datacentrum (<http://dx.doi.org/10.4121/uuid:9a2775c0-7c64-4fe1-bf02-221574825197>).

## 3.7 Data measurement of shoreline response

### 3.7.1 General

Measurement of the shoreline responses behind detached breakwaters is based on series of aerial imagery on Google Earth. Google Earth shows aerial images mostly in the period from 1972 until 2013. In general, the frequency of the aerial images is unbalanced at the different locations. It means that the images from the projects could be taken during this period, but they were normally taken once a year, some were taken several times a year, and others were taken only a few times during the whole period.

Identify the location of a project on Google Earth: Although the projects were usually mentioned in reports by the name of the local area, they were seldom shown with their global coordinates. From the name of the project location we can search out structure(s) parallel to the nearby coast. Based on additional information of the project such as number of schemes, parameters, even plan shape, it was possible to confirm that it is the correct site. After determining the exact location, it is useful to pin it down, to write down the project name, and to identify its global coordinates.

Investigation of images on the project sites, focusing on the location of four positions of shoreline in/around the middle of the structures, up and down-drift of the projects, and opposite gaps. Attaining data from the images, such as distance from the centre line along a structure to different parts of the coast behind and from a structure to the erosion points. The specific distances which we are concerned with are the tombolo width ( $T$ ), salient edge to the structure ( $X$ ), opposite gap distance to the structures' central axis ( $X_G$ ), maximum up and down-drift distances to the structure ( $X_U$  and  $X_D$ ), and distance along the centre line from the head of the first and the last structure to the maximum erosion point of up and down-drift, respectively ( $D_U$  and  $D_D$ ) (see figure 3.1).

Achievement of data, by using Google tools of measurement, runs as follows: at first, distinguish the objects of breakwaters, sandy beach, and water by colour and its characteristics on the images. Second, stretching the symmetry axis of the scheme (parallel to the shoreline).

And then measuring a length from the symmetry axis to the shoreline, making sure that the measurement is perpendicular and accurate. The details of the achievement of data of the different states will be shown in the next sections.

### 3.7.2 Measurement of the accretion

Sand was to be transported from areas nearby into the embayment zone and towards the shoreline. Inside the embayment sand was deposited around the axis of symmetry (perpendicular to the shoreline). From time to time, a sand siltation joined the shore and grew towards the breakwater. The term of “accumulation” means an increase in the beach profile by comparing the original beach between two heads of breakwater.

Nir (1982) found that for the detached breakwaters built inside the predominant surf zone **the static equilibrium state was achieved in three to five years from the construction date.** Applying the Nir’s theory to the field of observation, the aerial images also indicated that the new sand accretion behind each structure finally reached a certain shape and a specific magnitude. The shapes can be a tombolo or a salient, which seemed to fluctuate around an average size, to be observed in a series of the images after five years from construction. The shorelines from that time are called the ‘static equilibrium shorelines state’.

Choose the specific representative images: Two images during the static equilibrium state are concerned with features of the most recent highest and lowest sea water level, as well as the least cloudy effect. The most recent images attempt to ensure that at this time the shoreline meets stability, and recent images have a more accurate resolution. The second features are the highest and the lowest sea water level, which represent the mean high tide level and the mean low tide level. The facts, at the time the photos were taken, and at the time of sea tides going up and down, seem to have no correlation. However, we accept the hypothesis that the highest water level in the selected photo is the mean high tide level, and that the lowest water level in the selected photo is the mean low tide level. The last feature is the cloud effect, the less clouds the clearer the image, thus it is necessary to choose images without cloudy effects.

Distinguishing the forms of accumulation at the shoreline behind each breakwater: We need to divide accumulation into two types of siltation; a connected form to the breakwater and an unconnected form. In case of a connection, it is called a tombolo formation, and the width of tombolo alongside of the structure is measured. In the unconnected form, we make a measurement at the perpendicular distance from the edge of the equilibrium shoreline to the centre of breakwater. Measurement of the equilibrium shoreline behind the structure is applied for every individual breakwater in the schemes. Both representative images, mentioned above, are measured in the same way.

When we observed the two representative images, there were three cases: Case one: the accretions in both images were tombolos. Case two: the accretions in both images were salient. Case three: the accretion in one image meets salient, and in other image meets tombolo. The

different case forms will be separate in the statistics table. For instance, figure 3.12 and 3.13 illustrate measurements of equilibrium shorelines at two projects. In the Central Tel Aviv Coast project, both equilibrium shorelines appear as salient formations at low water levels and high water levels, shown in the aerial photos taken on 5/11/2011 and 19/6/2012, respectively. While in Elmer, the UK project, shapes occurred as tombolo at a low water level on 06/6/2013, but as salient shapes in photos taken on 14/5/2007.

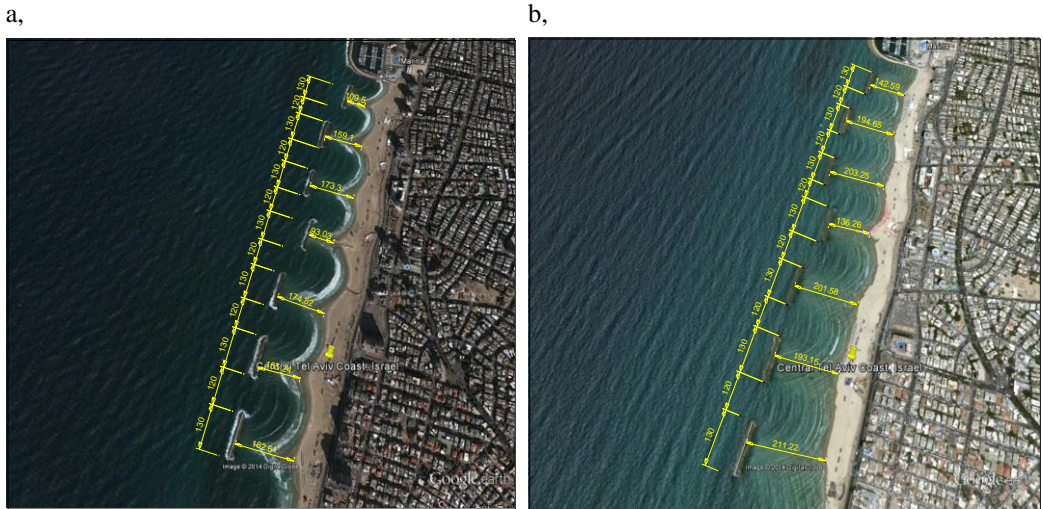


Figure 3.12: The salient measurements at low water level (a) and high water level (b) at Central Tel Aviv Coast, Israel



Figure 3.13: The tombolo measurements at low water level (a) and the salient measurements at high water level (b) at Elmer, the UK

Choose the mean value for each project in the observation of a single and a segmented project: If it is a single structure project, then the mean data of measurement is achieved as individual values. If it is a segment of a structures project, the mean data of a project is an average value of all individuals in this project; it has the same state of equilibrium. The mean value of accumulation is defined as the value at the Mean Water Level (MWL).

Conduct in the order of these steps above, the procedures for the 93 collected projects. The value achievement is shown in appendix 3 in the link <http://dx.doi.org/10.4121/uuid:9a2775c0-7c64-4fe1-bf02-221574825197>: There are 32 cases with a tombolo formation, 57 cases with a salient formation, 10 cases have both states – tombolo formation at low tide and salient formation at high tide, and 14 cases have no sinuosity – no response or erosion.

### 3.7.3 Measurement of the shoreline opposite the gap

When a project is built as segmented breakwaters, there are gaps between them. The shoreline opposite the gap is affected by waves, including diffraction waves and refraction waves. Diffraction waves are induced by waves interacting with the heads of structures; the refraction waves penetrate directly through the gaps. As the result of waves, current circulation cells are also induced. Behaviour of the shoreline opposite the gap changes from time to time. As a consequence, the shape of the equilibrium shoreline occurs like an arc. In terms of observation of the shoreline changes opposite the gap, the measurement of the furthest point in the arc is of concern.

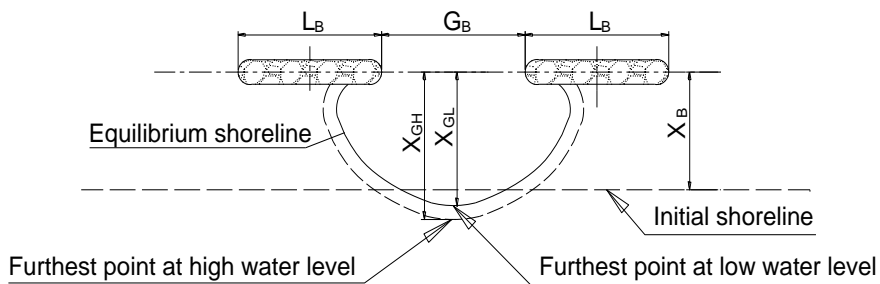


Figure 3.14: Definition of measurement the shore opposite the gap

The measurement is conducted on two aerial images, which are chosen to be the same as in the case of accumulation, mentioned in the previous section. The two values of distance from the centre axis to the furthest point are collected. Similar to the accumulation, these values are the representative distances at the high and at the low tide level. The distance value at the mean water level is the average distance of the high and the low water level (figure 3.14).

A total of 71 segmented projects are measured. In the survey, the 71 projects are divided into 83 cases of shoreline response, including 22 cases of tombolo, 42 cases of salient, 8 cases



of both tombolo and salient, and 11 cases of no sinuosity.

### 3.7.4 Measurement of the shoreline at up and down-drift

The purpose of this section is to survey the change of beach width at the up- and the down-drift in the states before and post construction. It is assumed that the initial shoreline at the up- and the down-drift coincided and was straight with the part of the shoreline just behind breakwaters. In other words, the distance from the up- and the down-drift to the centre line of the structures is the same initial offshore distance. The post construction state presents the behaviour of the up and down-drift by its positions. These distances will be measured and compared to the initial offshore distances.

At first, we should find out the distinguished areas by a qualitative theory of interaction of waves in the embayment. Three regions are defined: Region 1 - with wave height gradients and the turning of the front due to wave refraction – diffraction is important. Region 2 –presents wave height gradients and wave refraction is relevant. And, region 3 - structures have no effect on the wave field; the wave height gradients are slight and the wave fronts remain consistent (figure 3.15).

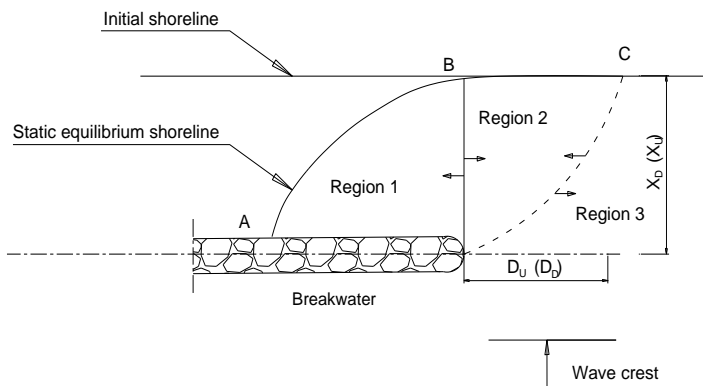


Figure 3.15: Sketch of the regions generated by detached breakwater

Secondly, to identify the impacted points: Gourlay (1974) examined the interaction between breakwater and the hydrodynamic field in dominant wave waters in the laboratory. He found rip currents are strong and narrow, these currents flowing seaward through the surf zone and affecting an adjacent sediment transport (see figure 3.16).

Then, points A, B, and C in figures 3.15 and 3.16 are the border points of the effect areas of the equilibrium shoreline by the breakwater. Point C is of interest as the limited point of structure effect at the up- or down-drift of post-construction. A portion of the equilibrium shoreline ABC stands like a curve, and the part of shore from point C outward (to the right) is

almost straight; thus, accepting point C as a transitional point from the curve to the straight line.

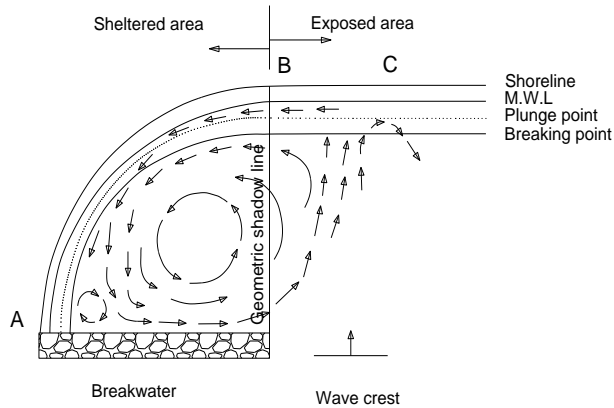


Figure 3.16: Rip currents in the lee of breakwater in a physical model

(modified from Gourlay (1974))

In the observation, the C points can be recognized on the two representative images as the “control point”. Measure two values of each C point, namely the distance to the centre shore parallel axis and the distance to the head of breakwater. The  $X_U$ ,  $D_U$  and  $X_D$ ,  $D_D$  stand for the C distances from adjacent breakwater’s head to the up- and down-drift, respectively (see figure 3.15). Each breakwater project will have one control point of the up-drift, and one control point of the down-drift.

Finally, to measure, by looking up the 93 projects that were listed and by finding the transitional point C, some situations occurred: At the control point another structure existed, or point C could not be defined. If the other structures were groins, revetments, and even other breakwaters, it was found that additional structures might prevent demerits of the consequences of breakwaters. In that situation, the C point is not a “natural” point per definition. The blocked structures at C points were taken out of the data series. If the situation could not identify the control point C on the equilibrium shoreline because of an unusual profile, then we accept these as the missing values. Therefore, the total number of the control points at the up-drift measured numbered 56, and at the down-drift a total of 52 points were found.

### 3.8 Concluding remarks

1. This chapter focused on the data of real projects in different countries. In total 93 projects with 1144 structures were collected. The data related to the projects are a combination of structure parameters, physical conditions, and measurements of shoreline results.

2. The inventory of the structure parameters mostly originated from reliable reports of projects, journal, and papers. Values of primary parameters exploited were: type of project (single or segmented), length of breakwater, offshore distance from the initial coast, gap width, structure freeboard, crest level width, water depth at structure, orientation of structure, and median grain size. Fortunately, most of the values were presented in several published documents, and, thus, we were able to use them.

3. Physical conditions at the projects mainly focussed on wave climate, tidal range, and current. Waves were achieved from two models, the re-analysis of the global atmosphere and surface conditions for over 45 years (ERA-40), and the model of estimating waves from past wind events (WIS). The data of these models were used to calculate the representative wave of each project. Moreover, other aspects of the physical conditions, such as tidal range and current were also listed.

4. Measurement methods were based on aerial images, which observed shoreline changes behind detached breakwater(s). The special points to make a comparison between pre-construction and post-construction shoreline that were measured included, the sand siltation, the opposite gap, controlled points at up- and down-drift. During measurements of shoreline change, several definitions were presented, such as the time of static equilibrium shoreline after construction, and the identity of limited effect of structures.

The database of inventory parameters, physical conditions, and measurement results will be used to analyse behaviour of parallel breakwater(s) on the shoreline behind and on the adjacent shoreline to the structures in the next chapter, chapter 4.

## CHAPTER 4: ANALYSIS OF PROTOTYPES DATA

### 4.1 Introduction

The previous chapter described how data were collected. In this chapter, the methods for analysing and the development of the relationship of the shoreline changes are described. In fact, the morphology of the shoreline behind the breakwaters is a consequence of many individual sediment transport events caused by successions of waves, tide, currents and structure interaction. In this sense, the shape of the beach in a sheltered and adjacent area may be realized as representative of an average form over time. The stability of a wide beach depends on the difference between the volumes of sediment entering and leaving due to waves, tide and currents interacting with structures. The position of a new shoreline will be eroding, accreting or will even remain in equilibrium. In these terms a situation will develop in which the location is evolving in response to a variety of conditions.

From the viewpoint of the modelling of the shoreline changes, and in order to make predictions, we measured the shoreline at several specific points as mentioned in the previous chapter. The data are used to analyse and to recognize the relationship trends of the points on the equilibrium shoreline; then to find out general functions of the empirical relationships.

Various authors have proposed models of the basic empirical relationships, however, the models used different types of data to develop the evaluation of the shoreline response. These models will be used in comparison to the developed models with the prototype development.

## 4.2 Analysis of shoreline siltation

In this section, we will analyse and find out the key parameters' effect on the siltation results, based on the basic analysis of each pair of dimensionless parameters. However, the siltation is the result of complex events driven by many parameters. On the basis of the collected data of the structure parameters, the physical conditions, sediment properties and the measurements of the equilibrium shorelines are taken into the account, then the relationships of the shoreline changes by a combination of these parameters will be found. Herein, the four states of siltation are tombolo, salient, both tombolo and salient, and no sinuosity will be analysed.

### 4.2.1 Classification based on the ratio of the breakwater length and the breakwater offshore distance ( $L_B/X_B$ )

From the observations and the measurements, the state of the equilibrium shore can be divided into four categories: Tombolo formation, salient formation, both tombolo and salient formation, and no sinuosity formation. The data of these different forms are sorted in detail in appendix 4 in the link <http://dx.doi.org/10.4121/uuid:9a2775c0-7c64-4fe1-bf02-221574825197>.

Take the statistics of a dimensionless parameter of the breakwater length and the offshore distance ( $L_B/X_B$ ), shown in table 4.1:

Table 4.1: Ratio of a dimensionless efficiency  $L_B/X_B$

$L_B/X_B$	Number of cases			
	Tombolo	Salient	Tombolo + salient	No Sinuosity
$\frac{L_B}{X_B} < 1$	7	39	3	3
$\frac{L_B}{X_B} \geq 1$	22	18	7	11
No ratio	3	0	0	0
Total	32	57	10	14

It can be seen from the table 4.1 that there are 22 cases of tombolo formation, accounting for 69% of the total when  $L_B/X_B \geq 1$ . While there are 7 cases, counting 22% when  $L_B/X_B < 1$ , there are also 3 cases which have no ratios of  $L_B/X_B$  because of the absence of information of  $X_B$  parameters. Contrary to the percentage of the tombolo form, there are 39 cases of the salient form, taking 75% of the total when  $L_B/X_B < 1$ , while 18 cases, accounting for 25%, are the salient form, when  $L_B/X_B \geq 1$ . In this state of both the tombolo formation at low tide and the salient formation at high tide, there are 3 cases when  $L_B/X_B < 1$  and 7 cases when  $L_B/X_B \geq 1$ , accounting for 30% and 70%, respectively. In a state of no sinuosity, there are 3 cases when  $L_B/X_B < 1$  and 11 cases when  $L_B/X_B \geq 1$ , accounting for 21% and 79%, respectively.

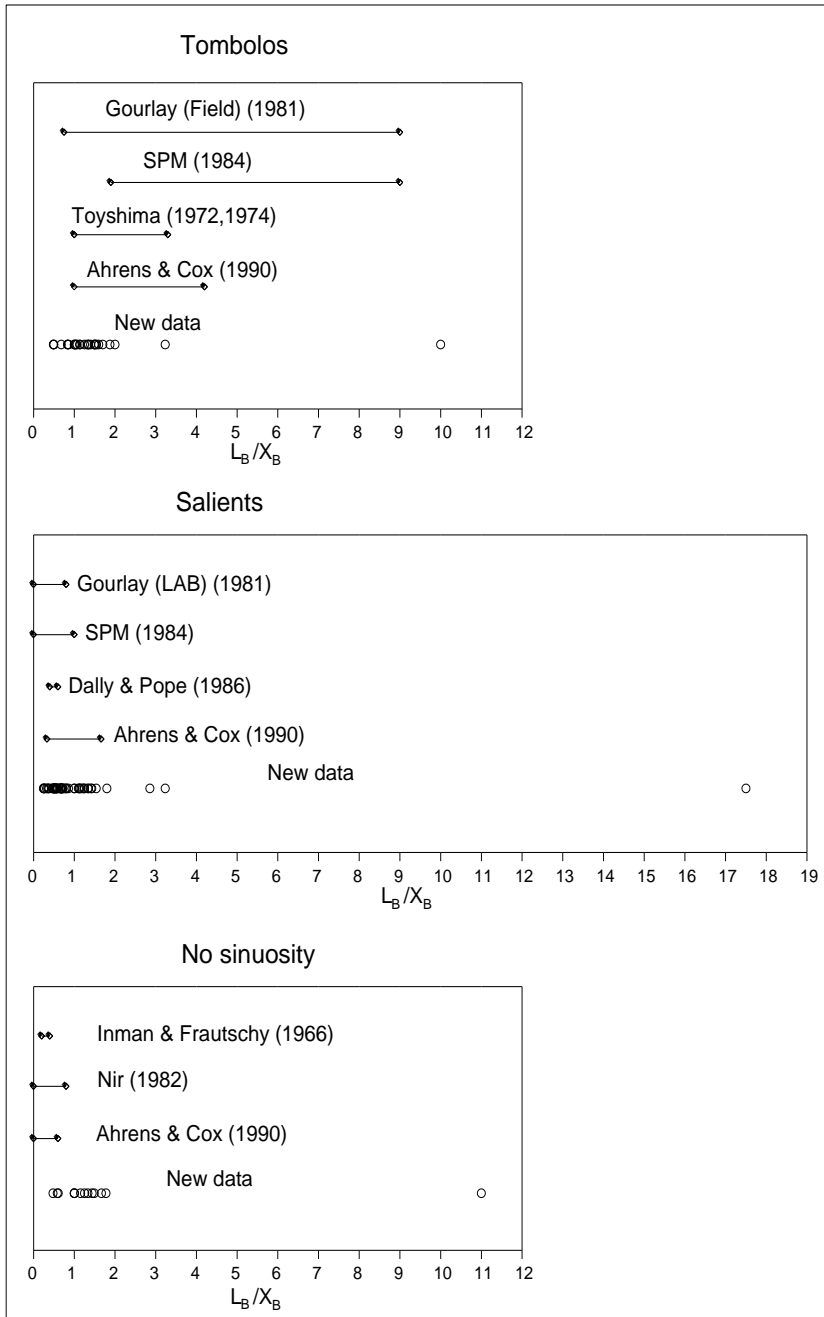


Figure 4.1: Comparing the field of the new data with the existing graph (after Rosati (1990))

In figure 4.1, the data of these prototypes has been plotted on the existing design graphs. The figures indicate that the expected coastline response of the previous studies is not always in agreement with the prototype measurements. This is possibly because many other parameters of the beach-breakwater interaction, such as tide, oblique wave, sediment property, and gap width, are not included in the existing design graphs. However, the Ahrens & Cox graphs are the closest prediction compared with the data of the tombolo and the salient cases.

Through the classified table and the comparison graphs, we realized that using the values of the  $L_B/X_B$  are a boundary to demonstrate that the different formation states are still unclear. However, it can be found that **1 is the boundary ratio to distinguish the state of the tombolo and the salient form** as acceptable. In other words, if  $L_B/X_B \geq 1$ , then a tombolo will most likely form, otherwise in the case of  $L_B/X_B < 1$ , a salient will most likely form. However, the no sinuosity formation is unclear under the ratio of  $L_B/X_B$ .

#### 4.2.2 The effect of dimensionless parameter of the breakwater length to the offshore distance

The effects of the dimensionless breakwater length to the offshore distance on the siltation in the difference states of the equilibrium shoreline will be analysed on the measurement data:

- **In the case of the tombolo**, finding the relationship between the three involved parameters, namely **the length of the breakwater ( $L_B$ )**, **the distance to the shoreline ( $X_B$ )** and **the tombolo width ( $T$ )**. These variables are taken to be dimensionless. Choosing  $X_B$  as a common and important variable. Using the  $X_B$  variable repeatedly in the two dimensionless parameters, then a linear relationship is found. In figure 4.2a this linear relation is shown when  $T/X_B$  values are plotted against  $L_B/X_B$  values, giving equation:

$$\frac{T}{X_B} = 0.85 \frac{L_B}{X_B} - 0.5 \quad (R^2=0.95) \quad (4.1)$$

As can be seen in figure 4.2a, most of the values of the  $L_B/X_B$  vary from 0.5 to 3.2, and the values of  $T/X_B$  from 0.1 to under 1.5, but only one “special point” has  $L_B/X_B = 10$  and  $T/X_B = 8.35$ . This case is the project in Metaurilia, Italy, which has seven breakwaters. The single structure is quite long with its length of 200 m, but its location is a very short distance from the initial shoreline, just 20 m. When we take this particular point out of the totality of the data, we can see that new relationship in figure 4.2b becomes:

$$\frac{T}{X_B} = 0.44 \frac{L_B}{X_B} - 0.003 \quad (R^2=0.51) \quad (4.2)$$

To compare equation 4.1 with 4.2, it seems that there are different constant values, slope values and, also, values of the R-squared. However, in general, they still have a linear relationship. The data with or without “special point” still have a linear trend.

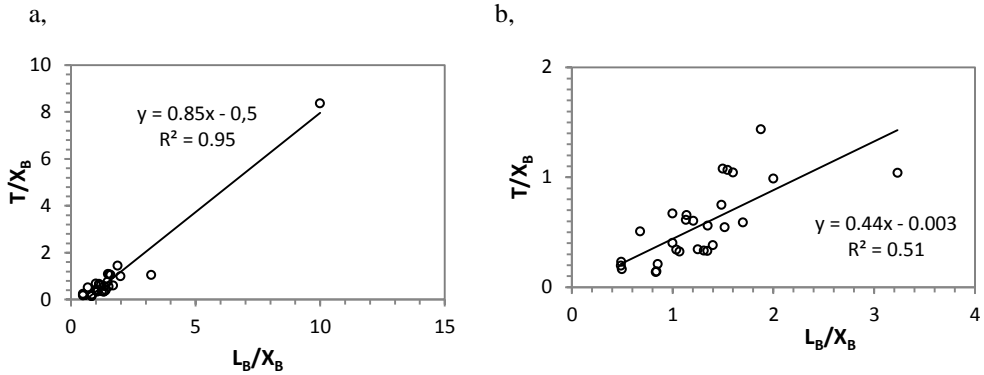


Figure 4.2: Relationship between  $T/X_B$  versus  $L_B/X_B$  of tombolo formation

- In the case of a salient, similar to the method of the tombolo analysis, the three involved parameter variables are the length of breakwater ( $L_B$ ), the distance to shoreline ( $X_B$ ), and the salient edge to breakwater ( $X$ ) to be dimensionless. Choose the  $X_B$  as a common and the most important variable. Push the  $L_B$  variable repetition in two parameters, which has relevance when the relationship is exponential. As shown in figure 4.3, the single curve results, when the values of the  $X/L_B$  are plotted versus  $L_B/X_B$ , having the equation:

$$\frac{X}{L_B} = 0.62 \left( \frac{L_B}{X_B} \right)^{-1.15} \quad (R^2 = 0.64) \quad (4.3)$$

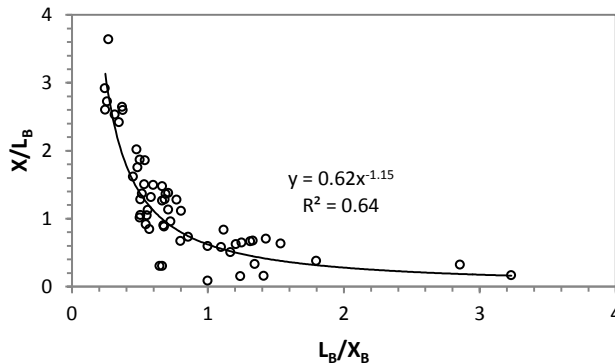


Figure 4.3: Relationship between  $X/L_B$  versus  $L_B/X_B$  of salient formation

The exponential trend of the data of the  $X/L_B$  and  $L_B/X_B$  is rather clear, also R-squared is quite high ( $R^2 = 0.64$ ). In addition, Hsu and Silvester (1990) presented the exponential relationship based on the combined source data of the prototype, the physical models and numerical models. Therefore, the relationship of dimensionless of the breakwater length to the offshore distance and the salient edge distance ratio is acceptable for the exponent relationship.



- Similarly the relationship of the three parameters in the salient form. The relationship between  $X/L_B$  and  $L_B/X_B$  is plotted with the dataset in a state of no sinuosity. It is shown in figure 4.3a, and giving the equation:

$$\frac{X}{L_B} = 1.25 \left( \frac{L_B}{X_B} \right)^{-0.83} \quad (R^2 = 0.89) \quad (4.4)$$

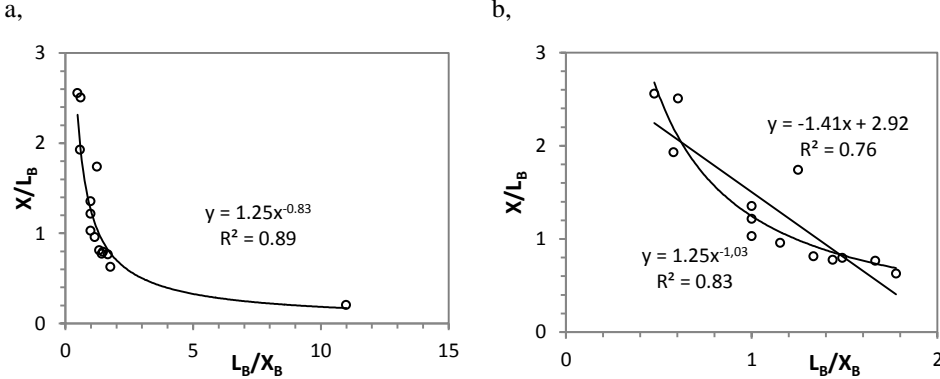


Figure 4.4: Relationship between  $X/L_B$  versus  $L_B/X_B$  of no sinuosity formation

In figure 4.4a, the majority of the points of  $L_B/X_B$  were from 0.5 to 1.9, and the points  $X/L_B$  were from 0.6 to just over 2.5, but there was one special point with  $L_B/X_B = 11$  and  $X/L_B = 0.203$ . This point represents the project at Grottammare (South of the Tesino River mouth), Italy. This project has an uncommon structure with a length of 550 m long and a 50 m offshore distance. If we take this point out of the data, which might be driving the relationship, we have a new scatter in figure 4.4b. The relationship equation in figure 4.4b can be linear or exponential as follows:

$$\frac{X}{L_B} = -1.41 \frac{L_B}{X_B} + 2.92 \quad (R^2=0.76) \quad (4.5)$$

$$\frac{X}{L_B} = 1.25 \left( \frac{L_B}{X_B} \right)^{-1.03} \quad (R^2= 0.83) \quad (4.6)$$

From the equations 4.4 and 4.5, the R-squared of the exponent relationship ( $R^2 = 0.83$ ) is higher than that of the linear relationship ( $R^2 = 0.76$ ). It means that, when the special point is omitted, the relationship is still the preferred exponent equation. Then, the exponent relationship between dimensionless of the breakwater length to the offshore distance and dimensionless of the siltation edge is accepted.

#### 4.2.3 The effect of dimensionless parameter of the gap width to the representative wavelength

The ratio of the gap width to the wavelength strongly effects the distribution of the wave height in the bay of segmented detached breakwaters. Simply understood, if increasing the ratio of gap to wavelength, then the amount of wave energy transmitted into the bay increases,

while reducing the effects of diffraction (showed in figures 2.42 to 2.52 of Shore Protection Manual – SPM 1984) . The more wave energy transmission, the more the fluid motion increases in the bay. Consequently, the sediment in the shadow zone behind the breakwater might tend to prevent accumulation. Then accumulation parameters should be analysed with the ratio of the gap width to the wavelength.

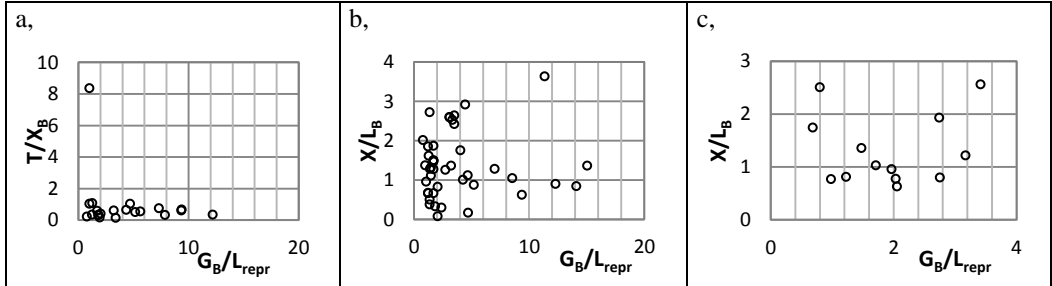


Figure 4.5: Effect of dimensionless of the gap width to the representative wavelength

a, Tombolo form; b, Salient form; c, No sinuosity form.

Based on the collected data from the mentioned projects above, we need to examine a relationship of wave energy transmission ratios ( $G_B/L_{repr}$ ) to accumulation ratios ( $T/X_B$  or  $X/L_B$ ) (see figure 4.5). **The scatters of the three cases indicate an unclear trend.** However, we can see that in the tombolo form (figure 4.5a) there were a wide range of transmission ratios, from 0.5 to 12, while the accumulation ratios were mostly under 1.5, except only one value was just over 8.0. In the case of the salient form (figure 4.5b), similar to tombolo form the wave transmission ratios were variable, ranging from 0.8 to 15, while more than half of the ratios of the salient's edge distance to breakwater length were lower than 1.0, and less than half of the ratios were from 1.0 to just under 4.0. The no sinuosity form has ratios of wave transmission from 0.7 to 3.5, but the measure of shore response seem to vary from 0.8 to slightly over 2.5. Therefore, the breakwaters were built with the variety ratios of the gap width to the representative wave length.

#### 4.2.4 The effect of dimensionless parameter of the oblique incident wave ( $\sin\alpha_0$ )

For the oblique incident wave cases, the sediment accumulation in the sheltered area of the up-drift of the breakwater is larger than at the down-drift. Moreover, the oblique incident waves result in deflection of the salient and the tombolo in the direction of littoral drift. Actually, the incident wave climate at any given site typically consists of a variety of wave directions. In addition, the detached breakwaters are usually oriented to be parallel to the initial shoreline, which is typically at a moderate angle to the dominant wave direction. Furthermore, the oblique predominant incident waves effect the longshore transport in the sheltered area. Thus, practically, in the option of the evaluation stage of the equilibrium shoreline, the angle of the waves approaching the shore should be used.

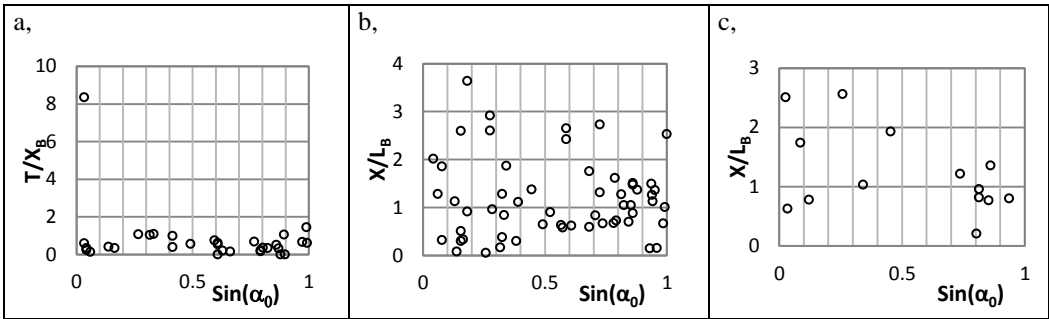


Figure 4.6: Effect of the oblique predominant incident waves on dimensionless of the sediment in the lee. a, Tombolo form; b, Salient form; c, No sinuosity form.

Figure 4.6 shows the scatters of the accumulation ratios ( $T/X_B$  or  $X/L_B$  versus the oblique predominant incident waves angle  $\sin\alpha_0$ ). In the three cases of planform, the relationship between them seems to be unclear. However, in the tombolo formation (4.6a), the dominant wave angles spread evenly from 0 to 90 degrees, but the dimensionless ratios of the tombolo width and the breakwater distance were under two, except one value is just over eight. In contrast to ratios of the salient edge distance to breakwater and its length (4.6b), these ratios fluctuated widely and ranged from close to 0 to just under 4 during the variety oblique angles. In the case of the no sinuosity form, through the scatter on figure (4.6c) it shows that it seems to be similar to the salient case, the distance of siltation edge ranged from 0 to 3, and predominant waves approach breakwaters at spread angles.

Taking a look at the planforms behind the breakwater schemes in the aerial images, the shoreline planform shapes are highly dependent on the waves direction climate. This is particularly noticeable for the tombolo, which seems to point into the waves. Normally, tombolos at the up-drift side were filled and its apexes were near the center of structures, also tombolos at the down-drift side were less filled. In case of the salient form, the orientation of the incident waves was related to degree of salient development. The salient angle was quite similar to the tombolo case, as well as the oblique dominant incident waves, and salients at the up-drift also seem larger than at the down-drift. Thus, the position of tombolo and salient equilibrium is dependent upon the predominant wave direction. If the dominant wave direction changes significantly in seasons, the equilibrium position of the bulge may readjust accordingly. In addition, strong oblique predominant incident waves will drive the sheltered area by the longshore currents, which can restrict the size of the salients and prevent them to reach the breakwaters. Unfortunately, the different magnitude of the siltation at the up- and down-drift as well as the orientation of the siltation, were not presented in the statistics. Only the mean values of the segmented projects were used as the representative values. The seasonal fluctuation was not mentioned either, but the equilibrium shoreline as the static shoreline after five years of construction was accepted.

#### 4.2.5 The effect of dimensionless parameter of the tidal range to the representative wave height

It is extremely difficult to predict which effect of a tidal range induces a tidal current on the shoreline response to detached breakwaters. However, a large tidal range tends to interrupt permanent tombolo formation. Especially if a breakwater is considerably overtopped during the high tide, the salient will certainly be prohibited to reach the breakwater and even have difficulty attaining a smooth salient shape. Therefore, it is necessary to examine the impact of the tidal range associated with waves to shore formation.

Figure 4.7 presents **scatters** of relationships of the ratios; on the horizontal axis the ratios of the tidal range to representative wave height ( $h_{\text{tide}}/H_{\text{repr}}$ ) are shown, and the vertical axis shows the ratios of the shore response ( $T/X_B$  or  $X/L_B$ ). In general, all cases did not show a clear relationship between the two ratios. In the tombolo and the salient cases (figure 4.7a,b), a majority of the values  $h_{\text{tide}}/H_{\text{repr}}$  was lower than 1.0, occupying more than 70% of the total. In contrast, the ratios in the no sinuosity case (figure 4.7c) were quite small, just 14%. In addition, the ratios of accumulation in the tombolo form were under 1.4, except one value was just over 8.0. The magnitude of the salient ratios ( $X/L_B$ ) fluctuated from 0.15 to slightly under 4.0 in both cases of the salient and the no sinuosity.

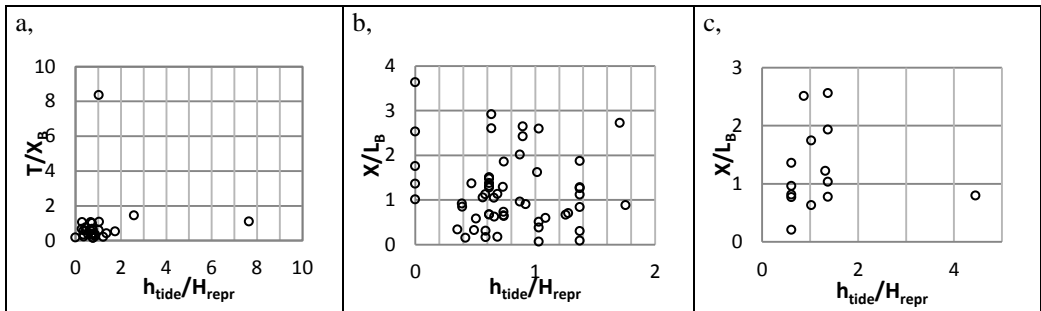


Figure 4.7: Effect of dimensionless tidal range to representative wave height

a, Tombolo form; b, Salient form; c, No sinuosity form.

#### 4.2.6 The effect of dimensionless representative wave height to median sand diameter

The longshore transport rates and the characteristic profile of the equilibrium beaches are affected by the sediment size and the sediment distribution. The sediment size can have an effect on the shore planform as well as on the rate of the beach response. Normally, a coarser sediment beach will have a steeper equilibrium profile than a finer sediment beach. In case of waves approaching a coarse beach, there seems to be less refraction, because of a steeper offshore bathymetry; hence, these waves can reach the project at more oblique angles. Additionally, the coarse sediment beach will respond more slowly and attain an equilibrium shape later than a fine sediment beach. Consequently, with the same wave conditions tombolo

formation might not happen on a coarse sand beach, but instead a tombolo can be formed on a fine sand beach.

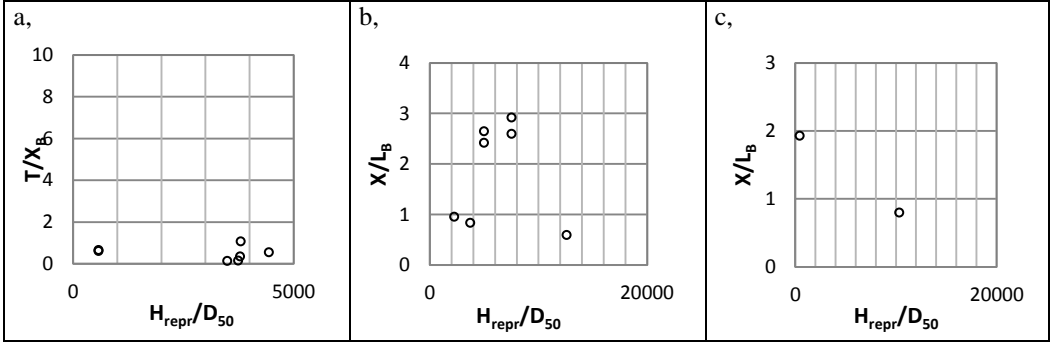


Figure 4. 8: Effect of sediment size (relative sediment uplift ability,  $H_{repr}/D_{50}$ ) on planform a, Tombolo form; b, Salient form; c, No sinuosity form.

In the data set of the pre-construction parameters of the projects, the sediment properties are shown in a limitation, so that the contribution is just 21. Considering an influence of grain size to the planforms in the lee, the sediment uplift ability ( $H_{repr}/D_{50}$ ) is related to the accumulation ratios ( $T/X_B$  or  $X/L_B$ ). In the three cases in figure 4.8, it is difficult to find out a clear trend of relationship because of the availability of few data in each case. However, the sediment uplift ability values in the tombolo state tend to be smaller than in the two other states.

#### 4.2.7 Combination of the effects

According to the analysis of qualitative and quantitative data in the pair of ratios in the sections above, it can be said that the dimensionless ratios of the shoreline response ( $T/X_B$  or  $X/L_B$ ) clearly have a relationship with the ratios of the breakwater blocking ( $L_B/X_B$ ). There is a linear relationship in the tombolo formation and in the exponential relationship in the other formation of the salient as well as in the no sinuosity.

The other dimensionless ratios also have a considerable influence on the shoreline response. The dimensionless ratios occurring are: the wave energy transmission ( $G_B/L_{repr}$ ), the oblique incident wave angle ( $\sin\alpha_0$ ), the tidal range effect ( $h_{tide}/H_{repr}$ ), and the sediment uplift ability ( $H_{repr}/D_{50}$ ). Although in theory these factors can certainly have an effect on the accumulation ratios, the data however do not show a clear trend on the scatters.

The fact is, that in the lifetime of a breakwater, not only each individual impact factor has an effect on the shoreline response, but also the combined effects of these the factors need to be acknowledged. Therefore, we suppose that the dimensionless parameters for the equilibrium state of the shoreline behind detached breakwaters are a function of the following parameters:

$$\frac{T}{X_B} \left( \text{or } \frac{X}{L_B} \right) = f \left( \frac{L_B}{X_B}, \frac{G_B}{L_{repr}}, \sin\alpha_0, \frac{h_{tide}}{H_{repr}}, \frac{H_{repr}}{D_{50}} \right) \quad (4.7)$$

Where :

$\frac{T}{X_B}$  is the ratio measure of magnitude of tombolo;

$\frac{X}{L_B}$  is the ratio measure of magnitude of salient or no sinuosity;

$\frac{L_B}{X_B}$  is the ratio measure of the efficient breakwater blocking;

$\frac{G_B}{L_{repr}}$  is the ratio measure of the wave transmission through gaps;

$\sin(\alpha_0)$  is the ratio measure of the dominant incident wave direction;

$\frac{h_{tide}}{H_{repr}}$  is the ratio measure of tide range effect;

$\frac{H_{repr}}{D_{50}}$  is the ratio measure of sediment uplift ability.

a. *Tombolo function*

Because of the clear linear relationship between  $T/X_B$  and  $L_B/X_B$  (see figure 4.1), the other four variables in function 4.7 ( $G_B/L_{repr}$ ,  $\sin\alpha_0$ ,  $h_{tide}/H_{repr}$ , and  $H_{repr}/D_{50}$ ) do not have such a clear relationship with the tombolo magnitude ratio ( $T/X_B$ ). Then, we accept a general relationship of the tombolo case in function 4.7 driven by the relationship of  $T/X_B$  and  $L_B/X_B$ . In other words, the tombolo formation has a linear function with the variables. Inferring from equation 4.7, it thus can be written:

$$\frac{T}{X_B} = a_0 + a_1 \left(\frac{L_B}{X_B}\right) + a_2 \left(\frac{G_B}{L_{repr}}\right) + a_3(\sin\alpha_0) + a_4 \left(\frac{h_{tide}}{H_{repr}}\right) + a_5 \left(\frac{H_{repr}}{D_{50}}\right) \quad (4.8)$$

Where :  $a_i = \text{constant } (i= 0 \div 5)$

The linear function 4.8 rewritten as the simple function is:

$$Y = a_0 + a_1X_1 + a_2X_2 + a_3X_3 + a_4X_4 + a_5X_5 \quad (4.9)$$

Where :

$$Y = \frac{T}{X_B}; X_1 = \frac{L_B}{X_B}; X_2 = \frac{G_B}{L_{repr}}; X_3 = \sin\alpha_0; X_4 = \frac{h_{tide}}{H_{repr}}; \text{ and } X_5 = \frac{H_{repr}}{D_{50}} \quad (4.10)$$

Based on the initial data collection of  $L_B$ ,  $X_B$ ,  $G_B$ ,  $h_{tide}$ ,  $D_{50}$ , the physical data of  $H_{repr}$ ,  $L_{repr}$ ,  $\alpha_0$ , and the measurement data of  $T$ , using the linear regression method, find out the value of the  $a_i$ . In the data set of the collection, some data of the parameters mentioned above are unavailable or missing, which then need to be estimated through multiple imputation analysis. Run the linear regression of the new imputed data on the Statistical Package for the Social

Sciences (SPSS), then value  $a_i$  can be found. The result of the tombolo formation is the linear relationship in the following function:

$$\frac{T}{X_B} = -0.8 + 0.9 \frac{L_B}{X_B} + 0.03 \frac{G_B}{L_{repr}} - 0.26 \sin(\alpha_0) + 0.82 \frac{h_{tide}}{H_{repr}} - 0.096 \frac{H_{repr}}{D_{50}} \quad (R^2 \approx 1.0, \sigma = 0.022) \quad (4.11)$$

This complex variable equation has a very high R-squared, almost 1.0, and comparing the R-squared in the basic equation of the tombolo formation 4.1 and 4.2, we found that the general equation 4.11 is still more accurate than the simple equation. Then, an estimation of tombolo magnitude by the complex equation is more accurate than the basic equation.

In case of the single breakwater,  $G_B = 0$  the equation 4.11 is written:

$$\frac{T}{X_B} = -0.8 + 0.9 \frac{L_B}{X_B} - 0.26 \sin(\alpha_0) + 0.82 \frac{h_{tide}}{H_{repr}} - 0.096 \frac{H_{repr}}{D_{50}} \quad (4.12)$$

If the dominant incident wave is perpendicular to the structures, given  $\alpha_0=0$ , then

$$\frac{T}{X_B} = -0.8 + 0.9 \frac{L_B}{X_B} + 0.03 \frac{G_B}{L_{repr}} + 0.82 \frac{h_{tide}}{H_{repr}} - 0.096 \frac{H_{repr}}{D_{50}} \quad (4.13)$$

The formula for the single breakwater in condition of the perpendicular incoming waves is:

$$\frac{T}{X_B} = -0.8 + 0.9 \frac{L_B}{X_B} + 0.82 \frac{h_{tide}}{H_{repr}} - 0.096 \frac{H_{repr}}{D_{50}} \quad (4.14)$$

### b. Salient function

There is clear exponential function relationship between  $X/L_B$  and  $L_B/X_B$  (see figure 4.2), the same as in the tombolo case, while the other four variables in function 4.7 ( $G_B/L_{repr}$ ,  $\sin\alpha_0$ ,  $h_{tide}/H_{repr}$ , and  $H_{repr}/D_{50}$ ) have a less clear relationship with the salient magnitude ratio  $X/L_B$ . Then, to accept that a general relationship of the salient formation in function 4.7 is driven by the relationship of  $X/L_B$  and  $L_B/X_B$ . In other words, the salient formation has the nonlinear - the exponent function. From equation 4.7, it can thus be rewritten as:

$$\frac{X}{L_B} = b_0 \left(\frac{L_B}{X_B}\right)^{b_1} \left(\frac{G_B}{L_{repr}}\right)^{b_2} (\sin\alpha_0)^{b_3} \left(\frac{h_{tide}}{H_{repr}}\right)^{b_4} \left(\frac{H_{repr}}{D_{50}}\right)^{b_5} \quad (4.15)$$

Where :  $b_i = \text{constant } (i= 0 \div 5)$

Making the natural logarithm on both sides of the equation 4.15, having

$$\ln\left(\frac{X}{L_B}\right) = \ln(b_0) + b_1 \ln\left(\frac{L_B}{X_B}\right) + b_2 \ln\left(\frac{G_B}{L_{repr}}\right) + b_3 \ln(\sin\alpha_0) + b_4 \ln\left(\frac{h_{tide}}{H_{repr}}\right) + b_5 \ln\left(\frac{H_{repr}}{D_{50}}\right) \quad (4.16)$$

$$\text{If } Y = \ln\left(\frac{X}{L_B}\right); b_0^* = \ln(b_0) \quad X_1 = \ln\left(\frac{L_B}{X_B}\right); X_2 = \ln\left(\frac{G_B}{L_{repr}}\right); X_3 = \ln(\sin\alpha_0); X_4 = \ln\left(\frac{h_{tide}}{H_{repr}}\right); X_5 = \ln\left(\frac{H_{repr}}{D_{50}}\right) \quad (4.17)$$

Then, 4.16 can be written as the simple function:

$$Y = b_0^* + b_1X_1 + b_2X_2 + b_3X_3 + b_4X_4 + b_5X_5 \quad (4.18)$$

Instead of finding the value of  $b_i$  ( $i=0 \div 5$ ) in the nonlinear equation 4.15, we can find the constant value  $b_0^*$  and  $b_i$  ( $i=1 \div 5$ ) in the linear equation 4.18 with conditions in 4.17. From the dataset,  $Y$  and  $X_j$  ( $j=1 \div 5$ ) can be determined through equation 4.17, but the missing data can be estimated through a multiple imputation analysis. The new imputed dataset is run in the linear regression in SPSS, with  $Y$  as a dependent variable and  $X_j$  as independent variables, and the equation is:

$$Y = 3.03 - 1.29 X_1 + 0.58 X_2 - 0.37 X_3 + 1.54 X_4 - 0.50 X_5 \quad (4.19)$$

or

$$\ln\left(\frac{X}{L_B}\right) = 3.03 - 1.29 \ln\left(\frac{L_B}{X_B}\right) + 0.58 \ln\left(\frac{G_B}{L_{repr}}\right) - 0.37 \ln(\sin\alpha_0) + 1.54 \ln\left(\frac{h_{tide}}{H_{repr}}\right) - 0.50 \ln\left(\frac{H_{repr}}{D_{50}}\right) \quad (4.20)$$

Taking the natural exponent  $e$  ( $e = 2.71828$ ) of both sides of the equation 4.20, the salient formation is the nonlinear relationship in the following function:

$$\frac{X}{L_B} = 20.68 \left(\frac{L_B}{X_B}\right)^{-1.29} \left(\frac{G_B}{L_{repr}}\right)^{0.58} \sin^{-0.37}(\alpha_0) \left(\frac{h_{tide}}{H_{repr}}\right)^{1.54} \left(\frac{H_{repr}}{D_{50}}\right)^{-0.50} \quad (R^2=0.99, \sigma =0.11) \quad (4.21)$$

This complex variables equation predicts more closely than the basic formula 4.3 in the case of the salient formation, because of the higher R-squared. Hence, equation 4.21 estimating salient growth is more precise than equation 4.3.

*c. No sinuosity function*

In the no sinuosity formation, similar to the salient state, the shoreline response is driven by the relationship between  $X/L_B$  and  $L_B/X_B$  (see figure 4.3) because the four other variables ( $G_B/L_{repr}$ ,  $\sin\alpha_0$ ,  $h_{tide}/H_{repr}$ , and  $H_{repr}/D_{50}$ ) do not show a strong relationship with  $X/L_B$ . It means that the shoreline response can be the same as in the salient case. Although the steps of finding the expected relationship is similar as the salient formula 4.15, the data of  $D_{50}$  is very limited, and thus the missing data cannot be imputed correctly in the SPSS. Hence, with the no



sinuosity formation we accept that the variable  $\frac{H_{repr}}{D_{50}}$  is omitted from the shoreline response relationship. The final equation of this state is:

$$\ln\left(\frac{X}{L_B}\right) = 0.42 - 1.03\ln\left(\frac{L_B}{X_B}\right) - 0.37\ln\left(\frac{G_B}{L_{repr}}\right) + 0(\sin\alpha_0) + 0.13\ln\left(\frac{h_{tide}}{H_{repr}}\right) \quad (4.22)$$

$$\text{or} \quad \frac{X}{L_B} = 1.52\left(\frac{L_B}{X_B}\right)^{-1.03}\left(\frac{G_B}{L_{repr}}\right)^{-0.37}\left(\frac{h_{tide}}{H_{repr}}\right)^{0.13} \quad (R^2=0.96, \sigma = 0.16) \quad (4.23)$$

Let's compare the R-squared of equations 4.23 and 4.4, represented in the no sinuosity formation, it is found that the complete equation is more accurate than the basic one, because of a higher R-squared. So that, the complete equation is more acceptable than the basic equation as predicted.

#### 4.2.8 Validation of the proposed formulation

##### a. Correlation coefficients

The Pearson partial correlation coefficients of the prediction in the equations of the tombolo, the salient and the no sinuosity relations are presented in the table 4.2, 4.3 and 4.4.

Table 4.2: Correlation coefficients of variables in tombolo equation 4.11

Variable	T/X <sub>B</sub>	L <sub>B</sub> /X <sub>B</sub>	G <sub>B</sub> /L <sub>repr</sub>	sinα <sub>0</sub>	h <sub>tide</sub> /H <sub>repr</sub>	H <sub>repr</sub> /D <sub>50</sub>
T/X <sub>B</sub>	1	0.778	0.271	0.145	0.340	0.419
L <sub>B</sub> /X <sub>B</sub>	0.778	1	0.022	-0.129	0.116	0.392
G <sub>B</sub> /L <sub>repr</sub>	0.271	0.022	1	0.283	0.486	0.451
Sinα <sub>0</sub>	0.145	-0.129	0.283	1	-0.145	-0.292
h <sub>tide</sub> /H <sub>repr</sub>	0.340	0.116	0.486	-0.145	1	0.935
H <sub>repr</sub> /D <sub>50</sub>	0.419	0.392	0.451	-0.292	0.935	1

Table 4.3: Correlation coefficients of variables in salient equation 4.20

Variable	Ln(X/L <sub>B</sub> )	Ln(L <sub>B</sub> /X <sub>B</sub> )	Ln(G <sub>B</sub> /L <sub>repr</sub> )	Ln(sinα <sub>0</sub> )	Ln(h <sub>tide</sub> /H <sub>repr</sub> )	Ln(H <sub>repr</sub> /D <sub>50</sub> )
Ln(X/L <sub>B</sub> )	1	-0.830	0.066	0.079	0.107	-0.055
Ln(L <sub>B</sub> /X <sub>B</sub> )	-0.830	1	-0.305	-0.034	-0.037	-0.336
Ln(G <sub>B</sub> /L <sub>repr</sub> )	0.066	-0.305	1	0.088	-0.292	0.489
Ln(Sinα <sub>0</sub> )	0.079	-0.034	0.088	1	-0.028	-0.335
Ln(h <sub>tide</sub> /H <sub>repr</sub> )	0.107	-0.037	-0.292	-0.028	1	0.450
Ln(H <sub>repr</sub> /D <sub>50</sub> )	0.055	0.336	0.489	-0.335	0.450	1

Table 4.4: Correlation coefficients of variables in no sinuosity equation 4.22

Variable	Ln(X/L <sub>B</sub> )	Ln(L <sub>B</sub> /X <sub>B</sub> )	Ln(G <sub>B</sub> /L <sub>repr</sub> )	Ln(sinα <sub>0</sub> )	Ln(h <sub>tide</sub> /H <sub>repr</sub> )
Ln(X/L <sub>B</sub> )	1	-0.946	0.328	-0.324	0.190

Variable	$\text{Ln}(X/L_B)$	$\text{Ln}(L_B/X_B)$	$\text{Ln}(G_B/L_{\text{repr}})$	$\text{Ln}(\sin\alpha_0)$	$\text{Ln}(h_{\text{tide}}/H_{\text{repr}})$
$\text{Ln}(L_B/X_B)$	-0.946	1	-0.664	0.238	-0.254
$\text{Ln}(G_B/L_{\text{repr}})$	0.454	-0.664	1	0.097	0.562
$\text{Ln}(\sin\alpha_0)$	-0.324	0.238	0.097	1	-0.053
$\text{Ln}(h_{\text{tide}}/H_{\text{repr}})$	0.190	-0.254	0.562	-0.053	1

From the Pearson correlation coefficients in table 4.2, it can be clearly seen that in the case of tombolo the independent variable  $L_B/X_B$  is the highest correlation coefficient to the dependent variable, equal to 0.778. It means that the variable  $L_B/X_B$  is the most important variable in the equation of the relationship. Also, it seems the variable  $\sin\alpha_0$  is the least important, because of the lowest correlation ratio, just 0.145. However, table 4.2 also shows the correlation of the ratios between the independent variables. Most of these ratios are quite small, except the ratio of 0.935, representing the correlation between  $h_{\text{tide}}/H_{\text{repr}}$  and  $H_{\text{repr}}/D_{50}$ , which is still a high relationship.

From the Pearson correlations between all variables in the case of salient in table 4.3, it can be understood that the independent variable  $\text{Ln}(L_B/X_B)$  is still the most important of the dependent variables, the correlation coefficient being -0.83. The other correlation coefficients to the dependent variable are relative to small. However, the three least important variables to the dependent variable are  $\text{Ln}(H_{\text{repr}}/D_{50})$ ;  $\text{Ln}(G_B/L_{\text{repr}})$ ; and  $\text{Ln}(\sin\alpha_0)$  with correlation ratios - 0.055, 0.066, and 0.079, respectively. The correlations between the independent variables are also small. Then, it can be said that there is no connection between the independent variables.

Table 4.4 shows the correlations in the case of no sinuosity, where two independent variables have a high correlation ratio with dependent  $\text{Ln}(L_B/X_B)$  is -0.946. The lowest correlation ratio is 0.190 with variable  $\text{Ln}(h_{\text{tide}}/H_{\text{repr}})$ . Also, there is a high relationship between independent variable  $\text{Ln}(G_B/L_{\text{repr}})$  and  $\text{Ln}(L_B/X_B)$ , where the correlation ratio is 0.664.

b. Residuals

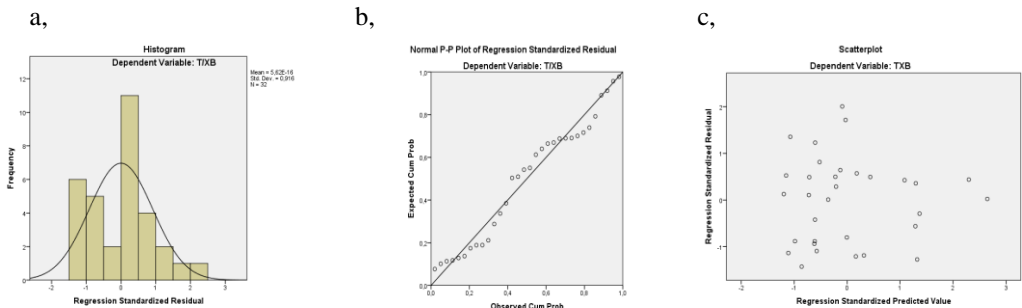


Figure 4.9: Regression standardized residual of dependent variable in equation 4.11

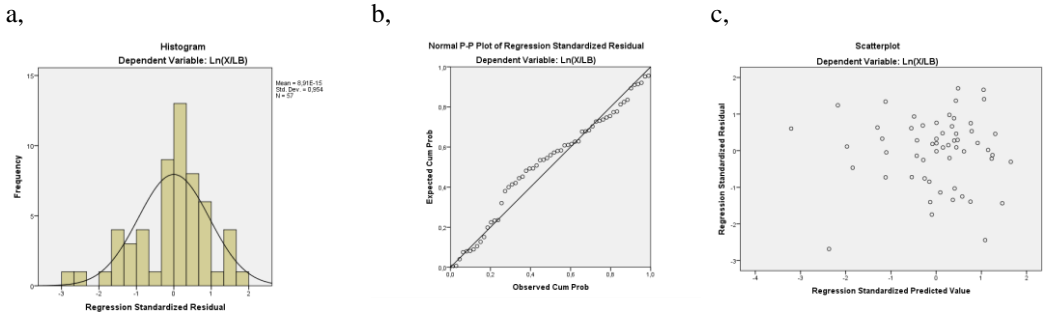


Figure 4.10: Regression standardized residual of dependent variable in equation 4.20

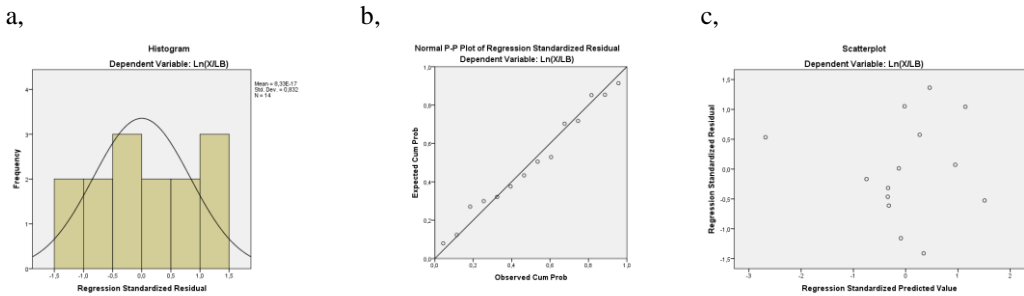


Figure 4.11: Regression standardized residual of dependent variable in equation 4.22

In figures 4.9, 4.10, and 4.11 the residual of the developed functions 4.11, 2.20, and 4.22 is shown. In the normal plots of a regression-standardized residual, the expectation values are very close to the observation values (figure 4.9b, 4.10b, 4.11b). The values of the residuals fluctuate mostly around zero. However, in the scatter plots, several points are still farther from zero (figure 4.9c, 4.10c, 4.11c).

c. Comparison the measured data with the previous studies data

- Comparison of the basic empirical relationship of the previous studies:

The basic empirical relationship of the shoreline response by considering the ratios between the two basic geometric parameters, namely the length of the detached breakwater ( $L_B$ ) and the distance of the structure from the initial offshore distance ( $X_B$ ). The ratio of  $L_B/X_B$  is greater than, less than, or equal to a certain number. The basic relations that were studied, as shown in table 4.5, by Inman (1966), Noble (1978), Gourlay (1981), Nir (1982), the Coastal Engineering Research Center (1984), Dally and Pope (1986), Suh and Dalrymple (1987), Herbich (1989), Hsu and Silvester (1990), Ahrens and Cox (1990), were separated into tombolo, salient, and no sinuosity. However, they show different values of ratio  $L_B/ X_B$  for classifying the types of response.

Table 4.5: Fitting the measured data to the previous empirical suggestions

$N_Q$	Author (year)	Tombolo $L_B/X_B > \dots$	Salient $L_B/X_B < \dots$	No sinuosity $L_B/X_B < \dots$
1	Inman and Frautschy (1966)	-	-	0.33 (0%)
2	Noble (1978)	-	-	0.17 (0%)
3	Gourlay (1981)	0.8 (86.2%)	0.5 (22.8%)	-
4	Nir (1982)	-	-	0.5 (7.1%)
5	Coastal Engineering Research Center (1984)	2 (6.9%)	1 (71.9%)	-
6	Dally and Pope (1986)	1.5 (27.6%)	1.5 (91.2%)	0.5 (7.1%)
7	Suh and Dalrymple (1987)	1 (69%)	1 (71.9%)	-
8	Herbich (1989)	1 (69%)	1 (71.9%)	0.5 (7.1%)
9	Hsu and Silvester (1990)	1.33 (44.8%)	1.33 (84.2%)	-
10	Ahrens and Cox (1990)	2.5 (6.9%)	2.5 (94.7%)	0.76 (21.4%)

The measured data, fitted to the suggested ratios of the various authors are presented in table 4.5. The percentages, which show the fitted projects, are between brackets. From this table it can be seen that the predictions of each author are not satisfactory for the whole of our prototypes dataset. The results of these studies were the most accurate in predicting the salient formation. However, Suh and Dalrymple (1987) and Herbich (1989) chose the ratio of  $L_B/X_B$  as the most relevant value in the prediction of the tombolo and salient formation.

- Tombolo data comparison :

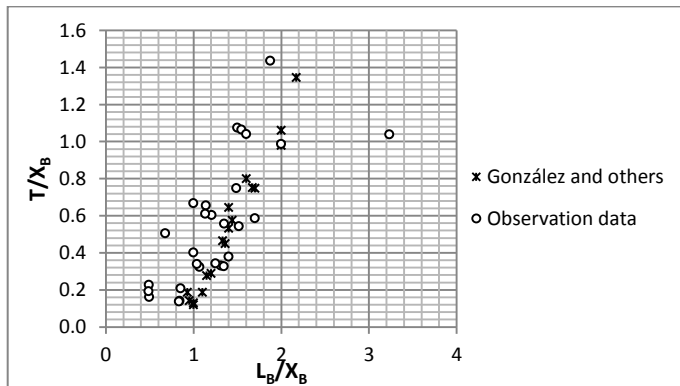


Figure 4.12: Measurement data versus Mauricio Gonz lez data

Measurement data of the tombolo on the prototypes has been compared to the field and experiment data reported by Toyoshima (1974), Nir (1976), Rosen and Vajda (1982), Ming and Chiew (2000), and Mauricio Gonz lez (2001). It can be seen from figure 4.12 that the value of the dimensionless parameters,  $T/X_B$ , was close to the measured data. Then, we can come to the

conclusion that the data of the observation on tombolo formation is wider spread than in the previous data. However, the two dataset have a similar trend.

- Salient formation comparison:

Comparison of the dimensionless data between Hsu and Silvester (1990) and prototype observation data is shown in figure 4.13. Hsu and Silvester used the mixed data of the prototypes, models, and the numerical data from the different authors. They collected 46 series cases and developed the model of the dimensionless relationship for the salient state. However, the new prototype data are only observations on the 57 real projects.

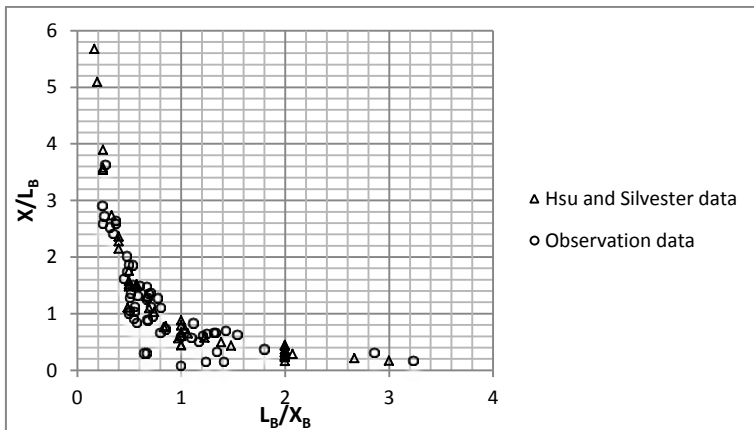


Figure 4.13: The observations versus Hsu and Silvester (1990) data

In the scatter of comparison, the Hsu and Silvester data were in good agreement with the present data. We can conclude that the data of the measurements of the prototypes can also be useful to predict the salient relations.

Considering the final equation based on the mixed data, the equation Hsu and Silvester established for the single breakwater with the perpendicular incoming waves is:

$$\frac{X}{L_B} = 0.6784 \left( \frac{L_B}{X_B} \right)^{-1.1248} \tag{4.24}$$

The equation we developed from the prototypes data, which is the same as for the Hsu and Silvester conditions, is:

$$\frac{X}{L_B} = 0.62 \left( \frac{L_B}{X_B} \right)^{-1.15} \tag{4.25}$$

When recalculating the recent data of the prototypes in Hsu and Silvester’s equation, the different values between the two formulae ranged from -10% to +12%. This is possible, because of Hsu and Silvester’s equation based on the variety types of data. On the other hand,

the new equation is based on only the mean data of the projects, including the single structure projects and the segmented structure projects.

From the validation, it can clearly be seen that the data of the two states, the tombolo and the salient of shoreline response compare well with the previous data. Although there is no previous function to compare with the new tombolo relations, the mixed data has the linear trend of the dimensionless  $T/X_B$ . Besides, the new salient equation is not much different from Hsu and Silvester's equation. However, the new equation includes more variables of the physical parameters than the previous equation.

### 4.3 Analysis of shoreline at opposite the gap

In the previous section, the relationships of the siltation growth were developed. In this section we will analyse the shoreline opposite the gap relationships as a consequence of the effect of segmented breakwaters.

#### 4.3.1 States of the shoreline opposite the gaps

The shoreline opposite gap in the scheme of the structures is generally a smooth arc. The term of the "opposite the gap states" is defined as: "the positions of the furthest points on the arc of the static shoreline between two adjacent accumulations". State one is a state of erosion and means that the shoreline was eroded compared to the original shoreline (the shoreline pre-construction of breakwaters) ( $X_G > X_B$ ). State two is a state of expansion; a state in which the width of the beach increases at the furthest point ( $X_G < X_B$ ). In other words, the original shore grows towards the sea (see detail in Figure 3.1). However, in the image observations, the third state, the unidentified state, is showing. This state of the shore opposite the gap is protected by a revetment or other structures and, then, cannot identify the natural shore behaviour.

In the four categories of the images: Tombolo, salient, both tombolo and salient and no sinuosity, they all have both accretion and erosion state at opposite the gap (see Figure 4.14). The percentage of the chance of gap accretion of both the tombolo and salient is the highest at 87.5% of identified gaps; the second biggest gap accretion chance is the tombolo, with 77.2%. But the erosion occurrence of the opposite gaps of 73%, is the highest in no sinuosity, and the second highest of gap erosion is in the salient, with 26%. The trend of the sand increase in the gaps is clearer than the loss of sand trend in these first three expected states. It can be said that the shoreline opposite the gaps is more likely to accumulate.

Considering the change of magnitude of the net sediment by analysing the ratio of  $\Delta X_G/X_B$  ( $\Delta X_G = X_B - X_G$ ) in the dataset, found the following arrangements:

- From -98% to +58% in case of tombolo;
- From -155% to +60% in case of salient;

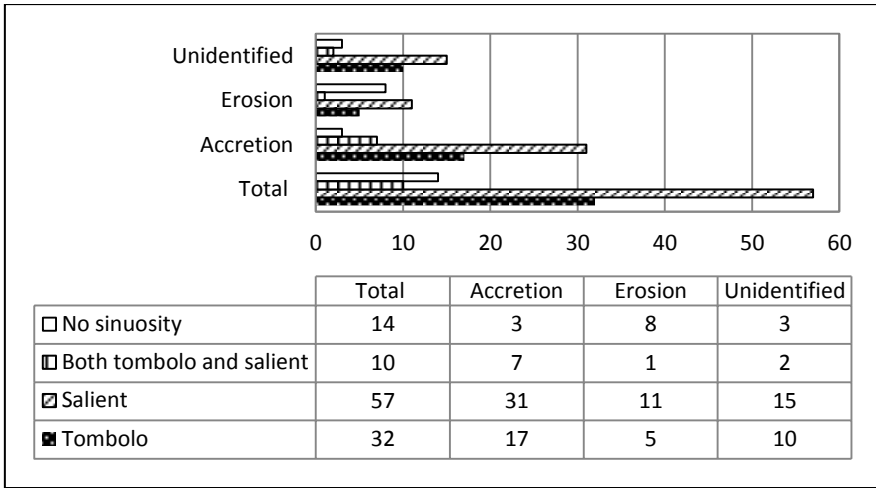


Figure 4.14: Inventory of the state of opposite gaps

4.3.2 Develop the relationships

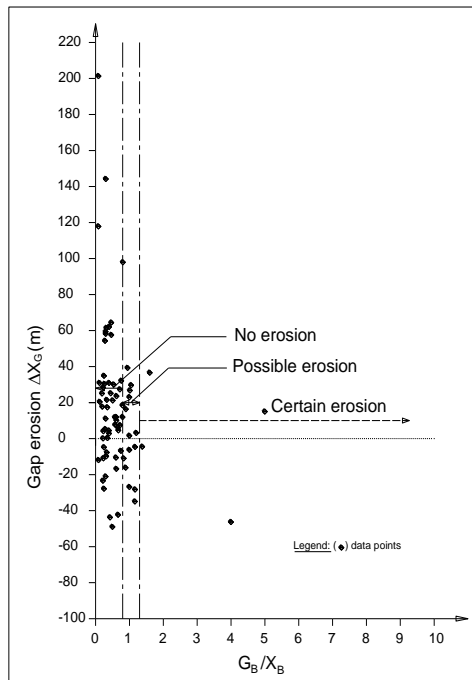


Figure 4.15: Comparison of the evaluation of Seiji and the measurement data for the shoreline erosion opposite the gaps (after Rosati (1990))

- From -50% to +58% in case of both tombolo and salient;
- From -94% to +13% in case of no sinuosity.

The negative values express the degree of erosion and positive values indicate the degree of accretion. Hence, it can be concluded that the shorelines opposite the gaps are not only eroded, but also are accreted. However, the magnitude of the net sediment changes compared with the original offshore distance is widely varied.

Seiji et al. (1987) presented the ranges to predict the opposite gap erosion in figure 4.15. The prediction of “no erosion” occurring for the lower boundary ( $G_B/X_B \leq 0.8$ ), was a reason for either accretion or very little erosion. The gap erosion occurred if the boundary ratio of  $G_B/X_B$  was greater 0.8. However, the plot of the measurement data on the Seiji’ graph shows that the existing estimation is very different from the actual field. The gap erosion is frequently presented in the prediction zone of “no erosion”. Therefore, the gap erosion cannot be predicted by the ratio of  $G_B/X_B$ .

Three parameters that should be taken into account are the gap width ( $G_B$ ), the original offshore distance ( $X_B$ ), and the post shore opposite gap distance ( $X_G$ ). Push these three variables to be dimensionless relations, and repetition of the  $G_B$  is a common and an important variable. The relevance of the relationship is linear. Apply this relationship for the four datasets of the four states of the shore response. The relationships are shown in the description in figure 4.16.

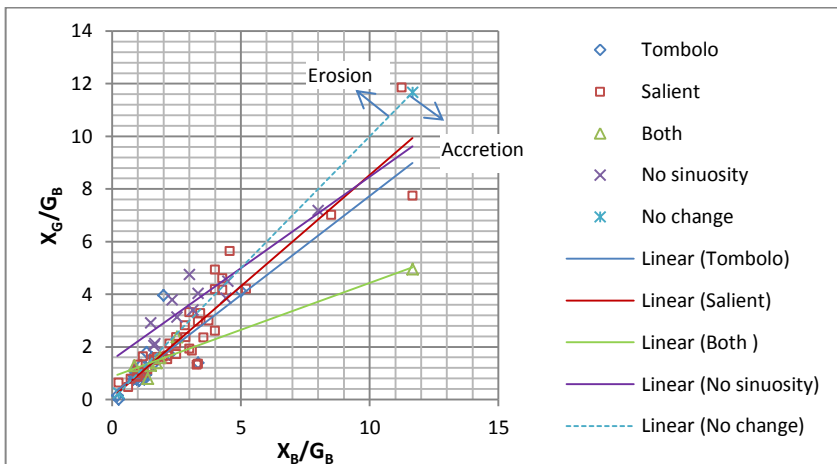


Figure 4.16: The relationships of gap dimensionless parameters

In figure 4.16, the green dotted line (the balance line) is representative of the shoreline, which remains unchanged. The area above the balance line is an expression of the erosion state, and the area on the other side indicates an expansion sediment state. As can be seen, the four lines are lying on both sides of the erosion zone and the acceleration zone, however, the



largest part of the no sinuosity line is in the erosion zone. These functions, driving the trend in figure 4.16 are :

- For tombolo

$$\frac{X_G}{G_B} = 0.196 + 0.75 \frac{X_B}{G_B} \quad (R^2 = 0.61) \quad (4.26)$$

- For salient

$$\frac{X_G}{G_B} = 0.076 + 0.85 \frac{X_B}{G_B} \quad (R^2=0.87) \quad (4.27)$$

- Both salient and tombolo

$$\frac{X_G}{G_B} = 0.86 + 0.36 \frac{X_B}{G_B} \quad (R^2 = 0.94) \quad (4.28)$$

- For no sinuosity

$$\frac{X_G}{G_B} = 1.52 + 0.69 \frac{X_B}{G_B} \quad (R^2=0.84) \quad (4.29)$$

As the discussion in section 4.2.7 pointed out, the interaction in the sheltered area is a combination of the effects of waves, currents, grains, and structure parameters. We suppose that the complex function of the dimensionless parameters on the shore opposite the gap is the following:

$$\frac{X_G}{G_B} = f\left(\frac{X_B}{G_B}, \sin\alpha_0, \frac{h_{tide}}{H_{repr}}, \frac{H_{repr}}{D_{50}}\right) \quad (4.30)$$

Where:

$\frac{X_G}{G_B}$  is the ratio measure of magnitude of the opposite gap resulting;

$\frac{X_B}{G_B}$  is the ratio measure of magnitude of the initial opposite gap;

$\sin(\alpha_0)$  is the ratio measure of the dominant incident wave direction;

$\frac{h_{tide}}{H_{repr}}$  is the ratio measure of the tide range effect;

$\frac{H_{repr}}{D_{50}}$  is the ratio measure of the sediment uplift ability.

Analysing the data of  $\sin(\alpha_0)$ ,  $\frac{h_{tide}}{H_{repr}}$ , and,  $\frac{H_{repr}}{D_{50}}$ , we found that these independent variables do not have a clear relation with the dependent variable  $\frac{X_G}{G_B}$ . Thus, the general function 4.30 is controlled by the trend of the variable  $\frac{X_B}{G_B}$ . The equation 4.30 can be rewritten:

$$\frac{X_G}{G_B} = c_0 + c_1 \frac{X_B}{G_B} + c_2(\sin\alpha_0) + c_3 \frac{h_{tide}}{H_{repr}} + c_4 \frac{H_{repr}}{D_{50}} \quad (4.31)$$

Where :  $c_i$  is constant (i=1÷4)

Based on the dataset we analyse the multi-variable function 4.31 with the different cases of the shoreline response by using the SPSS regression; the final relationships are:

- For tombolo

$$\frac{X_G}{G_B} = 1.006 + 1.09 \frac{X_B}{G_B} - 0.64\sin(\alpha_0) - 1.06 \frac{h_{tide}}{H_{repr}} - 0.04 \frac{H_{repr}}{D_{50}} \quad (R^2 = 1, \sigma = 0.001) \quad (4.32)$$

- For salient

$$\frac{X_G}{G_B} = -0.21 + 0.57 \frac{X_B}{G_B} + 0.68\sin(\alpha_0) + 0.26 \frac{h_{tide}}{H_{repr}} + 0.03 \frac{H_{repr}}{D_{50}} \quad (R^2 = 0.98, \sigma = 0.33) \quad (4.33)$$

- For both salient and tombolo

$$\frac{X_G}{G_B} = 0.57 + 0.38 \frac{X_B}{G_B} - 0.22\sin(\alpha_0) - 0.12 \frac{h_{tide}}{H_{repr}} + 0 \frac{H_{repr}}{D_{50}} \quad (R^2=0.98, \sigma = 0.38) \quad (4.34)$$

- For no sinuosity

$$\frac{X_G}{G_B} = 1.93 + 0.8 \frac{X_B}{G_B} + 0.25\sin(\alpha_0) - 0.71 \frac{h_{tide}}{H_{repr}} - 0.03 \frac{H_{repr}}{D_{50}} \quad (R^2=0.93, \sigma = 0.60) \quad (4.35)$$

It can be seen that the values of the R-squared in the complex variables formulae of the opposite gap relationships are relatively high, almost closed to 1.0. These values of the R-squared are in comparison still higher than the ones of basic equations 4.26 to 4.29. It means that the additional variables' contributions to the complex equations are acceptable.

To analyse the interrelation in these formulae of the developments, it is necessary to examine the correlation coefficients between the variables in the formulae. The ratios of the respective interactions will be apparent in the following tables.

As can be clearly seen in from table 4.6 to table 4.9, the highest correlation coefficient ratios are usually between the dependent variable  $X_G/G_B$  and the independent variable  $X_B/G_B$ . In other words, in these equations the independent variable  $X_B/G_B$  is the most important variable, driving the equations.

Table 4.6: Correlation coefficients of variables in tombolo case in equation 4.32

Variable	$X_G/G_B$	$X_B/G_B$	$\sin\alpha_0$	$h_{\text{tide}}/H_{\text{repr}}$	$H_{\text{repr}}/D_{50}$
$X_G/G_B$	1	0.530	-0.251	-0.114	-0.190
$X_B/G_B$	0.530	1	-0.245	0.600	-0.116
$\sin\alpha_0$	-0.251	-0.245	1	-0.137	-0.074
$h_{\text{tide}}/H_{\text{repr}}$	-0.114	0.600	-0.137	1	-0.581
$H_{\text{repr}}/D_{50}$	-0.190	-0.116	-0.074	-0.581	1

Table 4.7: Correlation coefficients of variables in salient case in equation 4.33

Variable	$X_G/G_B$	$X_B/G_B$	$\sin\alpha_0$	$h_{\text{tide}}/H_{\text{repr}}$	$H_{\text{repr}}/D_{50}$
$X_G/G_B$	1	0.931	-0.027	0.325	-0.730
$X_B/G_B$	0.931	1	-0.074	0.380	-0.505
$\sin\alpha_0$	-0.027	-0.074	1	-0.104	0.086
$h_{\text{tide}}/H_{\text{repr}}$	0.325	0.380	-0.104	1	0.212
$H_{\text{repr}}/D_{50}$	-0.730	-0.505	0.086	0.212	1

Table 4.8: Correlation coefficients of variables in both salient and tombolo case in equation 4.34

Variable	$X_G/G_B$	$X_B/G_B$	$\sin\alpha_0$	$h_{\text{tide}}/H_{\text{repr}}$	$H_{\text{repr}}/D_{50}$
$X_G/G_B$	1	0.991	0.188	-0.771	0.011
$X_B/G_B$	0.991	1	0.229	-0.751	-0.035
$\sin\alpha_0$	0.188	0.229	1	0.130	0.212
$h_{\text{tide}}/H_{\text{repr}}$	-0.771	-0.751	0.130	1	0.353
$H_{\text{repr}}/D_{50}$	0.011	-0.035	0.212	0.353	1

Table 4.9: Correlation coefficients of variables in no sinuosity case in equation 4.35

Variable	$X_G/G_B$	$X_B/G_B$	$\sin\alpha_0$	$h_{\text{tide}}/H_{\text{repr}}$	$H_{\text{repr}}/D_{50}$
$X_G/G_B$	1	0.882	-0.179	-0.448	-0.558
$X_B/G_B$	0.882	1	-0.181	-0.074	-0.376
$\sin\alpha_0$	-0.179	-0.181	1	0.170	0.304
$h_{\text{tide}}/H_{\text{repr}}$	-0.448	-0.074	0.170	1	0.603
$H_{\text{repr}}/D_{50}$	-0.558	-0.376	0.304	0.603	1

The residuals analysis of the equations 4.32 to 4.35 are shown below in figures 4.17 to 4.20 respectively:

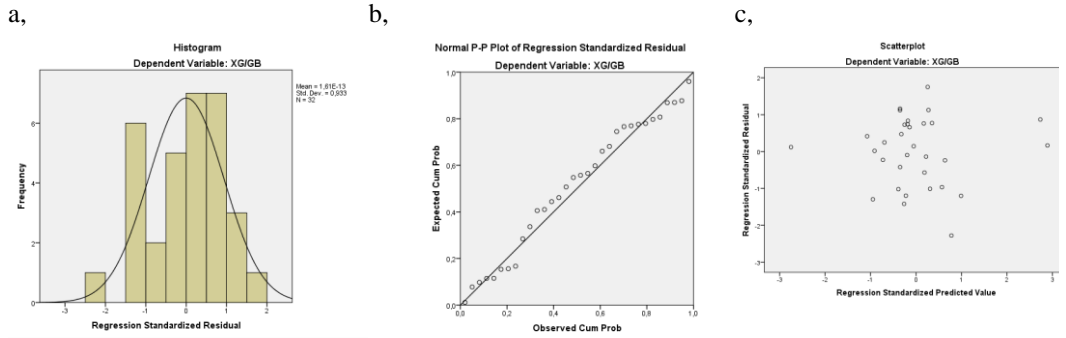


Figure 4.17: Regression standardized residual of dependent variable in tombolo case (e.4.32)

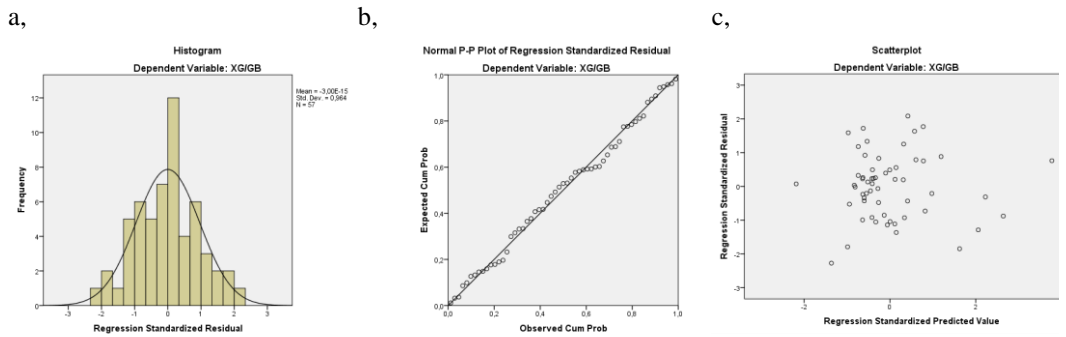


Figure 4.18: Regression standardized residual of dependent variable in salient case(e.4.33)

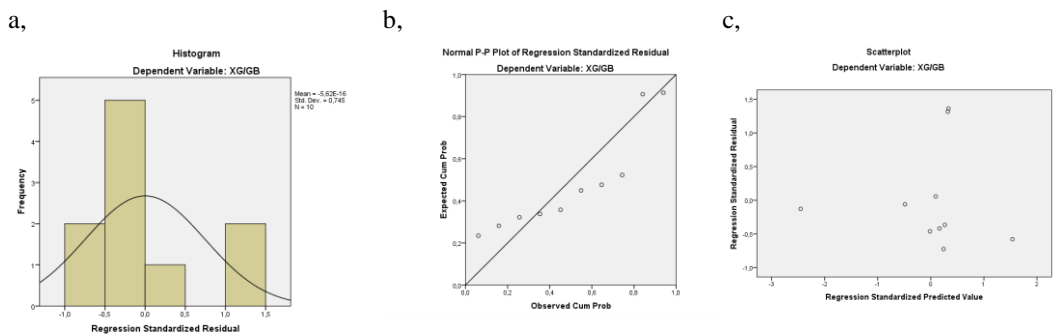


Figure 4.19: Regression standardized residual of dependent variable in both salient and tombolo case (e.4.34)

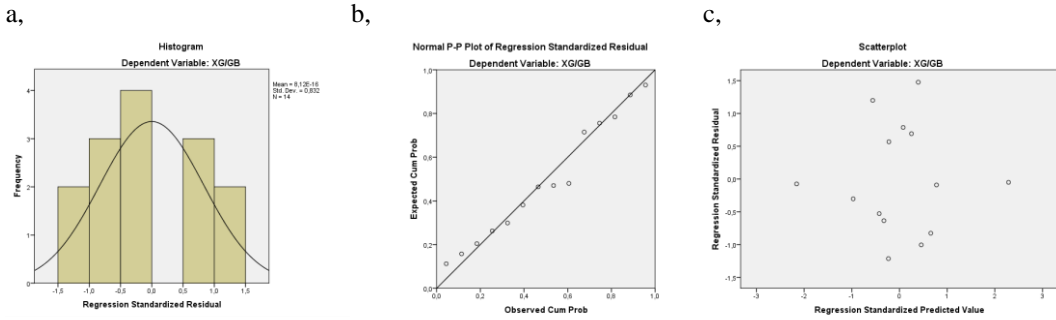


Figure 4.20: Regression standardized residual of dependent variable in no sinuosity case(e.4.35)

To sum up, the distances of the furthest points on the equilibrium shorelines opposite the gaps can be formulated under the linear relation equations of the dimensionless variables. These equations of component variables of complex interactions are gap width, breakwater distance, wave height, length, oblique angle, and median grain size. In these equations the ratio  $X_B/G_B$  is the most important variable, which is the key of driven functions.

#### 4.4 Analysis of shoreline at up and down-drift area

Applying the detached breakwater in a protected area may have an effect on the adjacent coasts. The changes of the beach on each side of the structure are approached differently as up-drift and down-drift. The up-drift of a structure is located at the wave-swept side compared to the predominant wave direction. The down-drift, at the other side of the structure, is the shadow shore of the predominant wave. We suppose that the maximum effect of the structure at the up- and down-drift are the transitional points, which distinguish a change from a curve of siltation accretion to a straight line of the shore. These points were explained in figure 3.16 as the position of C in chapter 3. The data of the transitional points will be used to develop the evaluation relations.

##### 4.4.1 Comparison of locations between the up-drift and the down-drift

The two parameters to identify the transitional point at the up- and down-drift are the distance to the shore parallel centre axis and the distance to the head of the adjacent breakwater. The data of these parameters will be used for the analysis:

First of all, an analysis of the data of the distances of the transitional points on the equilibrium shore at the up- and the down-drift to the breakwaters' centre axis ( $X_U$  and  $X_D$ , respectively). From the measurements we found that the two points at up- and down-drift were not in symmetry with the project. The results presented that the net amount of sand is different between the up- and the down-drift, although from the transitional points outward of the structure were under the same wave conditions. This difference can be explained by the change

of the longshore sand transport rate before and after the breakwater(s). Figure 4.21 illustrates the net sandy beach at the up-drift ( $\Delta X_U = X_B - X_U$ ) and the down-drift ( $\Delta X_D = X_B - X_D$ ) of the measurement data. In the case of the 93 projects, the data can be accepted for 62 cases, while other projects are inappropriate because of additional structures or because they are unobservable from the observation points.

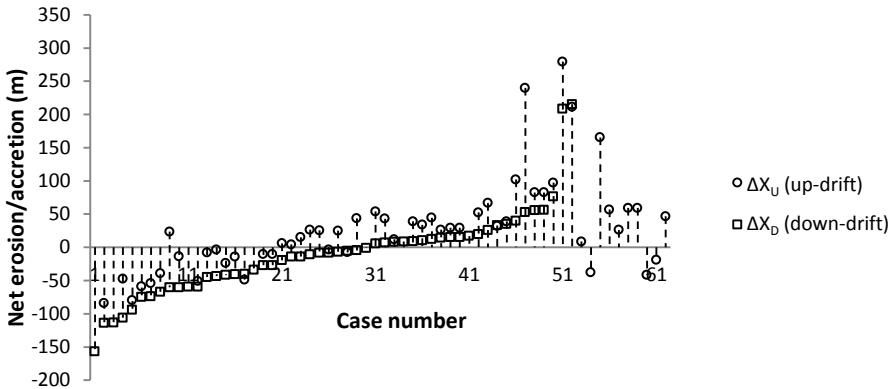


Figure 4.21: Net sand beach at up-drift and down-drift in comparison

It can be clearly seen from figure 4.21 that, at the up- and the down-drift, both states of erosion (negative values) and accretion (positive values) appeared at the controlled points. However, the net sand beach at the up-drift was higher than at the down-drift in most cases. In other words, the up-drift tends to less erosion than the down-drift. Thus, the down-drift will lead to more potential shore damage than the up-drift.

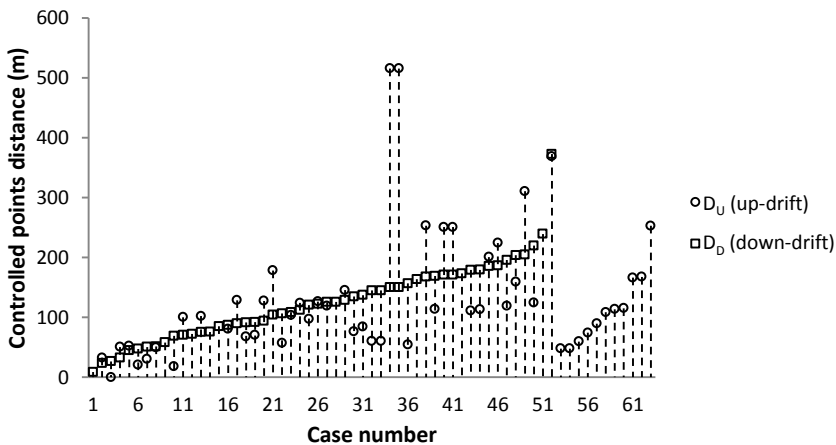


Figure 4.22: Controlled point distances at up and down-drift comparison

Secondly, an analysis data of distances from the controlled points to the heads of the adjacent breakwaters (Figure 4.22). The measurements showed a total of 63 cases, but only 51 cases attained the values at both the up- and the down-drift. Usually, the longer the distance from the controlled point to the breakwater's head, the larger the area of the circulation effect. However, the dataset includes 19 cases of the up-drift having longer distances than the down-drift.

#### 4.4.2 Development of basic relationships

The development of relationships is aimed to identify the location of the controlled points at the up- and the down-drift by their coordination: the distance to the adjacent breakwater's head and the distance to the shore parallel centre axis. The representative values of the coordination at the mean water level (MWL) are  $X_U$ ,  $D_U$  (up-drift) and  $X_D$ ,  $D_D$  (down-drift). The data of the measurements are separated into the four situations on image observations of the equilibrium shoreline as well as the siltation analysis. Thus pushing the two dimension variables  $X_U$  (or  $X_D$ ,  $D_U$ ,  $D_D$ ) and  $X_B$  into a relation. The relevant relationships seem to be the linear. However, the relationships have unequal ratios and have a different goodness of fit. The results will be presented in the following subsections below.

##### *a, For tombolo formation*

The linear relationships that are fitted by the measurement data in the projects have a tombolo formation. The data of the shore at up- and down drift taken to analyse, were the avoidance of the effects of other structures, such as groin and revetment. Then the number of the data is limited to just over 10 cases for each. Figure 4.23 shows the fitted lines between  $X_U$  (and  $X_D$ ,  $D_U$ ,  $D_D$ ) and  $X_B$  is:

In figure 4.23 the formulae representing the trends are:

- Up-drift:

$$X_U = 31.8 + 0.8X_B \quad (R^2=0.47) \quad (4.36)$$

$$D_U = 21.3 + 0.86X_B \quad (R^2=0.40) \quad (4.37)$$

- Down-drift:

$$X_D = 62.3 + 0.47X_B \quad (R^2=0.60) \quad (4.38)$$

$$D_D = 62.9 + 0.41X_B \quad (R^2=0.55) \quad (4.39)$$

The two up-drift formulae have a quite low of R-squared, just around 0.4. But these values are higher with the data at the down-drift, around 0.6. Thus, in the tombolo formation, the linear trends are not so clear.

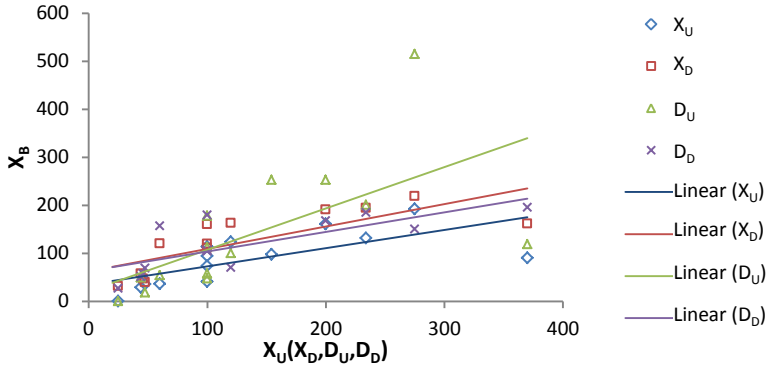


Figure 4.23: Up and down drift relations in tombolo formation

b, For salient formation

The data in the salient formation in figure 4.24 are denser than the data of the tombolo case, and the trends of these data are found to be linear. Herein, the trend is quite clear because of a R-squared higher than 0.5; especially, at the down-drift, the R-squared are close to 0.7 (see equations 4.40 to 4.43).

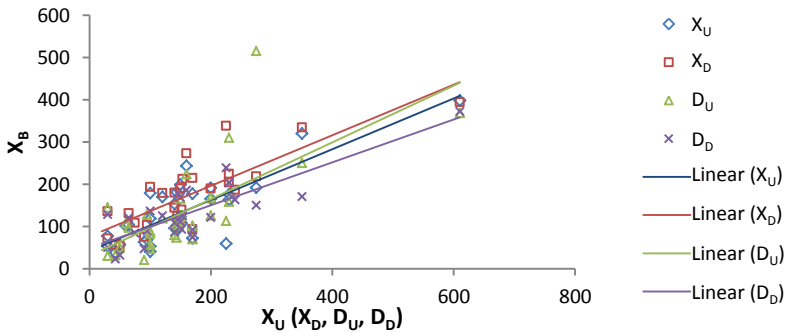


Figure 4.24: Up and down drift relations in salient formation

Up-drift:

$$X_U = 42.7 + 0.6X_B \quad (R^2=0.66) \quad (4.40)$$

$$D_U = 31 + 0.67X_B \quad (R^2=0.51) \quad (4.41)$$

- Down-drift:

$$X_D = 10.1 + 0.7X_B \quad (R^2=0.69) \quad (4.42)$$

$$D_D = 76.7 + 0.6X_B \quad (R^2=0.67) \quad (4.43)$$



c, For both tombolo and salient formation

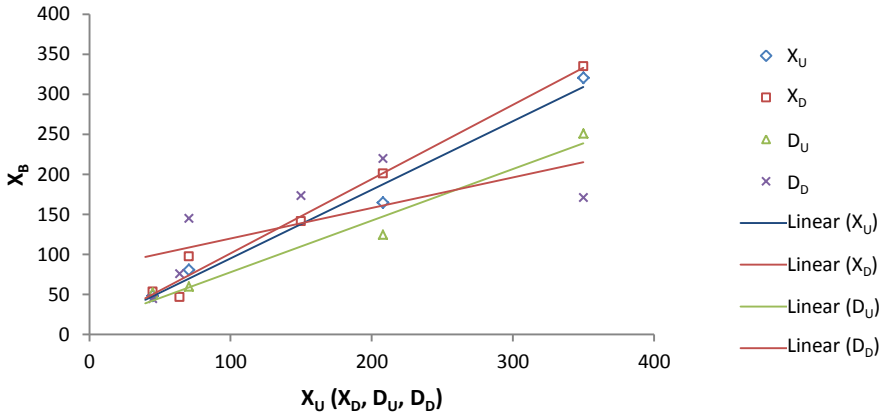


Figure 4.25: Up and down drift relations in both tombolo and salient formation

This formation presents the up- and the down-drift data of the sites at which accumulations have occurred with the tombolo at high tide and the salient at low tide. The data are limited for the ten projects and, only three of four offer a strong evident linear trend. However, the distance of the down-drift ( $D_D$ ) is slightly weaker with the R-squared of almost 0.46.

The equation from 4.44 to 4.47 present the fitted data are:

- Up-drift:

$$X_U = 9.4 + 0.86X_B \quad (R^2=0.98) \quad (4.44)$$

$$D_U = 13.6 + 0.64X_B \quad (R^2=0.97) \quad (4.45)$$

- Down-drift:

$$X_D = 8.8 + 0.93X_B \quad (R^2=0.98) \quad (4.46)$$

$$D_D = 82 + 0.38X_B \quad (R^2=0.46) \quad (4.47)$$

d, For no sinuosity

The data in the no sinuosity formation is very limited and therefore cannot show a trend (figure 4.26). In fact, the total number of projects of the no sinuosity state is fourteen, but only for a few of them the measurements were taken, as other additional structures, such as revetments, groins, even detached breakwaters, were close to them. Generally, we can conclude that these projects were unsuccessful to protect the shore.

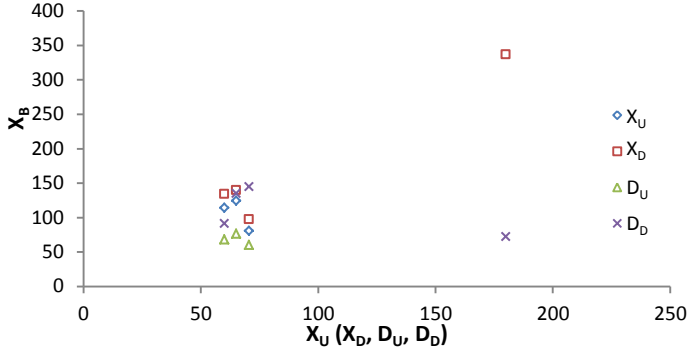


Figure 4.26: Up and down drift relations in no sinuosity formation

#### 4.4.3 General relationships

In this section will develop the relations of the coordination of the control points at the up- and the down-drift of the structures. The coordination is identified by the horizontal and by the vertical distance to the head of the adjacent breakwater. Understanding that, from the control point outward of the structures, the circulation currents and the wave diffraction are unreachable, consequently the sand transport from the control point outward is not affected by the circulation currents induced by the breakwater nor by the wave diffraction.

To assume that the coordination of the control points is related to the variable of the parameters of the initial offshore distance, the wave height, the oblique wave angle, the tidal range and the median grain size, then the general equation relationship is written:

$$X_{U(D)} \text{ or } D_{U(D)} = f(X_B, H_{repr}, \sin \alpha'_0, h_{tide}, D_{50}) \quad (4.48)$$

Where:

$X_U, D_U$  are distances from the control point of the up-drift to the centre axis and the head of breakwater;

$X_D, D_D$  are distances from the control point of the down-drift to the centre axis and the head of breakwater;

$\sin \alpha'_0 = 1 \text{ meter} * \sin \alpha_0$ , is the parameter effect from the oblique of the predominant wave.

Taking the analysis of the relations between the individual the dependent variable  $X_U$  (or  $X_D$  or  $D_U$ , or  $D_D$ ) with each independent variable  $H_{repr}$  (or  $\sin \alpha'_0$ , or  $h_{tide}$ , or  $D_{50}$ ) in the general equation, we found rather low correlations. Hence, accepting that the linear relationship between the dependent variable  $X_U$  (or  $X_D$  or  $D_U$ , or  $D_D$ ) and  $X_B$ , which controls the general equation is linear too.

From the prototype data, the following equations in the different formations are developed:

a. Tombolo formation

- For up-drift:

$$X_U = 82.1 + 0.28X_B + 92.03H_{repr} - 51.9 \sin \alpha'_0 - 101.84h_{tide} - 8.75D_{50} \quad (R^2 \approx 1, \sigma = 0.01) \quad (4.49)$$

$$D_U = 553 - 3.07X_B + 33.2H_{repr} + 250 \sin \alpha'_0 - 91.6h_{tide} - 153.05D_{50} \quad (R^2=0.99, \sigma = 8.0) \quad (4.50)$$

- For down-drift:

$$X_D = -70.4 + 1.5X_B + 17.6H_{repr} - 87.4 \sin \alpha'_0 + 37.7h_{tide} + 37.02D_{50} \quad (R^2 = 0.93, \sigma = 14.8) \quad (4.51)$$

$$D_D = 81.2 + 0.48X_B - 36.8H_{repr} + 26.9 \sin \alpha'_0 + 7.2h_{tide} - 15.6D_{50} \quad (R^2=0.73, \sigma = 31.6) \quad (4.52)$$

The four equations 4.49 to 4.52 for the tombolo formation are regressed from the data of 32 projects with tombolo siltation. However, the data is not fully complete, then, the missing data are imputed before running regression. The results of the regression equations have the high values of R-squared, of over 0.7. But the equations 4.51 and 4.52 have the high standard error of the estimate ( $\sigma$ ), with 14.8 and 31.6, respectively.

b. Salient formation

The analysis for up- and down-drift of salient formation based on the data set of the 57 projects. Similar to the tombolo case, it is needed to impute the missing data, and then regress for the estimation equations. The final equations are:

- For up-drift:

$$X_U = 42.4 + 0.64X_B - 112.3H_{repr} + 16.7 \sin \alpha'_0 + 88.4h_{tide} + 74.2D_{50} \quad (R^2= 0.90, \sigma =24.6) \quad (4.53)$$

$$D_U = -69.7 + 1.3X_B - 245.5H_{repr} + 12.2 \sin \alpha'_0 + 198.3h_{tide} + 272.5D_{50} \quad (R^2= 0.80, \sigma= 42.8) \quad (4.54)$$

- For down-drift:

$$X_D = 79.9 + 0.35X_B + 41.7H_{repr} + 101 \sin \alpha'_0 - 22.2h_{tide} - 129.3D_{50}$$

$$(R^2 = 0.88, \sigma = 25.9) \quad (4.55)$$

$$D_D = -46 + 0.5X_B + 73.1H_{repr} + 110.6 \sin \alpha'_0 - 36.5h_{tide} - 37.4D_{50}$$

$$(R^2 = 0.72, \sigma = 35.1) \quad (4.56)$$

The four equations 4.53 to 4.56 show the estimation of the distances of the limited effect points at up- and down-drift in the salient formation. These equations are presented with the high R-squared, of which the lowest is 0.72 . However, the error of estimation ( $\sigma$ ) is the highest of 42.8. It means that, the actual result can be a variation from -42.8m to +42.8m around the estimation. Therefore, the equations with a higher standard error of estimation are a less accurate result.

*c. Both tombolo and salient formation*

The both tombolo and salient formation is divided by observation of the aerial images in which the tombolo form on the images is taken at low tide and the salient form on the images is taken at high tide. There are ten projects pertaining to this case. The data of these projects is analysed as a linear relation to the distances of the limited points, having the equations:

- For up-drift:

$$X_U = 103.8 + 0.58X_B + 95.6H_{repr} - 83.4 \sin \alpha'_0 - 10.2h_{tide} - 77.1D_{50}$$

$$(R^2 = 0.82, \sigma = 44.9) \quad (4.57)$$

$$D_U = 30.9 + 0.51X_B + 51.4H_{repr} - 21.7 \sin \alpha'_0 - 5.8h_{tide} + 45.8D_{50}$$

$$(R^2 = 0.81, \sigma = 34.7) \quad (4.58)$$

- For down-drift:

$$X_D = 178.1 + 0.74X_B - 62.6H_{repr} - 71.7 \sin \alpha'_0 + 1.9h_{tide} - 67.8D_{50}$$

$$(R^2 = 0.95, \sigma = 28.1) \quad (4.59)$$

$$D_D = 107.04 + 0.24X_B + 14.6H_{repr} - 79.6 \sin \alpha'_0 + 0.18h_{tide} - 74.8D_{50}$$

$$(R^2 = 0.88, \sigma = 25.5) \quad (4.60)$$

As can be seen, the four equations from 4.57 to 4.60 have the high coefficients of determination  $R^2$ , however, several equations also have high standard error of estimation  $\sigma$ . The values of the R-squared is higher than 0.7 to approximately 1.0; the standard error is higher than 0.01 to biggest is 44.9.

To sum up, the parameters of the shoreline at the up-drift and the down-drift have been developed. The analysis of the correlation coefficients between independent variables for these equations, shows that the highest correlation coefficients are among  $X_U$  (or  $X_D$ , or  $D_U$ , or  $D_D$ ) and  $X_B$ . Thus it can be said that  $X_B$  is the most important variable in these equations. However, the regression-standardized residuals show that the estimation values are not really accurate in relation to the observation values, except in the case of the up-drift of the tombolo formation.

#### 4.5 Discussion

1. The siltation response is influenced by the ratio of the breakwater length and its offshore distance ( $\frac{L_B}{X_B}$ ). This ratio of the prototypes data of the tombolo and the salient is mostly in agreement with a greater and a smaller than one, respectively. And, the data of the no sinuosity formation shows a ratio mostly greater than one (see figure 4.1). However,  $\frac{L_B}{X_B} > 1$  is not applicable for the no sinuosity condition, because the 14 cases have a limited shoreline response; among them 9 cases were located close to river mouths, or a sailing port, or a groin. Therefore, sediment supply can be driven by the river flow or be mainly deposited in front of the structures at the upstream, leading to the no sinuosity formation of the detached breakwater project.

2. The bounds of opposite the gap response were pointed out by Seiji et al. (1987), which were based on the ratio of the gap width and the offshore distance ( $\frac{G_B}{X_B}$ ). When the prototype data are fitted on the Seiji graph (see figure 4.15), the prediction of Seiji was found to be inappropriate. In addition, Seiji did not mention the difference between the opposite gap with the tombolo and the salient. Thus, the shore at the opposite of the gap cannot be predicted by the ratio of  $\frac{G_B}{X_B}$ .

3. A low-crested rubble mound structure is normally used for breakwaters of shoreline protection, which has wave transmission, consisting of wave penetration through the structure and wave overtopping. The wave transmission is the one of the parameters' effect on sediment movement. Van der Meer (1991) developed the wave energy transmission model which showed that the wave transmission coefficient depends on the relations of breakwater freeboard, wave height, crest width and median stone size. However, the effect of wave transmission on the shoreline changes was not presented in the relationship equations.

4. Tidal currents have a role in sediment transport in sheltered area by their bed shear stress, however, tidal currents did not appear in the relationship equations. Tidal currents have more impact on sediment movement in macro-tidal beaches and less impact on sediment movement in micro-tidal (or non-tidal) beaches. To understand the effects of tidal currents on the shore, the bed shear stress needs to be obtained, but it is not available in the collected data. Therefore, further research should be done about the variable of tidal currents.

## 4.6 Conclusions

In this chapter, the equations of empirical relationships for the four important positions in the equilibrium shoreline were developed. These are the relationships between the equilibrium shore parameters and the detached breakwaters parameters, the wave parameters, the tidal range and sediment size. The analysis of the relationships started with the finding of the basic relationships to shoreline changes and continued with the development of the relationships of the shoreline changes including the other parameters. The collective relationships of the shoreline changes are a combination of the total effects, however, the general relationships are driven by the strongest parameter. The main findings are summarized below for the siltation, opposite the gap, the up-drift and the down-drift:

1. The siltation of tombolo, salient and limited response were expressed by the dimensionless equations and how they related to the eight parameters: the breakwater length, the offshore distances, the gap width, the representative wave height, the representative wave length, the oblique representative wave angle, the tidal level and the median sediment size. However, the oblique representative wave angle was not presented in the limited response equation. In these siltation equations, the highest correlations are between dimensionless of the tombolo width to the offshore distance ( $\frac{T}{X_B}$ ) in tombolo formation (or dimensionless parameter of the salient edge distance to breakwater to the breakwater length  $\frac{X}{L_B}$  in salient formation) and dimensionless of the breakwater length and the breakwater offshore distance ( $\frac{L_B}{X_B}$ ).

2. In the ratio of the breakwater length and the breakwater offshore distance ( $\frac{L_B}{X_B}$ ), it is appropriate to distinguish between siltation as tombolo and a salient. If  $\frac{L_B}{X_B} \geq 1$ , then a project will create a tombolo, otherwise in the condition of  $\frac{L_B}{X_B} < 1$ , a project will create a salient. The limited response is unfortunately unclear under the ratio of  $\frac{L_B}{X_B}$ .

3. The data and the equations of the tombolo and salient formation are compared with the data and the equation of the previous studies, respectively. The data, taking in comparison of previous studies, are a combination of numerical data, laboratory data and prototype data under the basic conditions of a single structure and perpendicular incident waves in the papers of Mauricio González (2001) and Hsu and Silvester (1990), Yamada et al., (2010). The equation of Hsu and Silvester for salient was compared to the newly developed equation; however, no equation for tombolo in the previous studies was compared to the new tombolo equation.

4. The equilibrium shoreline opposite the gap was presented by the dimensionless equations, which are the relationship between the ratio measure of the equilibrium shore opposite the gap ( $\frac{L_B}{X_B}$ ) and the ratios measure of the original shore opposite the gap ( $\frac{X_B}{G_B}$ ), the representative wave

oblique angle ( $\sin\alpha_0$ ), the tide effect ( $\frac{h_{tide}}{H_{repr}}$ ), the sediment uplift ability ( $\frac{H_{repr}}{D_{50}}$ ). In these equations for the shoreline at opposite the gap, the highest correlations were found between the ratio measure of the equilibrium shore opposite the gap and the ratio measure of the initial shore opposite the gap.

5. The up-drift and the down-drift were supposed as the furthest points, where hydrodynamics are changed by the structures. These points were determined by their coordination on the cross shore and the alongshore axes, which are dependent on the five parameters of the structure's offshore distance, the representative wave height, the representative oblique wave angle, the tidal range and the median sediment size. The most effective parameters are the wave height, the oblique wave angle, the tidal range and the sediment size. The equations of the relationship have the high coefficients of determination (R-squared). Nevertheless, some of these equations are still less accurate, because they have a high standard error of estimation ( $\sigma$ ).

In the next chapter will analyse the roles of the parameters influence on the shoreline changes.

## CHAPTER 5: INFLUENCE OF THE PARAMETERS ON THE SHORELINE CHANGES

### 5.1 Introduction

The previous chapter developed the relationship equations for the parameters of the four particular positions on the static shoreline behind detached breakwaters. In this chapter, the method of analysis of the shoreline changes by individual parameters will be interpreted.

The aspects concerning the shoreline changes are a fluctuation of the tombolo width, the salient length, the net shoreline changes at opposite the gap, and the distances of the up and the down-drift. These parameters can be defined as the net of the beach changes, which are determined through specific structure dimensions under particular natural conditions. Thus, we need to recalculate the shoreline changes based on a restructuring of the relationship equations, as developed in the previous chapter. Because the shoreline changes relate to multiple parameters, then, the trends of the net shore changes will be analysed separately on each parameter, while keeping the other parameters unchanged. The values resulting of the shoreline changes are plotted in a sequence of changes of this particular parameter. Comparison between the slopes of the shoreline changes caused by the different parameters, thus, will show which parameters have more influence on the shoreline changes.

On the basis of the sample values of the parameters to be analysed, we will recommend the applicability of the parameter ranges, which will be appropriate in practice. The estimation equations were originally developed for the generalizations about the shoreline changes. However, the equations developed based on the limited data set within the narrow input



parameter ranges leading to these equations, are only accurate in specific conditions. Therefore, it needs to be known which sector is most relevant for application.

## **5.2 Influence of the parameters on the cross shore axis**

In this section we will discuss the effects of various parameters of segmented detached breakwaters, i.e. wave climate, tidal range and sediment size, on the changes of the shore on the cross shore axis (seaward or landward).

On the equilibrium shoreline, the four positions, siltation, the opposite gap, the down-drift and the up-drift, known as the marked points A, B, C and D on the planform, are evaluated. In the previous sections the relationship of distances of these points to the parallel centre axis and the adjacent breakwater's head were calculated. Here, the estimation of the accumulation and the erosion of these positions based on the shoreline changes, extracted from the developed equations, are:

$S = X_B - X$  : Salient length (m);

$T$  : Tombolo width (m);

$\Delta X_G = X_B - X_G$  : The shoreline change at the opposite gap (m);

$\Delta X_U = X_B - X_U$  : The shoreline change at the up-drift (m);

$\Delta X_D = X_B - X_D$  : The shoreline change at the down-drift (m).

From the developed equations, if we know the salient apex distance ( $X$ ), the tombolo width ( $T$ ), the opposite gap distance ( $X_G$ ), the up-drift distance ( $X_U$ ) and the down-drift distance ( $X_D$ ), the shoreline changes parameters are then determined. However, the magnitude of the shoreline changes depends on the individual parameter value, and then the contribution of each parameter to the shoreline changes needs to be reviewed. In order to do this, first, we choose the specific values of all input parameters, namely breakwater parameters, wave characteristics, tidal level and sediment size (called independent variables), which contribute to the equations of  $X$ ,  $T$ ,  $X_G$ ,  $X_U$  and  $X_D$  (called dependent variables). Herein, the particular examined parameters, namely  $L_B = 50\text{m}$ ,  $X_B = 50\text{m}$ ;  $G_B = 50\text{m}$ ,  $H_{\text{repr}} = 2\text{m}$ ,  $L_{\text{repr}} = 40\text{m}$ ,  $\alpha_0 = 30$  degrees,  $h_{\text{tide}} = 2\text{m}$  and  $D_{50} = 0.5\text{mm}$ , are chosen as the basis values. Second, to adjust one of the independent variables while the other independent variables remain constant. Then we find the trend of the shoreline at the survey points, as well as the changed estimated values of the net sediment.

The shoreline change affected by the eight parameters will be analysed in the states of the salient and the tombolo in sections below.

5.2.1 Effect of the breakwater length ( $L_B$ )

In order to analyse the effects of the breakwater length on the sediment accumulation and sediment erosion, the ratios of the breakwater length and the breakwater offshore distance ( $L_B/X_B$ ) are selected to be the salient formation smaller than one; the tombolo formation greater than one (as concluded in section 4.2.1). In the salient formation, the values of the breakwater length are increased, varying from 5 to 50 m and in the tombolo formation, the values of the length of the breakwater are increased, varying from 50 to 140 m, while the other parameters, the offshore distance ( $X_B = 50$  m), the gap width ( $G_B = 50$  m), the representative wave height ( $H_{repr} = 2$  m), the representative wave length ( $L_{repr} = 40$  m), the predominant wave direction ( $\alpha_0 = 30$  degrees), the tidal level ( $h_{tide} = 2$  m) and the median sediment size ( $D_{50} = 0.5$  mm), are kept to be constant. The results of the shoreline changes are shown in figure 5.1 and figure 5.2.

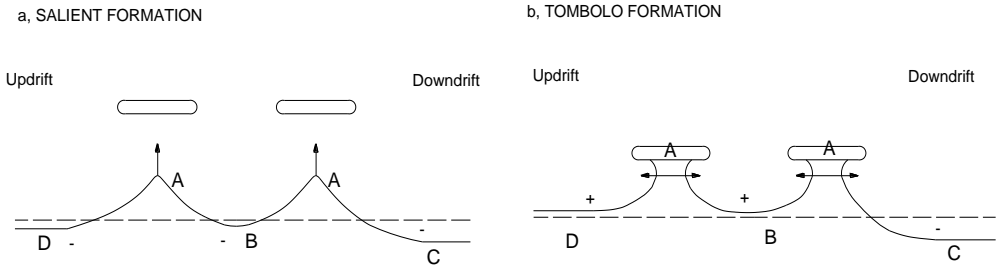


Figure 5.1: The trends of the shoreline when the breakwater length increases

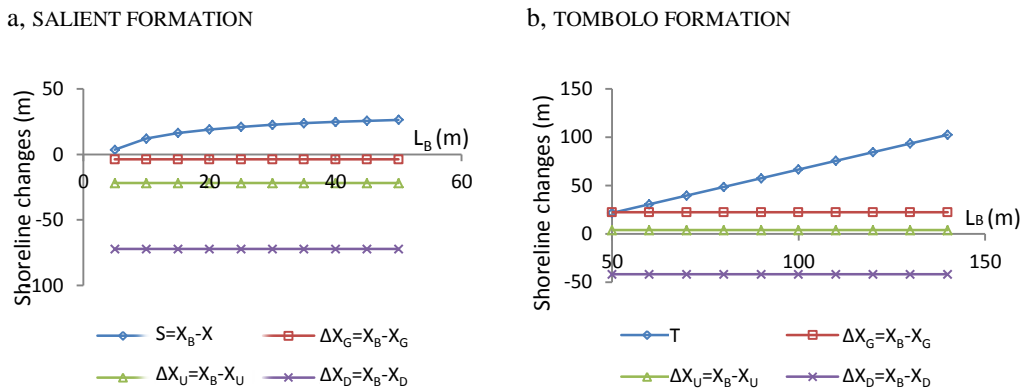


Figure 5.2: The evaluation of the shoreline change as the breakwater length increases

As can be seen from figure 5.1, the length of the breakwater affects the shore at point A as salient or tombolo, while it does not affect the shore at points B, C and D, known as the

opposite gap, the down-drift and up-drift, respectively. The shore at position A has a growth trend of sediment: the salient grows toward the breakwater and the tombolo gets wider.

The estimation values in figure 5.2 show that both the salient length and the tombolo width have an increasing trend, however, the increase of the salient length ( $X$ ) is a curve, while the increase of the tombolo width is a linear line. When the breakwater length increases gradually from 5 to 50m, the salient length increases moderately from just over zero to 26m. The salient length is always smaller than the offshore distance within the data set collected of the breakwater length, as it ranges from 30 to 350 m. The tombolo width expands quickly from 20 to 100m as the breakwater length increases from 50 to 140m. In applying the tombolo calculation with the maximum value of the breakwater length in the data set with 280m, we found that the tombolo reaches close to the proximity of the breakwater length.

The shore changes at point B, C and D are the constant values, while the length of the breakwater increases. The results of the three positions in the salient formation show negative values. It means that the shoreline at these positions will usually erode, within the values of the other input parameters; however, the gap erosion  $\Delta X_G$  (point B) is the smallest - just under zero, and the down-drift erosion  $\Delta X_D$  is the largest - with over 70m (figure 4.40a). In the tombolo formation, position B and D are different from the positions in the salient formation, they actually show accretion. The value of the accretion at the opposite gap (point B) is around 20m, while the value of the accretion at point D is close to zero (figure 5.2b). Similar to point C in the salient formation, point C in the tombolo formation is eroded with a value of erosion of just over 40 m.

### *5.2.2 Effect of the breakwater offshore distance ( $X_B$ )*

The analysis of the shoreline changes in the trend and the magnitude of the breakwater, as the offshore distance increases, while the others parameters remain unchanged at the same chosen basis values, will be discussed. The salient and tombolo occur under the condition of the ratio of the breakwater length and the breakwater offshore distance ( $L_B/X_B$ ). Then, herein, we analyse the breakwater offshore distance changes with increased values from 50 to 140m for the salient formation and an increase of values from 5 to 50m for the tombolo formation. The overall trends are shown in figure 5.3, which presents the directions of the shoreline growth during the offshore distance increases; the quantitative sediment is plotted in the figure 5.4.

As can be seen in figure 5.3a, the shoreline in the salient formation has an incremental trend for all detected points. Waves lose energy on entering the embayment between the breakwaters and the shoreline. When the breakwater is moved further to the shoreline, the wider the sediment supply through the embayment, the greater the increasing rate of the sediment entrapment. In figure 5.4a the increase of values at the four positions, which have the strongest effect of the breakwaters on the shoreline, is shown. The four increasing trends are almost parallel when increasing the offshore distance. However, the salient length is the highest line

with always positive values, in contrast to the down-drift, being the lowest line with always negative values, while both the opposite gap and the up-drift change from negative values into positive values. This graph shows that the down-drift is certain to be eroded, the up-drift is likely eroded and the opposite gap is least eroded.

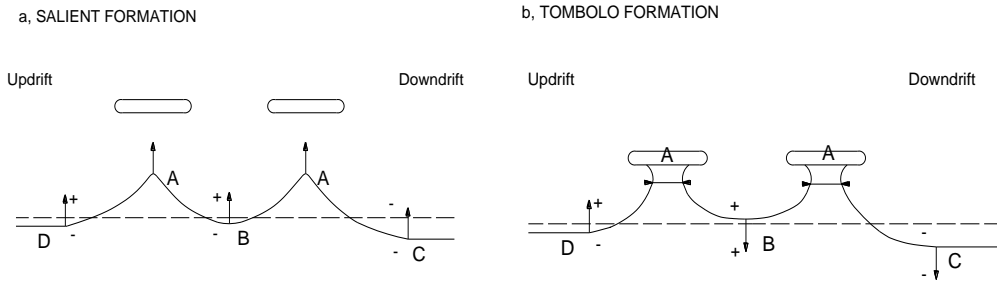


Figure 5.3: The trends of the shoreline when the breakwater offshore distance increases

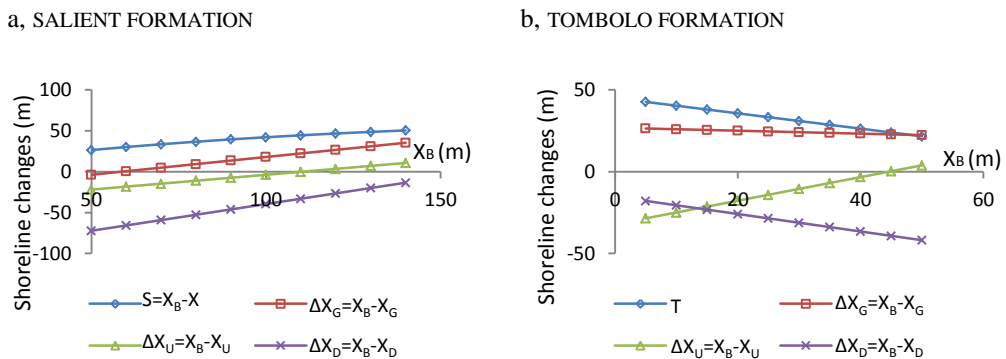


Figure 5.4: The evaluation of the shoreline change as the breakwater offshore distance increases

In case of the tombolo formation, the shore has a very different trend from the salient formation – reduction trends, except the up-drift has an increase trend (figure 5.3b), when the breakwater gets further away the shoreline, the amount of wave energy transmitted into the embayment is larger. Because the tombolo works as a groin, which stops the sediment transport along the shore by the up-drift tombolo, then the sediment deposition at the up-drift increases. In contrast to the positions at the opposite gap and the down-drift, the longshore transport rate reduces as a consequence of the lower sediment supply, leading to erosion. The quantitative net sediment, figure 5.4b illustrates the values change. The tombolo, the opposite gap and the down-drift have different decrease trends. The tombolo, the opposite gap and the down-drift decrease significantly, from 43 to 22m and from -18 to -42m, respectively, and the opposite gap has a

slight decrease, from 26 to 22m. However, the graph indicated that accretion usually occurs at the opposite gap and that the down-drift a certain eroded occurs. The up-drift goes up, but most values are negative, from -28 to 4m.

5.2.3 Effect of the gap width ( $G_B$ )

To determine the effects of the gap width in segmented breakwaters on the shoreline changes, ten gap widths between breakwaters are chosen, with widths ranging from 10 to 100m while the other parameters are constant.

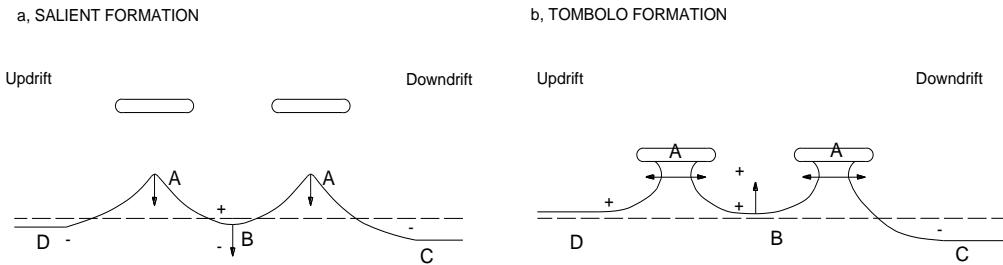


Figure 5.5: The trends of the shoreline when the breakwater gap increases

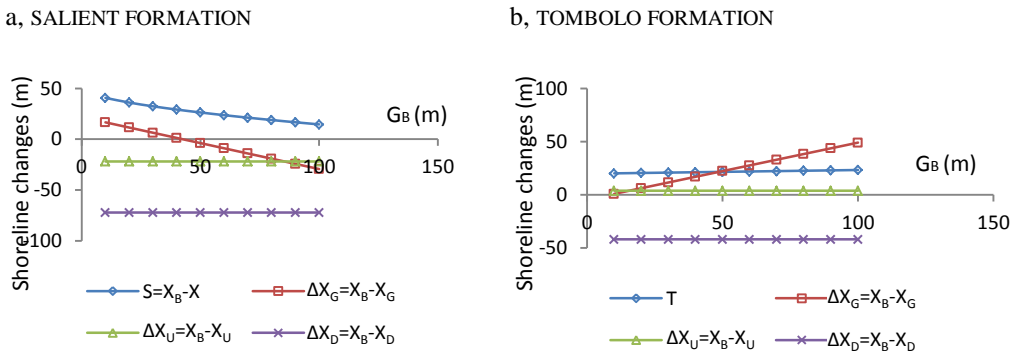


Figure 5.6: The evaluation of the shoreline change as the breakwater gap increases

Figure 5.5 shows the effects of the gap width on the shoreline with the change of the siltation at position A and the change of the opposite gap at point B, but the down-drift and the up-drift (points C and D) remaining unchanged. The two cases of the formation have opposite trends, the salient drops in contrast to the tombolo growth, the opposite gap moves landward in the salient case in contrast to the opposite gap moving seaward in the tombolo case.

As known in figure 5.6a, both the salient length and the gap loose a moderately amount of sand: from 40 to 15m for the salient and from 17 to -29m for the opposite gap. Herein, if we extrapolate the graphs, the salient goes to zero, when the gap width goes to infinity and at the

shore opposite gap occurs infinity erosion, however, the gap width ranges from 20 to 220m in the data set. Both the up-drift and the down-drift remain unchanged when the gap width changes; they will have a state of erosion. Comparing the two positions, the down-drift has more potential erosion than the up-drift.

In the gathered graphs of the tombolo (figure 5.6b), the opposite gap has the largest change in size: the net sediment increases quickly from just over zero to slightly under 50m. The tombolo width has a similar trend, however, it increases slightly, from 20 to 23m. The up-drift has an accelerated and a stable value of 4 m, while the down-drift shows erosion and a stable value of -40m.

#### 5.2.4 Effect of the representative wave height ( $H_{repr}$ )

The wave height is the main cause of sediment transport on the long shore and the cross shore. The sediment changes after breakwater construction will analyse the variation of the representative wave height with the set of wave heights, varying from 0.5 to 5.0m. The description of the shoreline changes and the estimation of its values are presented in figures 5.7 and 5.8.

The tendency of the beach changes at the four positions is shown in figure 5.7. When the representative wave height increases, three of the four positions in the salient formation, the salient, the opposite gap and the up-drift (points A, B and D), show increasing trends, whereas the position at the down-drift has a decreasing trend, while the four positions in the tombolo formation have similar trends, which have decreased.

Commonly, a higher wave height tends to interrupt tombolo formation, because of increased wave penetration through the structure and increased wave overtopping. However, sand spits of the salient tend to have less impact by the wave penetration and the wave overtopping, while the sediment rate still increases inside of the embayment. These reasons lead to a continuation of the growth of the salient.

The evaluation values of the shoreline parameters are shown in the figure 5.8. The salient and the tombolo change with the complicated curves. Both of them change significantly when the representative wave height is smaller than one metre, after that they have a moderate change. The values of the salient length are negative when waves heights are rather low and the values of the tombolo width are negative when waves heights are rather high. It can be assumed that, the siltation estimation is inappropriate in certain areas of the wave height.

In the salient formation, although the shore opposite gap always has a growth trend, however, the net sediment at this position is always negative (figure 5.8a). In contrast with the shore opposite gap in the tombolo formation, the shore has a landward trend, yet, the shore is still always accreted in the wave height range.

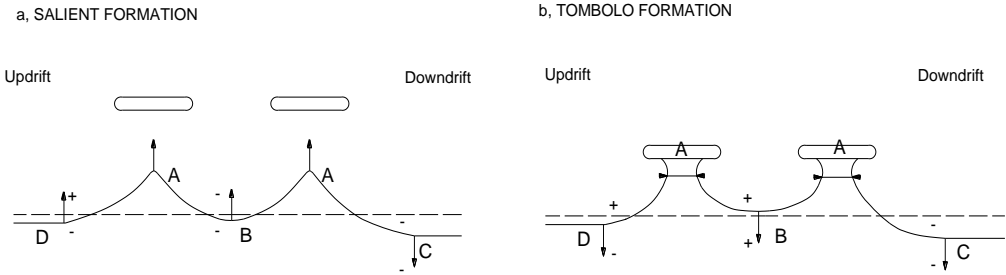


Figure 5.7: The trends of the shoreline when the wave height increases

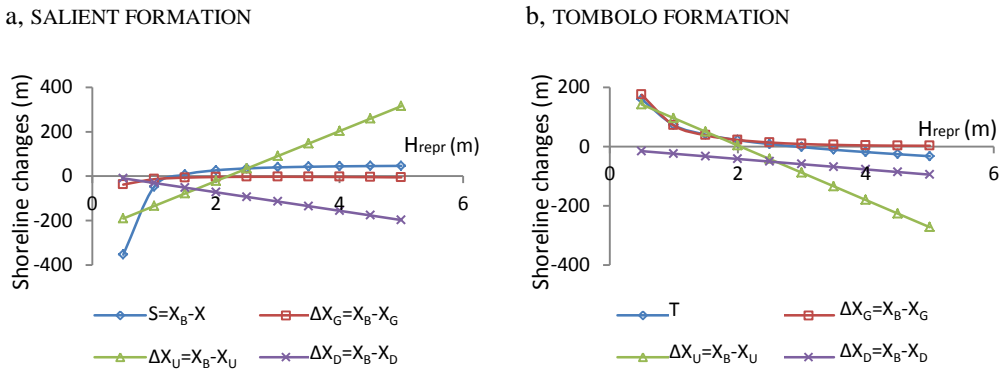


Figure 5.8: The evaluation of the shoreline change as the wave height increases

The up-drift changes rapidly in both cases of formation. The up-drift has an increase from heavily eroded sand to strongly accreted sand (from -190 to +310m). A completely different trend is seen in the tombolo formation; the up-drift has a decreasing trend, from wide accretion to deep erosion (from +140 to -270m).

The down-drift has a moderate decrease in both formations. Hence, the wave height increases as a consequence of the more severe erosion at the down-drift.

In the collection data, the range of the representative wave height varies from 0.4 to 2.3m. Then, the estimation of the shoreline change might be inaccurate if the wave height is outside of this range.

### 5.2.5 Effect of the representative wave length ( $L_{repr}$ )

The representative wavelength is found in the effect on siltation of the salient and the tombolo, while the effect is not found in the other positions. In the analysis, to raise the

representative wavelengths in steps of 5m, from 15 to 60m, we may find out the change of the siltation. The salient increases as the representative wave height increases as well. The values of the salient length rise moderately, from 8 to just over 30m (figures 5.9a and 5.10a). The tombolo width shows a trend of reduction, however, it reduces only slightly, from 24 to 20m (figure 5.10b).

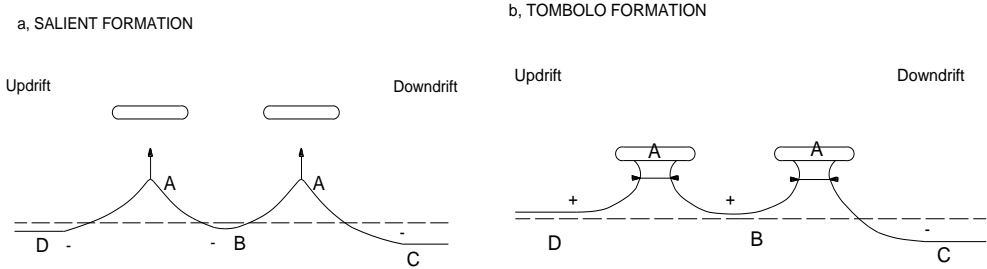


Figure 5.9: The trends of the shoreline when the wave length increases

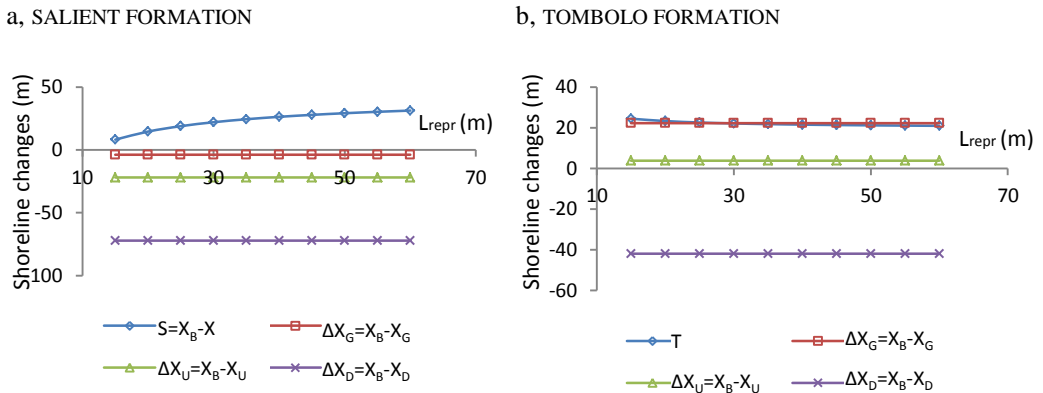


Figure 5.10: The evaluation of the shoreline change as the wave length increases

The three positions: The opposite gap, the up- and the down-drift are independent from the representative wavelength. Their values remain unchanged. In the salient formation these points are found as negative values (or the eroded shore). It is shown that, the down-drift is the most eroded position, while the opposite gap is the least eroded position. The state of the opposite gap and the up-drift in the tombolo formation are different from the state of the salient formation, which is a state of accretion. However, the down-drift is still eroded as in the same state of the salient.

The data set shows the values of the wavelength running from 13 to 60m. However, the estimation of the shoreline change can be extrapolated with a higher wavelength than the collected range.



5.2.6 Effect of the representative wave direction ( $\alpha_0$ )

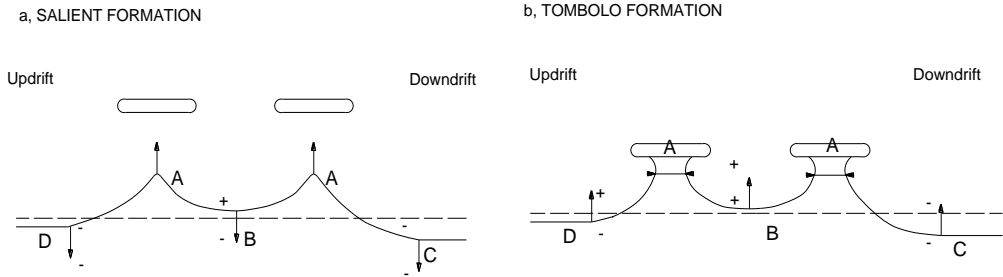


Figure 5.11: The trends of the shoreline when the wave direction increases

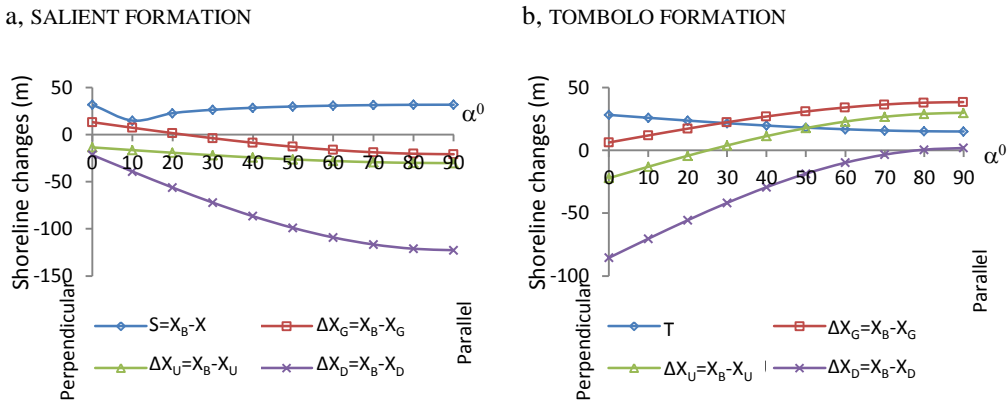


Figure 5.12: The evaluation of the shoreline change as the wave direction increases

The oblique predominant wave is one of the main reasons of sediment movement along the shoreline. Evaluated results are used for the wave perpendicular to the shore to parallel to the shore ( $0^\circ < \alpha_0 < 90^\circ$ ), with other constant parameters, namely  $L_B = 50\text{m}$ ,  $X_B = 50\text{m}$ ;  $G_B = 50\text{m}$ ,  $H_{\text{repr}} = 2\text{m}$ ,  $L_{\text{repr}} = 40\text{m}$ ,  $h_{\text{tide}} = 2\text{m}$  and  $D_{50} = 0.5\text{mm}$ . The descriptions of the trends are given in figures 5.11 and the results obtained from the model are presented in figure 5.12.

In figure 5.11, we can see the opposite trends between the salient formation and the tombolo formation. At the siltation – position A, the salient has an expansion of length; by contrast, the tombolo has a reduction of width. Three other positions, the opposite gap, the up-and down-drift have a decreased trend in the salient formation, and have an increased trend in the tombolo formation.

In figure 5.12 the magnitude of the changes in net sediment during the wave angle increases is shown. In the salient formation (figure 5.12a), the salient length (S) decreases from 30m at the perpendicular wave to 15 m at a wave angle of 10 degrees, and then it grows gradually as a

curve to over 30 m at parallel wave; by contrast, the down-drift ( $\Delta X_D$ ) shows the fastest erosion and it falls from -20m to under -120m. Both the up-drift and the opposite gap lose moderate amounts of sand. The state of the equilibrium shore at the opposite gap ( $\Delta X_G$ ) changes from accretion at small wave angles into erosion at bigger wave angles. But, the state of the equilibrium shore at the up-drift ( $\Delta X_U$ ) is more and more eroded. In the tombolo formation (figure 5.12b), the tombolo width (T) reduces slightly from 28 to 15m. By contrast to the down-drift, it raises quickly, but it is mostly eroded, from -85m to just over zero. The up-drift and the opposite gap have a medium change. Both increase in size, but the up-drift increases ( $\Delta X_U$ ) from an erosion of -20m to an accretion of 30m, while the opposite gap ( $\Delta X_G$ ) gains more and more accretion, from 6 to 38m.

### 5.2.7 Effect of the tidal range ( $h_{tide}$ )

The effects of the tidal range on the change of shoreline are calculated with the increase tidal level from 0 to 4.5m, during which the other parameters are constant. Figure 5.13 explains the tendency at the four positions concerned. The quantitative changes are shown in figure 5.14.

Generally, the trends of the four positions in the salient formation are opposite the trends of these positions in the tombolo formation (figure 5.13). Points A, B and D have a decreasing trend in the salient formation compared to an increasing trend of these points in the tombolo formation, and point C has an increasing trend in the salient formation compared to a decreasing trend in the tombolo formation.

As can be seen from figure 5.14, the up-drift has the biggest change in both of the formations. The net sediment value falls down from 150 to -240m in the salient formation and it climbs up from -200 to 88m in the tombolo formation. The second biggest change is the down-drift; its values go up from -116 to -17m in the salient formation and go down from 34 to -136m in the tombolo formation. In the salient formation, the opposite gap is the least changed; it has a downward trend from a small accretion of 9m to a slight erosion of 20m. The opposite gap in the tombolo formation has an up-trend; it increases gradually from an erosion of 30m to an accretion of 88m. The salient length decreases from the longest it can be (equal to the structure offshore distance, 50m) to -32m. The tombolo width increases from -19 to 73m.

The values of the evaluation show that the tide is one of the most difficult variables to estimate the equilibrium shoreline. The up-drift and the down-drift present the wide range of change. The values of the estimated siltation have negative values with the condition of a tide greater than 3.5 m in the salient formation and smaller than 1.0m in the tombolo formation. It can be concluded that in some areas of tidal range, the functions of estimation of the shoreline change are inappropriate.

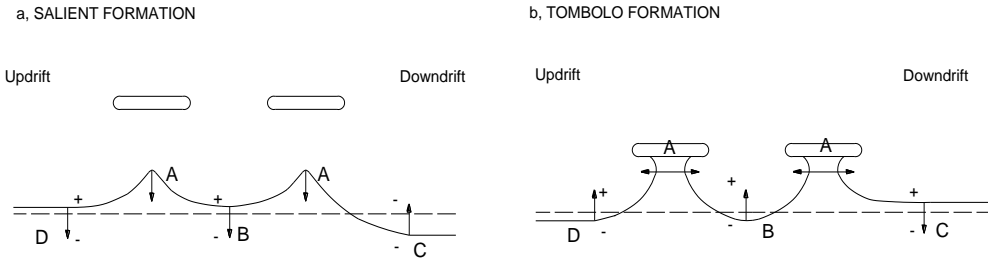


Figure 5.13: The trends of the shoreline when the tide increases

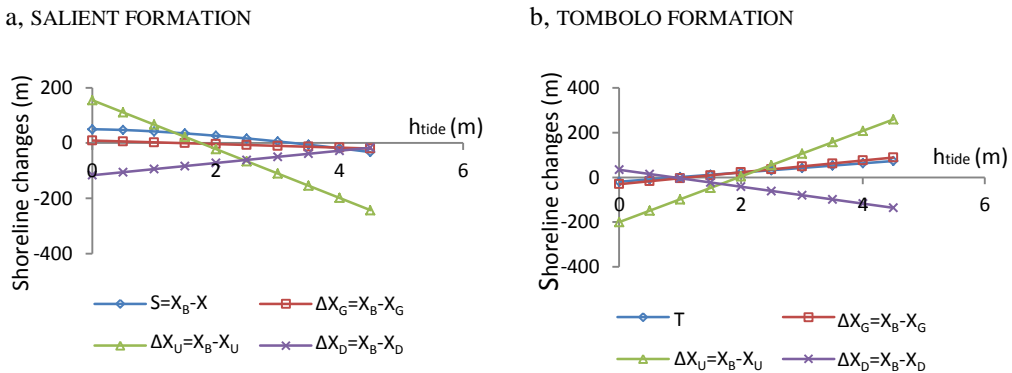


Figure 5.14: The evaluation of the shoreline change as the tide increases

### 5.2.8 Effect of the median sediment size ( $D_{50}$ )

The median sediment size contributes to the equilibrium shore at all of the four positions. To analyse the effects of the sediment size on the shore behind the breakwaters, the sediment size is increased from 0.2 to 2.0mm (this sediment size range is contributed of the data set). The tendencies of the shoreline growth/loss are presented in figure 5.15. The results of the estimation are shown in figure 5.16.

In figure 5.15, it can be seen that the trends of the net sediment at the four positions in the salient formation have opposite trends of these positions in the tombolo formation. The up-drift and the salient lose sand in the salient formation which are compared with the growth sand at the up-drift and the tombolo in the tombolo formation. The gap and down-drift grow sand in the salient formation and are compared with the loss of sand at these points in the tombolo formation.

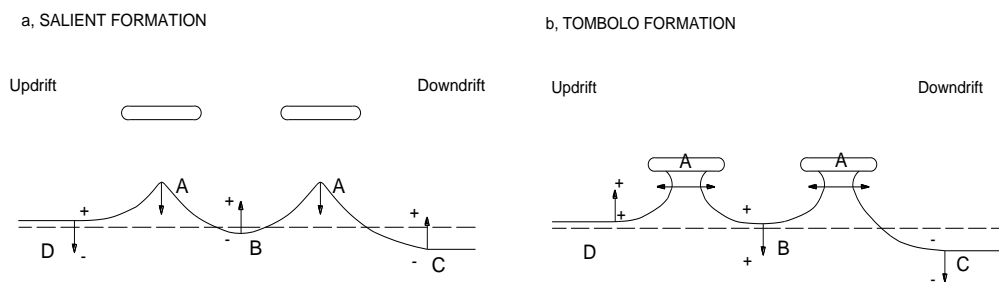


Figure 5.15: The trends of the shoreline when the median sediment size increases

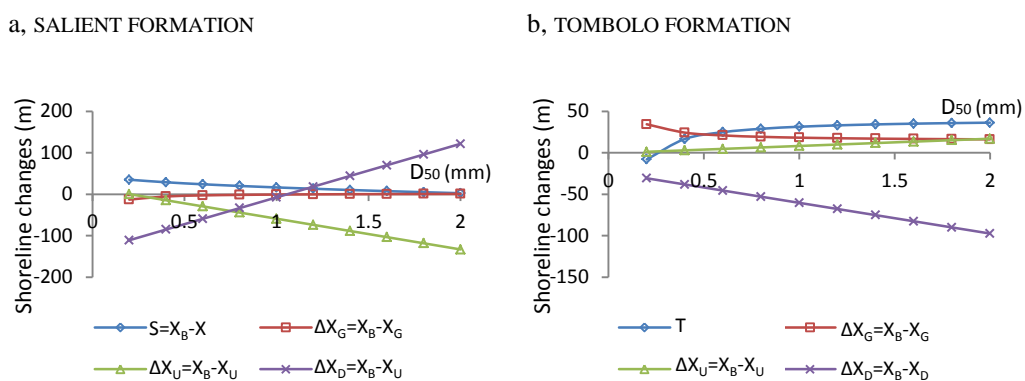


Figure 5.16: The evaluation of the shoreline change as the median sediment size increases

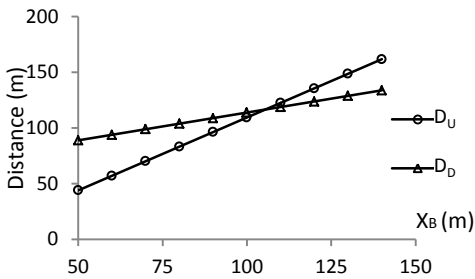
In figure 5.16 the quantitative values of the net sediment, when increasing sediment size with the other parameters remaining constant, are shown. Both formations have a significant change at the down-drift. The down-drift in the salient formation grows rapidly from erosion of 110 m to accretion of 120 m, while the down-drift in the tombolo formation drops quickly from an erosion of 30m to an erosion of 97m. The up-drift has a second significant change in the formation form; it is usually eroded from zero down to -130 m. However, the up-drift in the tombolo formation is the least changed; a slight increase from just over zero to 17m. The opposite gap in the salient increases slightly, but it seems to be slightly eroded. In contrast to the opposite gap in the tombolo formation, it decreases gradually, but it always accretes (from 35m down to 15m). The siltation shows a moderate change: the salient is backward, it gradually loses sand from 35m to almost zero; the tombolo is forward, it grows fast when the sediment size is rather small (fine sand) and remains fairly unchanged when the sediment size is large (coarse sand).

### 5.3 Influence of the parameters on the alongshore axis

As the analysis of the detached breakwaters demonstrates, the width of the shore behind the project is impacted from the limited point of the up-drift to the limited point of the down-drift. The distances alongshore of the limited points are known as a function of the offshore parameters, namely, the wave height, the wave angle, the tidal range and the sediment size. In this section the effects of each parameter, based on changes while the other parameters are constant, will be analysed. The basis values taken in the analysis are similar to the basis values in the cross shore analysis.

#### 5.3.1 Effect of the offshore distance ( $X_B$ )

a, SALIENT FORMATION



b, TOMBOLO FORMATION

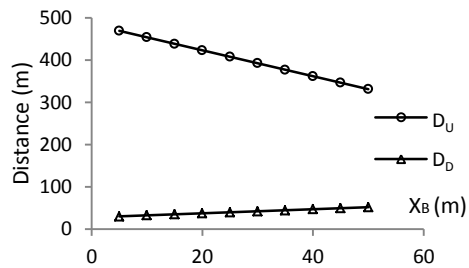


Figure 5.17: Estimation of alongshore effect as the offshore distance

The effect of the offshore distance on the shore at the up- and down-drift as linear lines is analysed (figure 5.17). Both the up-drift and the down-drift in the salient formation show an increase trend as the offshore distance increases. The affected shore is approximately from 50 to 150m at the up-drift and from 90 to 130m at the down-drift. When the offshore distance is less than 100m, the effect of the distance at the up-drift is smaller than at the down-drift distance. However, it is changed when the offshore distance is greater than 100m (figure 5.17a). In the tomboLO formation, the up-drift has a declining trend, while the down-drift has a slight increasing trend. However, the distance effect at the up drift is much more than the distance effect at the down-drift: the up-drift affected distance is reduced from 460m down to 330m compared to the down-drift increase from 30m up to 50m (figure 5.17b).

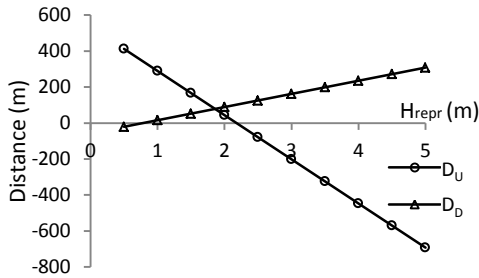
#### 5.3.2 Effect of the wave height ( $H_{repr}$ )

The shore is significantly changed when the wave height increases. The along shore effect distance changes into linear lines in the two formations. It can be seen from figure 5.18, that the trends of the change in the two formations are opposite: a downward trend at the up-drift of the salient is compared to an upward trend of the tomboLO, and an increase trend at down-drift

of the salient is compared to a decrease trend of the tombolo. The distances of the shore effect at the up-drift and the down-drift in the salient is equal at a wave height of around 2m. In contrast to the tombolo formation, the affected distances at the up-drift and the down-drift differ more as the wave height increases.

The data of the wave height ranges from 0.4 to 2.3m, then the equations estimate of the values is incorrect with a higher wave. In the figure, the up-drift of the salient and the down-drift of the tombolo have negative values.

a, SALIENT FORMATION



b, TOMBOLO FORMATION

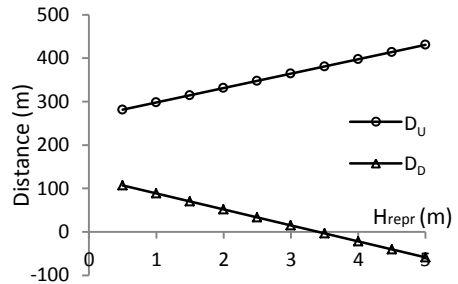
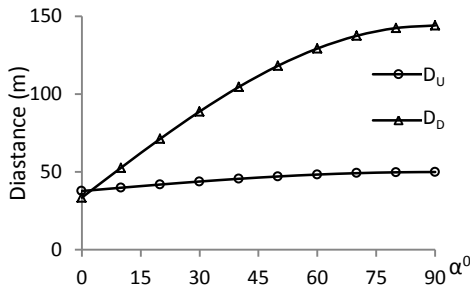


Figure 5.18: Estimation of alongshore effect as the wave height

### 5.3.3 Effect of the oblique wave angle ( $\alpha_0$ )

a, SALIENT FORMATION



b, TOMBOLO FORMATION

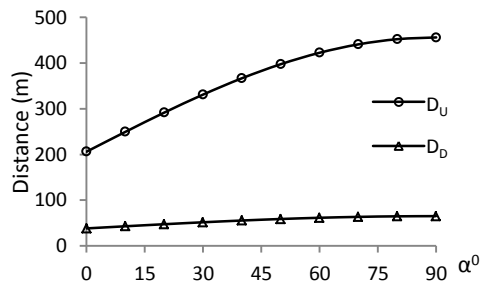


Figure 5.19: Estimation of alongshore effect as the oblique wave angle

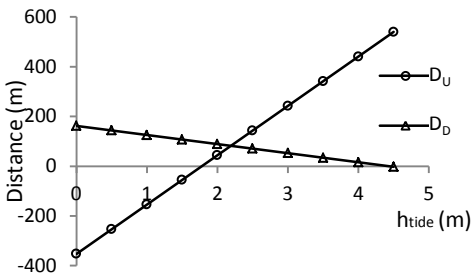
Figure 5.19 shows the more oblique the wave angle, the greater effect of the distance alongshore. In the salient formation, the distances grow as a curve. It increases quickly at the down-drift from 30 to 140m, while the up-drift distance increases slightly from 37 to 50m as the oblique wave angle increases from 0 to 90 degrees. The tombolo formation has increased

curves, however, the up-drift is the much higher curve compared with the curve of the down-drift. The up-drift grows from 200 to 450m, while the down-drift grows from 40 to 65m.

5.3.4 Effect of the tidal range ( $h_{tide}$ )

The tidal range drives the distances effect, which is presented in figure 5.20. It shows that the up-drift of both formations changes significantly: from a negative value of -350m up to 540m in the salient formation, and from 510m down to 100m in the tombolo formation. However, the down-drift of both formations has moderate changes in the decrease trends, from 160m down to zero for the salient formation, and in the increase trend, from 37m to 70m for the tombolo formation.

a, SALIENT FORMATION



b, TOMBOLO FORMATION

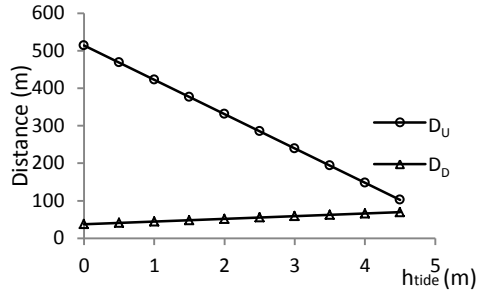


Figure 5.20: Estimation of along shore effect as the tidal range

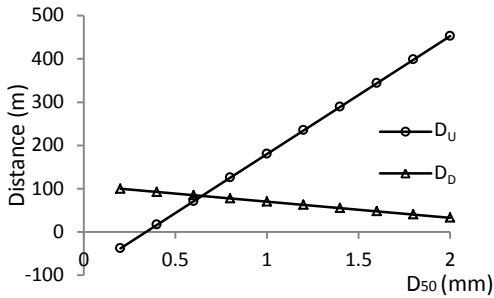
In the estimation result of the tidal change, the up-drift shows the negative values with a tidal range of less than 1.7m in the salient formation. On the other hand, the up-drift can reach high values with a high tide level. AS a consequence, these equations for the up-drift may be inaccurate estimations in several cases of tidal ranges. The fact is, that the tidal range applicability in the data set is from zero to 3.0m.

5.3.5 Effect of the sediment size ( $D_{50}$ )

The median sediment size causes a significant change of the distance at the up-drift and a moderate change of the distance at the down-drift. They both show an increase trend and a decrease trend in the salient formation, but they only result in decrease trends in the tombolo formation (figure 5.21). In the salient formation, the effect distance ranges from under zero up to 450m at the up-drift, and the effect distance ranges from 100m down to 30m at the down-drift. In the tombolo formation, the distance at the up drift ranges from 370m down to 100m, and at the down-drift ranges from 55m down to 30m.

In both graphs of the up-drift distance, we see that, they change quickly and reach really big values in some conditions of different sediment sizes. Hence, these results need to be considered.

a, SALIENT FORMATION



b, TOMBOLO FORMATION

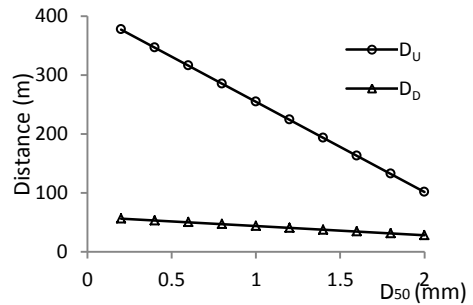


Figure 5.21: Estimation of alongshore effect as the sediment size

#### 5.4 Discussion

Although the estimation equations of the shoreline changes have achieved their goal, the results are under discussions.

First of all, there is a limited range of data. The limited data collection of the projects is taken into account in regression. The contribution of the parameters are not covered in all cases of estimation: the length of breakwater ranges from 15 to 350m; the offshore distance ranges from 20 to 370m; the gap width ranges from 15 to 300m; the representative wave height ranges from 0.37 to 2.31m; the representative wave length ranges from just over 13 m to under 60 m; the predominant wave angle spreads from 2.5 degrees to 83.5 degrees; the tidal level is less than 3.6m; and the median sediment size is from 0.13mm to maximum of 1.86mm. Hence, the estimation of the shoreline changes might be imprecise when it extrapolates outside of the ranges of these data sets mentioned above.

Secondly, imputation of the missing data might lead to unexpected results. As the definition in the planform in figure 3.1 (chapter 3) indicates, the values of the tombolo width (T), the salient length (S), and the distances of the up and the down-drift ( $X_U$ ,  $D_U$ ,  $X_D$ ,  $D_D$ ) are greater and equal to zero. However, negative values of these parameters are found, when interpreting the effects: the salient S has some negative values in the wave height analysis in figure 5.8a; the tombolo T has small negative values in the graphs of the tide and the sediment size analyses in figures 5.14b and 5.16b, and the distance from the up-drift point to the head of the adjacent breakwater shows some negative values in figures 5.20a and 5.21a. Therefore, the



missing values of some parameters imputed to create the relationships are the logical values, but they cast a doubt about the actual prototype values.

Third, the values of the structure parameters, wave parameters, tidal range and sediment size were used as one basis of the interpretation of the shoreline changes. If a random project has new conditions, a recalculation is necessary.

Finally, it has been possible to develop generalizations about the net shoreline changes based on the data collected from the 93 projects. However, in order for the prediction of the shoreline changes to be widely applicable and to be more accurate, the data set needs a larger population of projects.

## **5.5 Conclusions**

In this chapter, the shoreline changes behind the detached breakwaters influenced by the detached breakwaters parameters, the wave parameters, the tidal range and sediment size were reviewed in order to analyse the role and impact of each parameter. The following conclusions are drawn on the developments of the salient and the tombolo formation.

1. Within the values of the parameters taken in the analysis, the four positions on the shoreline always have results, consisting both of negative and positive values. It means that, at least one of the four positions caused erosion, and at least one of the four positions caused accretion. Hence, the detached breakwater constructed has both advantages and disadvantages.
2. The shoreline changes on the cross shore direction are various at the four positions, and they are also different between the salient formation and the tombolo formation:

The results of the evaluation show that the down-drift affects the most frequent erosion on the shoreline. The down-drift in the tombolo formation certainly causes erosion within any values of the parameters, while the down-drift in the salient formation is likely to cause erosion, however seldom, it is accreted.

The shore at the up-drift is impacted by the structures. The up-drift fluctuating from accretion to erosion depends on the magnitude of the input parameters. It is found that the up-drift in the salient formation is probable to erode, while this position in the tombolo formation is less frequently eroded than that of the salient.

The shoreline opposite the gap is affected differently in the two states of formation. The shore at opposite the gap in the tombolo formation is most likely accreted. Compared with the shore opposite the gap in the salient formation, a balance between accretion and erosion may be possible.

The siltation of the tombolo and the salient, both have a loss of sediment and a growth of sediment. The changes of the salient trends are completely opposite the tombolo trends when

the influenced parameters change.

3. The eight parameters contribute sediment on the shore behind breakwater. However, each position has different groups of the influenced parameters on the cross shoreline:

The effects of the wave height, the tidal range and the offshore distance are found to be the most important factors on the variation in sand of the siltation (salient and tombolo).

The other important factors affecting the equilibrium shore at the up- and the down-drift are the wave height, the oblique wave angle, the tidal range and the sediment size.

The most effective factors that have an impact on the shore opposite the gap are the gap width and the wave height.

4. The shore effect we must be concerned about, is not only the inner structures' length, but also the width from the affected up-drift point to the affected down-drift point. The main causes of concern relating to the extra shore are wave climate, tides and sediment.
5. The limited effect point at the down-drift is usually closer to the structure than the up-drift effect point in the project, which has a tombolo formation. However, in the project, which has a salient formation, the dominance of the distance effect points at the up-drift and the down-drift is unclear.
6. The shoreline changes evaluation is more appropriate when the input parameters fluctuate inside the range of the data set. If we extrapolate the shoreline changes outside the range of the input parameters, it might lead to the inaccurate results in several cases.



## CHAPTER 6: CONCLUSIONS AND RECOMMENDATIONS

### 6.1 Conclusions

The research was set out to analyze the shoreline changes behind emerged detached breakwaters under varying geometrical layouts and conditions. We have been able to identify where and when the presence of this structure along the shoreline shows accretion and erosion, as well as to establish a rational and motivation for shore protection. The resources for the prototypes' data, required for the analysis of the impact of breakwaters on the shoreline, have been collected. The equilibrium shoreline has been observed and measured through the aerial images series at four important positions. Consequently, the empirical relationships have been developed between the impact parameters and the equilibrium shoreline parameters, and thereby, the magnitude of the shoreline changes behind the breakwater is quantified under specific conditions. The research has also investigated whether the shoreline can result in effective accretion, and whether the shoreline can result in potential erosion. In the approach to the subject, our attention focused on emerged detached breakwaters and we sought to answer the four following questions:

1. Where are the most sensitive positions on the equilibrium shoreline behind breakwaters?
2. Which parameters are involved in the shoreline behaviour?
3. What are relationships between variables and the shoreline response?
4. How do the individual variables influence the shoreline changes?

The main findings of the research are outlined below:

Previous studies of the empirical relationships can be applicable in limited conditions, with good results in the prediction of the parameters of the tombolo and the salient, but by themselves lack the data to be developed for their application to investigate the changes of all affected beaches, or, to predict the behaviour of a shore with a multiple breakwaters project, including beaches that are impacted simultaneously at the shore opposite the gap, the up-drift and the down-drift.

In this study, new empirical relationships have been developed, based on data of prototypes to investigate the parameters of the equilibrium shoreline at four critical points, namely the siltation point, the shore opposite the gap, the up-drift and the down-drift point. The analysis found that the equilibrium shore behind detached breakwaters was related to eight variables: breakwater length, breakwater offshore distance, gap width, representative wave height, representative wave length, representative wave direction, tidal range and sediment size. The siltation parameters of the tombolo and of the salient that were developed with the dimensionless functions of these eight variables are:

$$\frac{T}{X_B} \left( \text{or } \frac{X}{L_B} \right) = f \left( \frac{L_B}{X_B}, \frac{G_B}{L_{repr}}, \sin \alpha_0, \frac{h_{tide}}{H_{repr}}, \frac{H_{repr}}{D_{50}} \right)$$

The shoreline opposite the gap was also found in the dimensionless relationship, but the function consisting of seven of the eight variables is:

$$\frac{X_G}{G_B} = f \left( \frac{X_B}{G_B}, \sin \alpha_0, \frac{h_{tide}}{H_{repr}}, \frac{H_{repr}}{D_{50}} \right)$$

The shoreline at the up-drift and the down-drift distances were the dimensional functions of the five variables are:

$$X_{U(D)} \text{ or } D_{U(D)} = f(X_B, H_{repr}, \sin \alpha'_0, h_{tide}, D_{50}).$$

The new data analysis of the equilibrium shoreline is to determine whether a tombolo or a salient is formed as a function of the breakwater length ( $L_B$ ) and breakwater offshore distance ( $X_B$ ). The good agreement for the data showed that a tombolo is formed if the ratio of the breakwater length and the breakwater offshore distance is greater than one, and that a salient is formed if the ratio of the breakwater length and breakwater offshore distance is smaller than one.

Detached breakwaters reduced but did not eliminate erosion in the field of the structures. Evaluation of the shoreline showed that of the three positions at the opposite gap, the up-drift and the down-drift, at least one of them is always eroded. The chances of erosion in the tombolo formation presented the possibility of erosion at the down-drift, might a chance of erosion at the up-drift, and rare erosion at opposite the gap. The chance of erosion in the salient formation showed that in these three positions there is not much difference; both situations of

erosion and accretion exist. However, the down-drift has more potential for erosion than the other positions.

Seiji et al. (1987) suggested the boundary of the shore opposite the gap responses, based on the ratio of the gap width and the offshore distance ( $\frac{G_B}{X_B}$ ). However, the data of the prototypes did not fit with the Seiji boundary. New findings found that gap erosion or accretion is likely to refer to the relationship between the ratio of the offshore breakwater distance and the gap width ( $\frac{X_B}{G_B}$ ), and the ratio of the shoreline opposite the gap to breakwater and the gap width ( $\frac{X_G}{G_B}$ ); while the shore opposite the gap in the tombolo formation is most likely accreted, compared with the possibility of both accretion and erosion of the shore opposite the gap in the salient formation.

The magnitude of a tombolo width is possible to be determined if the eight parameters are known. The model results for the tombolo showed that the tombolo width increases as the breakwater length, the gap width, the tidal range and the sediment size are increased. Herein, the breakwater length is the most effective parameter for the tombolo growth, and the gap width is the least effective parameter. The tombolo width reduces by an increase of the offshore distance, the wave height, the wave length and the oblique wave angle. The fastest reduction of the tombolo width is an increment of the wave height, but the wavelength is the lowest active parameter.

The magnitude of a salient length can be calculated through the salient equations as well. The models for the salient formation showed that the sediment accumulates more in the salient siltation in the lee, as the breakwater length, the offshore distances, the wave height, the wave length and the oblique wave angle are increased, where it is unclear which parameter is dominant, as they have an equal role in the increasing of the salient length. The relative salient length decreases as the gap width, the tidal range and the sediment size are increased. In this case, the tidal range is slightly more active than the gap width and sediment size.

Limited responses of the shoreline in the lee may happen when the breakwater is constructed close to other structures, which interrupt long-shore sediment transport. From observations it was shown that unsuccessful breakwaters were placed in the field of the down-drift of a groin, or near a port with breakwaters, nearby river mouths, or even at the down-drift side of a long segment.

The shore opposite the gap response is different with siltation occurring. In the situation of a tombolo and when siltation is occurring, the shore opposite the gap is likely to accrete in most conditions. The magnitude of the shoreline opposite the gap increases as the gap width, the oblique wave angle and the tidal range are increased. Here, the increasing of the gap width is the strongest parameter to encourage sediment deposition, while the oblique wave is the least influential parameter in comparison with the other three parameters. The shoreline opposite the gap decreases with increasing offshore distances, wave height and sediment size. Herein,

increasing the wave height results in the fastest recession of the shore opposite the gap; by contrast, increasing the offshore distance results in the lowest recession in the area. Another case of salient siltation occurs when the shore opposite the gap has both chances of erosion and accretion. The sediment accumulates more at the shoreline opposite the gap as the offshore distances is farther away, and as the wave height and the sediment size are increased. The offshore distance increase is the main result of the sediment accumulation, while the two other parameters are less important. The shoreline opposite the gap is reduced by increasing the gap width, the oblique wave angle and the tidal range. The most active parameter is the gap width, while the tidal range is the least active parameter.

The shore at the up-drift may be eroded in the breakwater fields. Considering a scenario of frequent erosion, found that the up-drift of the salient formation is more frequently eroded than the up-drift of the tombolo formation. The most effective parameter, resulting in the up-drift of the tombolo formation and losing sediment quickly, is an increasing of the wave height. The tidal range most is important in changes of the shore at the up-drift of salient formation; its increases lead to more up-drift erosion.

The shore at the down-drift has the greatest potential for erosion in the breakwater fields. The model results showed that the down-drift is certain of erosion, when a project creates a tombolo. The amount of erosion in the down-drift is generally reduced with increasing values of the influential parameters, except the oblique wave angle. Herein, the tidal range and the wave height that are the most impacted factors. The model for the down-drift of the salient formation showed that the down-drift is most likely to cause erosion, however, it is seldom accreted. An increase of the offshore distance, the tidal range and the sediment size is the relative cause for sediment accumulation more in the down-drift, while the relative sediment loses more by increasing the wave height and the oblique wave. The important factors of the shoreline changes in the salient formation are the wave height and the sediment size.

However, the widths alongshore of the erosion area at the up-drift and at the down-drift are a fluctuation, which can be estimated. The erosion length along the down-drift is usually shorter than that of the up-drift in the tombolo formation, ranging mostly from 0.5 to 3 times the offshore distance at the down-drift, compared to 2 to 9 times the offshore distances at the up-drift. In the salient formation, the erosion length alongshore at both the up-drift and the down-drift occur within 0.5 to 5 times of the breakwater offshore distance from the head of the adjacent breakwater.

Although the aim of this research, i.e. the estimation of shoreline changes to be more widely applicable and to be more accurate, has been reached, the data set needs a larger population of projects in order to be complete.

## 6.2 Recommendations

The following recommendations are offered for related research in the field of hydraulic science and further academic investigation:

- Detached breakwaters can redistribute sand in the littoral zone, but do not provide or create sediment to a protected beach. As a consequence of accretion, which deposits in the embayment, erosion will occur in adjacent areas. It is strongly recommended that pre-beach fill at the up-drift areas will be included as a component of all breakwater projects, to supply a sediment source for planform and to reduce erosion impacts, pre-filling the volume of sand that is estimated to accumulate in the field.

- The measurements of the prototypes, taken in this study, will be valuable for physical and numerical model validation.

- Further investigation of the effect of varying freeboard height and crest width on the beach changes is advised. The wave energy dissipation rate depends on the freeboard height and crest width. The present research has investigated the effect of normal wave incidence on the low-crested breakwaters with uniform crest width. Thus, the effect of freeboard height and crest width of breakwater on the shoreline changes in this research is presently unclear;

- The effect of tidal currents was not included in the present study. A variation of sea water level leads to tidal currents, which transports sediment by bed shear stress. The effect of tidal currents must be different in the macro-tidal beaches and micro-tidal beaches. Further research on the effect of the tidal currents is necessary.

- Investigation of the different results between the breakwater at the up-drift and the breakwater at the down-drift in a long scheme is advised. The present research has developed, and is based on, the mean values of the projects, which supposes that the sediment transport rate is the same at any given breakwaters in the scheme. Therefore, the additional investigation will provide more information of the shoreline response at different structure positions in the long scheme.

- Further investigation of optimization of the detached breakwater on its plan shape and finding the appropriate parameters of the salient or tombolo formations, which have the minimum erosion impact on the shore at the opposite gap, the up-drift and the down-drift.

The new empirical relationships have been developed based on the data of prototypes, including structure parameters, physical conditions, sediment size and gathering equilibrium shoreline measurements from aerial photography.





## REFERENCES

- AHRENS, J. & COX, J. 1990. Design and performance of reef breakwaters. *Journal of Coastal Research*, 61-75.
- BATTJES, J. A. & JANSSEN, J. P. F. M. 1978. Energy loss and set-up due to breaking of random waves. *Coastal Engineering*, 19.
- BIRBEN, A. R., ÖZÖLÇER, İ. H., KARASU, S. & KÖMÜRÇÜ, M. İ. 2007. Investigation of the effects of offshore breakwater parameters on sediment accumulation. *Ocean Engineering*, 34, 284-302.
- BRICIO, L., NEGRO, V. & DIEZ, J. J. 2008. Geometric Detached Breakwater Indicators on the Spanish Northeast Coastline. *Journal of Coastal Research*, 245, 1289-1303.
- CENTER, C. E. R. 1984. Shore Protection Manual (SPM), 4th edition.
- CHASTEN, M. A., ROSATI, J. D., MCCORMICK, J. W. & RANDALL, R. E. 1993. Engineering Design Guidance for Detached Breakwaters as Shoreline Stabilization Structure. DTIC Document.
- CUR 97-2A 1997. Beach Nourishment and Shore Parallel Structures. *Technical report, Gouda, The Netherlands*, Phase 1.
- DALLY, W. R. & POPE, J. 1986. Detached breakwaters for shore protection. DTIC Document.
- DEAN, R., BEREK, E., GABLE, C. & SEYMOUR, R. 1982. Longshore transport determined by an efficient trap. *Coastal Engineering Proceedings*, 1.
- DEAN, R. G. Heuristic models of sand transport in the surf zone. Conferences on engineering dynamics in the surf zone, Sydney, NSW, Proceeding, 1973. 208-214.
- ENGINEERS, U. S. A. C. O. 2002. Coastal Engineering Manual. *Engineer Manual 1110-2-1100, U.S. Army Corps of Engineers, Washington, D.C.*
- FRIED, I. 1976. Protection by means of offshore breakwaters. *Coastal Engineering Proceedings*, 1.
- GALOFRÉ, J., MONTOYA, F. & MEDINA, R. 1997. Beach Nourishment in Altafulla, Spain: Verification of Theoretical Models. *Coastal Engineering*, 14.
- GOURLAY, M. R. 1974. Wave set-up and wave generated currents in the lee of breakwater or headland. *Coastal Engineering*, 14, 20.

- GOURLAY, M. R. 1981. Beach processes in the vicinity of offshore breakwaters and similar natural features. *Coastal and Ocean Engineering*, 5.
- HALLERMEIER, R. J. Sand transport limits in coastal structure designs. *Coastal Structures* 83, 1983. ASCE, 703-716.
- HANSON, H. & KRAUS, N. C. 1990. Shoreline response to a single transmissive detached breakwater. *Coastal Engineering Proceedings*, 1.
- HARRIS, M. M. & HERBICH, J. B. 1986. Effects of breakwater spacing on sand entrapment. *Journal of Hydraulic Research*, 24, 347-357.
- HERBICH, J. B. 1989. Shoreline changes due to offshore breakwaters. *International Association for Hydraulic Research Congress*, 23, 11.
- HSU, J. R. & SILVESTER, R. 1990. Accretion behind single offshore breakwater. *Journal of waterway, port, coastal, and ocean engineering*, 116, 362-380.
- ILIC, S., CHADWICK, A. J. & FLEMING, C. 2005. Investigation of detached breakwaters. Part 2 - morphodynamics. *Maritime Engineering* 158, 20.
- INMAN, D. L. & BAGNOLD, R. 1963. Littoral processes. *The sea*, 3, 529-553.
- INMAN, D. L. F., J.D. 1966. Littoral processes and the development of shorelines. *Coastal Engineering*, 10, 26.
- JOSÉ MA BERENQUER, J. E. 1988. Design of pocket beaches. The Spanish case. *Coastal Engineering*, 1411-1425.
- K.J. MACINTOSH, C. A. 1988. Artificial beach units on Lake Michigan.pdf. *Coastal Engineering*, 2840-2854.
- KAMPHUIS, J. W. 1991. Alongshore sediment transport rate. *Journal of Waterway, Port, Coastal, and Ocean Engineering*, 117, 17.
- KOMAR, P. D. & INMAN, D. L. 1970. Longshore sand transport on beaches. *Journal of geophysical research*, 75, 5914-5927.
- KRAUS, N. C., ISOBE, M., IGARASHI, H., SASAKI, T. O. & HORIKAWA, K. 1982. Field experiments on longshore sand transport in the surf zone. *Coastal Engineering Proceedings*, 1.
- KRIEBEL, D. L. 1983. *Beach and dune response to hurricanes*. University of Delaware.
- KRIEBEL, D. L. & DEAN, R. G. 1985. Numerical simulation of time-dependent beach and dune erosion. *Coastal Engineering*, 9, 221-245.
- LAMBERTI, A., ARCHETTI, R., KRAMER, M., PAPHITIS, D., MOSSO, C. & DI RISIO, M. 2005. European experience of low crested structures for coastal management. *Coastal Engineering*, 52, 841-866.
- MADSEN, O. S. & GRANT, W. D. 1976. Quantitative description of sediment transport by waves. *Coastal Engineering Proceedings*, 1.

- MAURICIO GONZÁLEZ, R. M. 2001. On the application of static equilibrium bay formulations to natural and man-made beaches. *Coastal Engineering*, 43, 209-225.
- MCCORMICK, M. E. 1993. Equilibrium shoreline response to breakwaters. *Journal of waterway, port, coastal, and ocean engineering*, 119, 657-670.
- MICHE, R. 1944. Mouvement ondulatoires de la mer en profondeur constante ou décroissante. *Annales des Ponts et Chaussées*.
- MING, D. & CHIEW, Y.-M. 2000. Shoreline changes behind detached breakwater. *Journal of Waterway, Port, Coastal, and Ocean Engineering*, 126.
- MOORE, B. D. 1982. *Beach profile evolution in response to changes in water level and wave height*. University of Delaware.
- NIR, Y. 1976. Detached breakwaters, groynes and artificial structures on the Mediterranean shore and their influence on the structure of the Israeli shore. *Report No.3,76/2, Jerusalem, March 1976 Ministry of Industry and Commerce, Geological Institute, Marine Geology Section*.
- NIR, Y. 1982. Offshore artificial structures and their influence on the Israel and Sinai Mediterranean beaches. *Coastal Engineering Proceedings*, 1.
- NOBLE, R. M. 1978. Coastal structures' effects on shorelines. *Coastal Engineering*, 16, 17.
- POPE, J. & DEAN, J. L. 1986. Development of design criteria for segmented breakwaters. *Coastal Engineering Proceedings*, 1.
- RICARDO DEL VAILE, R. M., AND MIGUEL A. LOSADA 1993. Dependence of Coefficient K on Grain Size. *Waterway, Port, Coastal, Ocean Engineering*, 119.
- ROELVINK, J. & STIVE, M. 1989. Bar-generating cross-shore flow mechanisms on a beach. *Journal of Geophysical Research: Oceans (1978–2012)*, 94, 4785-4800.
- ROSATI, J. D. 1990. Functional design of breakwaters for shore protection: Empirical methods. *Technical report CERC-90-15, U.S. Army Engineer Waterways Experiment Station, Vicksburg, MS*.
- ROSEN, D. S. & VAJDA, M. 1982. Sedimentological influences of detached breakwaters. *Coastal Engineering Proceedings*, 1.
- SAVILLE, J. T. 1962. An approximation of the wave run-up frequency distribution. *Coastal Engineering*, 8, 12.
- SEIJI, M., UDA, T. & TANAKA, S. 1987. Statistical study on the effect and stability of detached breakwaters. *Coastal Engineering in Japan*, 30, 131-141.
- SHEPARD, F. P. & INMAN, D. L. 1951. *Sand movement on the shallow inter-canyon shelf at La Jolla, California*, US Beach Erosion Board.
- SHINOHARA, K. & TSUBAKI, T. Model study on the change of shoreline of sandy beach by the offshore breakwater. *Coastal Engineering (1966)*, 1966. ASCE, 550-563.

## References

---

- STIVE, M. 1986. A model for cross-shore sediment transport. *Coastal Engineering Proceedings*, 1.
- SUH, K. & DALRYMPLE, R. A. 1987. Offshore Breakwaters in Laboratory and Field. *Journal of Waterway, Port, Coastal, and Ocean Engineering*, 113.
- TOYOSHIMA, O. 1974. Design of a detached breakwater system. *Coastal Engineering*, 14, 13.
- TOYOSHIMA, O. 1982. Variation of Foreshore due to detached breakwaters. *Coastal Engineering*, 20.
- UDA, T. 1988. Statistical analysis of detached breakwaters in Japan *Coastal Engineering*.
- VAN DER MEER, J. W. 1991. Stability and transmission at low-crested structures. *Delft Hydraulics Publication No. 453, Delft, The Netherlands*.
- WEN-JUINN, C. & CHING-TON, K. 1995. Effects of detached breakwater on shore protection. *International Conference on Coastal and Port Engineering in Developing Countries*.
- YAMADA, K., UDA, T., FURUIKE, K., SUWA, Y., SAN-NAMI, T. & ISHIKAWA, T. 2010. Mechanism of Offshore Sand Discharge into Submarine Canyon Triggered by Construction of Detached Breakwaters close to Shoreline

## WEBSITES

Low crested detached breakwaters data in Europe in the DELOS project. Link: <http://databases.eucc-d.de/plugins/projectsdb/project.php?show=258>

Detached breakwaters data in the US in CERC. Link: <http://chl.erdc.usace.army.mil/datas>

Wave data in the ERA-40. Link: [http://apps.ecmwf.int/datasets/data/era40\\_daily/](http://apps.ecmwf.int/datasets/data/era40_daily/)

Wave data in the WIS. Link: <http://wis.usace.army.mil/>

Ocean current data in OSCAR. Link: <http://www.oscar.noaa.gov/>

Dissertation online. Link: <http://repository.tudelft.nl/>

Appendixes of this dissertation. Link: <http://dx.doi.org/10.4121/uuid:9a2775c0-7c64-4fe1-bf02-221574825197>



## LIST OF SYMBOLS

**Roman symbols**

A	profile scale factor	-
$A_T$	accreted sand area	$m^2$
C	dimensional coefficient	-
$C_B$	crest width of breakwater	m
$C_f$	friction factor	-
$C_{g0}$	group velocity	m/s
D	dissipation energy flux into surf zone	J
d	grain diameter	mm
$D^*$	equilibrium energy dissipation per unit volume	$j/m\ s$
$D_{50}$	sand median size	mm
$D_D$	distance alongshore from down-drift point to an adjacent breakwater's head	m
$d_{sa}$	annual seaward limit of the littoral zone	m
$d_t$	average tombolo sand layer thickness	m
$D_U$	distance alongshore from up-drift point to an adjacent breakwater's head	m
E	wave energy per unit surface area	$J/m^2$
F	energy flux per unit width	$J/m\ s$
$F_B$	freeboard of breakwater	m
g	gravity	$m/s^2$
$G_B$	gap width between two successive breakwaters	m
h	water depth	m
$H_0$	deep water wave height	m
$H_0$	deep water wave height	m
$H_b$	breaking wave height	m
$h_B$	water depth at breakwater	m
$H_e$	deep-water wave height exceeding 12 hours per year	m
$H_{max}$	maximum wave height	m
$H_{repr}$	representative wave height	m
$H_s$	significant wave height	m



*List of Symbols*

---

$h_{\text{tide}}$	tidal range	m
$I_c$	dynamic transport rate	kg/s
$I_s$	Pope and Dean value	-
$J$	unit factor pointing shoreward	
$K$	Komar dimensionless parameter	-
$K_s$	shoaling coefficient	-
$K_T$	structure transmissivity	-
$L_0$	deep water wavelength	m
$L_B$	length of breakwater	m
$L_{\text{repr}}$	representative wavelength	m
$n$	ratio of wave group speed and phase speed	-
$n_w$	number of waves in the dominant direction	-
$p$	sediment porosity	-
$P_1$	alongshore energy flux per unit length of beach	J/m day
$Q$	amount of sediment moved alongshore	kg/s
$Q_b$	amount of sand deposition in the lee	m <sup>3</sup>
$q_s$	volumetric cross-shore sediment transport rate per unit width	m <sup>3</sup> /m
$R^2$	coefficient of determination (or goodness of fit)	-
$S$	distance from the land spit at its apex measured from original shoreline	m
$S_w$	wave steepness	-
$S_{xy}$	longshore current	N/m
$T$	wave period	s
$T$	tombolo width	m
$T/2-t_2$	time finish motion	s
$t_1$	time start motion	s
$T_e$	wave period corresponding to wave height exceeding 12 hours per year	s
$T_p$	breaking wave period	s
$T_{\text{repr}}$	representative wave period	s
$U$	near bed velocity of fluid	m/s
$U_c$	mean direction current	m/s
$X$	distance from salient edge to the breakwater's shore parallel centre axis	m
$X_B$	distance from breakwater to original shoreline	m
$X_{br}$	breaker line's distance from original shoreline	m
$X_D$	distance from down-drift point to the breakwater's shore parallel centre axis	m
$X_G$	distance shore opposite the gap to the breakwater's shore parallel centre axis	m

---

$X_U$	distance from up-drift point to the breakwater's shore parallel centre axis	m
$Y_T$	attachment width at the breakwater	m

**Greek symbols**

$\alpha_0$	oblique deep water wave angle	degree
$\alpha_b$	beach slop outside break point	degree
$\beta$	local bottom slope	-
$\Psi$	Shields parameter	-
$\Psi_m$	mobility number	-
$\varepsilon_0$	McCormick value	-
$\theta$	angle the wave ray makes with the onshore	degree
$\theta_B$	orientation of structure to the original shore	degree
$2\theta_b$	small value of breaking wave angle	degree
$\theta_N$	orientation of structure to the true North	degree
$\overline{i(y)}$	local mixed bedload and suspend load vector	
$\bar{\phi}$	mean transport rate over half a wave period	kg/s
$\Delta X_D$	net length of sediment erosion/accretion at down-drift shore	m
$\Delta X_G$	net length of sediment erosion/accretion at shore opposite gap	m
$\Delta X_U$	net length of sediment erosion/accretion at up-drift shore	m
$\pi$	Pi number	-
$\rho$	mass density of water	kg/m <sup>3</sup>
$\rho_s$	mass density of the sediment grains	kg/m <sup>3</sup>
$\omega$	fall velocity	m/s
$\sigma$	standard error of the estimate	-
$\sigma_H$	standard deviation of wave height	m
$\sigma_T$	standard deviation of period	s
$\sigma_a$	standard deviation of wave angle	degree



## LIST OF FIGURES

<i>Figure 1.1: Schematic of this research</i> .....	5
<i>Figure 2.1: Detached breakwaters (Coastal Engineering Manual, 2002)</i> .....	8
<i>Figure 2.2: Nearshore circulation system showing the rip currents and the feeder currents (modified from Shepard and Inman (1951)).</i> .....	11
<i>Figure 2.3: Waves near a single detached breakwater(CUR 97-2A, 1997)</i> .....	16
<i>Figure 2.4: Wave induced currents around segmented detached breakwaters</i> .....	17
<i>Figure 2.5: Zigzag movement of sediment (Adapted from Ming and Chiew (2000))</i> .....	18
<i>Figure 3.1: The definition of terms used in the thesis</i> .....	32
<i>Figure 3.2: How to recognize the objects by colours that appear in the aerial image</i> .....	34
<i>Figure 3.3: Number of the collected projects (a) and structures (b) in the different countries.</i> ..38	
<i>Figure 3.4: Histograms showing the distribution of cases and structures for each investigated parameters.</i> .....	41
<i>Figure 3.5: The direction measurement at San Antonio beach, Calonge, Spain project.</i> .....	42
<i>Figure 3.6: Significant waves height retrieved from the ERA-40</i> .....	43
<i>Figure 3. 7: Deep water wave at Kaike, Japan project</i> .....	45
<i>Figure 3.8: Wind rose (a) and wave rose (b) at the WIS station 92031 in Erie Lake. January 1980 – December 2012 (from USACE)</i> .....	46
<i>Figure 3.9: The distribution of projects and structures for representative wave parameters</i> ..	48
<i>Figure 3. 10: Comparison between waves collection and waves in the reports</i> .....	49
<i>Figure 3.11: The spring tidal range distribution</i> .....	49
<i>Figure 3.12: The salient measurements at low water level (a) and high water level (b) at Central Tel Aviv Coast, Israel</i> .....	52
<i>Figure 3.13: The tombolo measurements at low water level (a) and the salient measurements at high water level (b) at Elmer, the UK</i> .....	52
<i>Figure 3.14: Definition of measurement the shore opposite the gap</i> .....	53
<i>Figure 3.15: Sketch of the regions generated by detached breakwater</i> .....	54
<i>Figure 3.16: Rip currents in the lee of breakwater in a physical model</i> .....	55
<i>Figure 4.1: Comparing the field of the new data with the existing graph</i> .....	59
<i>Figure 4.2: Relationship between <math>T/X_B</math> versus <math>L_B/X_B</math> of tombolo formation</i> .....	61
<i>Figure 4.3: Relationship between <math>X/L_B</math> versus <math>L_B/X_B</math> of salient formation</i> .....	61

Figure 4.4: Relationship between  $X/L_B$  versus  $L_B/X_B$  of no sinuosity formation ..... 62

Figure 4. 5: Effect of dimensionless of the gap width to the representative wavelength ..... 63

Figure 4.6: Effect of the oblique predominant incident waves on dimensionless of the sediment in the lee. a, Tombolo form; b, Salient form; c, No sinuosity form. .... 64

Figure 4.7: Effect of dimensionless tidal range to representative wave height ..... 65

Figure 4. 8: Effect of sediment size (relative sediment uplift ability,  $H_{repr}/D_{50}$ ) on planform a, Tombolo form; b, Salient form; c, No sinuosity form..... 66

Figure 4.9: Regression standardized residual of dependent variable in equation 4.11 ..... 71

Figure 4.10: Regression standardized residual of dependent variable in equation 4.20..... 72

Figure 4.11: Regression standardized residual of dependent variable in equation 4.25..... 72

Figure 4.12: Measurement data versus Mauricio González data..... 73

Figure 4.13: The observations versus Hsu and Silvester (1990) data ..... 74

Figure 4.14: Inventory of the state of opposite gaps..... 76

Figure 4.15: Comparison of the evaluation of Seiji and the measurement data for the shoreline erosion opposite the gaps (after Rosati (1990)) ..... 76

Figure 4.16: The relationships of gap dimensionless parameters ..... 77

Figure 4.17: Regression standardized residual of dependent variable in tombolo case ..... 81

Figure 4.18: Regression standardized residual of dependent variable in salient case ..... 81

Figure 4.19: Regression standardized residual of dependent variable in both salient and tombolo case ..... 81

Figure 4.20: Regression standardized residual of dependent variable in no sinuosity case ..... 82

Figure 4.21: Net sand beach at up-drift and down-drift in comparison ..... 83

Figure 4.22: Controlled point distances at up and down-drift comparison ..... 83

Figure 4.23: Up and down drift relations in tombolo formation ..... 85

Figure 4.24: Up and down drift relations in salient formation ..... 85

Figure 4.25: Up and down drift relations in both tombolo and salient formation ..... 86

Figure 4.26: Up and down drift relations in no sinuosity formation..... 87

Figure 5.1: The trends of the shoreline when the breakwater length increases..... 95

Figure 5.2: The evaluation of the shoreline change as the breakwater length increases ..... 95

Figure 5.3: The trends of the shoreline when the breakwater offshore distance increases ..... 97

Figure 5.4: The evaluation of the shoreline change as the breakwater offshore distance increases..... 97

Figure 5.5: The trends of the shoreline when the breakwater gap increases..... 98

Figure 5.6: The evaluation of the shoreline change as the breakwater gap increases..... 98

Figure 5.7: The trends of the shoreline when the wave height increases..... 100

Figure 5.8: The evaluation of the shoreline change as the wave height increases..... 100

Figure 5.9: The trends of the shoreline when the wave length increases..... 101

Figure 5.10: The evaluation of the shoreline change as the wave length increases ..... 101

*Figure 5.11: The trends of the shoreline when the wave direction increases .....102*  
*Figure 5.12: The evaluation of the shoreline change as the wave direction increases .....102*  
*Figure 5.13: The trends of the shoreline when the tide increases.....104*  
*Figure 5.14: The evaluation of the shoreline change as the tide increases .....104*  
*Figure 5.15: The trends of the shoreline when the median sediment size increases .....105*  
*Figure 5.16: The evaluation of the shoreline change as the median sediment size increases .105*  
*Figure 5.17: Estimation of alongshore effect as the offshore distance.....106*  
*Figure 5.18: Estimation of alongshore effect as the wave height.....107*  
*Figure 5.19: Estimation of alongshore effect as the oblique wave angle .....107*  
*Figure 5.20: Estimation of along shore effect as the tidal range .....108*  
*Figure 5.21: Estimation of alongshore effect as the sediment size.....109*



## LIST OF TABLES

<i>Table 2.1: Empirical relationships for detached breakwater (from Chasten et al. (1993))</i> .....	24
<i>Table 2. 2: Conditions for shoreline response behind detached breakwater</i> .....	26
<i>Table 3.1: Summary of the US breakwater projects (from technical report CERC-93-19) ....</i> - 35 -	
<i>Table 3. 2: Projects of detached breakwater in Spain</i> .....	36
<i>Table 4.1: Ratio of a dimensionless efficiency <math>L_B/X_B</math></i> .....	58
<i>Table 4.2: Correlation coefficients of variables in tombolo equation 4.11</i> .....	70
<i>Table 4.3: Correlation coefficients of variables in salient equation 4.20</i> .....	70
<i>Table 4.4: Correlation coefficients of variables in no sinuosity equation 4.22</i> .....	70
<i>Table 4.5: Fitting the measured data to the previous empirical suggestions</i> .....	73
<i>Table 4.6: Correlation coefficients of variables in tombolo case in equation 4.32</i> .....	80
<i>Table 4.7: Correlation coefficients of variables in salient case in equation 4.33</i> .....	80
<i>Table 4.8: Correlation coefficients of variables in both salient and tombolo case in equation 4.34</i> .....	80
<i>Table 4.9: Correlation coefficients of variables in no sinuosity case in equation 4.35</i> .....	80





## ACKNOWLEDGEMENT

Doing the PhD research has been one of the most challenging work in my life. This thesis is my own results of study, but I received so much support and help from many people around me. It is a chance to thank all of them, including those I may have forgotten to mention herein.

First, I would like to express my deepest gratitude to Prof. J.K. Vrijling and Assoc.Prof. H.J. Verhagen, my promoters, for their enthusiastic guidance and encouragement. Prof. Vrijling gave me inspiring advice which broadened my mind, and also gave me complete freedom in my PhD life. All discussions with Assoc.Prof. Verhagen were so working detailed, his broad knowledge in hydraulic structures; all this promoted my progress, while on the thesis a lot.

Many thanks go to Prof. P.H.A.J.M van Gelder for your guidance in statistics and engineering software and you have always been encouraging and patient, which helped me to increase my confidence and to overcome difficulties in the study.

I am grateful to my graduation committee members: Dr.ir. N.T. Hoan, Prof.Dr.-Ing. H. Schüttrumpf, Dr.ir. B. Hofland, Prof.dr.ir. P.H.A.J.M. van Gelder, Prof.dr.ir. M.J.F. Stive and Prof.dr.ir. S.N. Jonkman for their critical comments and suggestions to improve the manuscripts.

My sincere thanks for the financial support by the Ministry of Education and Training of Vietnam (through Project 322) and the Valorisation Centre, especially Mrs. Tran Thi Nga and Mrs. Veronique van der Varst for their support and help.

I appreciate Mrs. Mariette van Tilburg for her encouragement during critical times and for her review of my thesis writing. I have learnt more from her in the academic writing.

I would like to thank the English teacher – Mrs. Clair Taylor. She has patiently corrected my English pronunciation when I just arrived.

Many thanks go to the staff in the Department of Hydraulic Structures and Flood Risk by their support: Judith, Inge, Agnes, Lenie, Madelon and Mark.

I will forever remember the Vietnamese Community in Delft (VCiD), which I joined in parties, BBQs, sightseeing, games, etc.; a small tennis group – where I played stress away after a hard working day. I love you all. I wish everyone happiness and success.

## *Acknowledgement*

---

I would like to thank the colleagues of the Port and Waterway Engineering Department, the National University of Civil Engineering (NUCE) – where I work. I especially acknowledge Assoc.prof.dr. Pham Van Giap, Assoc.prof.dr. Do Van De, Dr. Bui Viet Dong by their support and encouragement. Many thanks to Mrs. Dao Tang Kiem who helped me to connect to the Valorisation Center, Delft University of Technology to apply for a Ph.D. position.

Last but not least, to my wife to Hong Nhung for her love, sacrifices, patience, and taking care our children and to my children, Gia Bao and Gia Han; I hope that in the near future you will return to visit the attractive city – Delft, where you lived. I am really warmed with the frequent encouragement from my family members, I am grateful for my parents, brothers and sisters. I also keep in mind the support from the family company - KCON.

Tat Chien KHUONG

Delft, December 2015

## CURRICULUM VITAE

Tat Chien KHUONG was born in Nam Dinh province, Vietnam, on 21 February 1976. From 1994 to 1999, he studied Port and Waterway Engineering at National University of Civil Engineering (NUCE) and obtained BSc degree. During the period at university he won the silver medal for “Graduation Thesis” granted Ministry of Education and Training, Ministry of Construction and Vietnam construction organization (giai thuong Loa Thanh). Shortly after BSc graduation, in June 1999 he worked as an assistant lecturer at the Faculty of Hydraulic Engineering, NUCE. In the meanwhile he continued to do his Master degree at the Faculty of Postgraduates, NUCE and obtained his Master degree in 2002. From 2002 to the present, he works as a lecturer at the Department of Port and Waterway Engineering, NUCE. In June 2011, he started his PhD study at the Section of Hydraulic Structures and Flood Risk, Delft University of Technology, the Netherlands. This PhD study was financially supported by the Ministry of Education and Training of Vietnam (through 322 project).